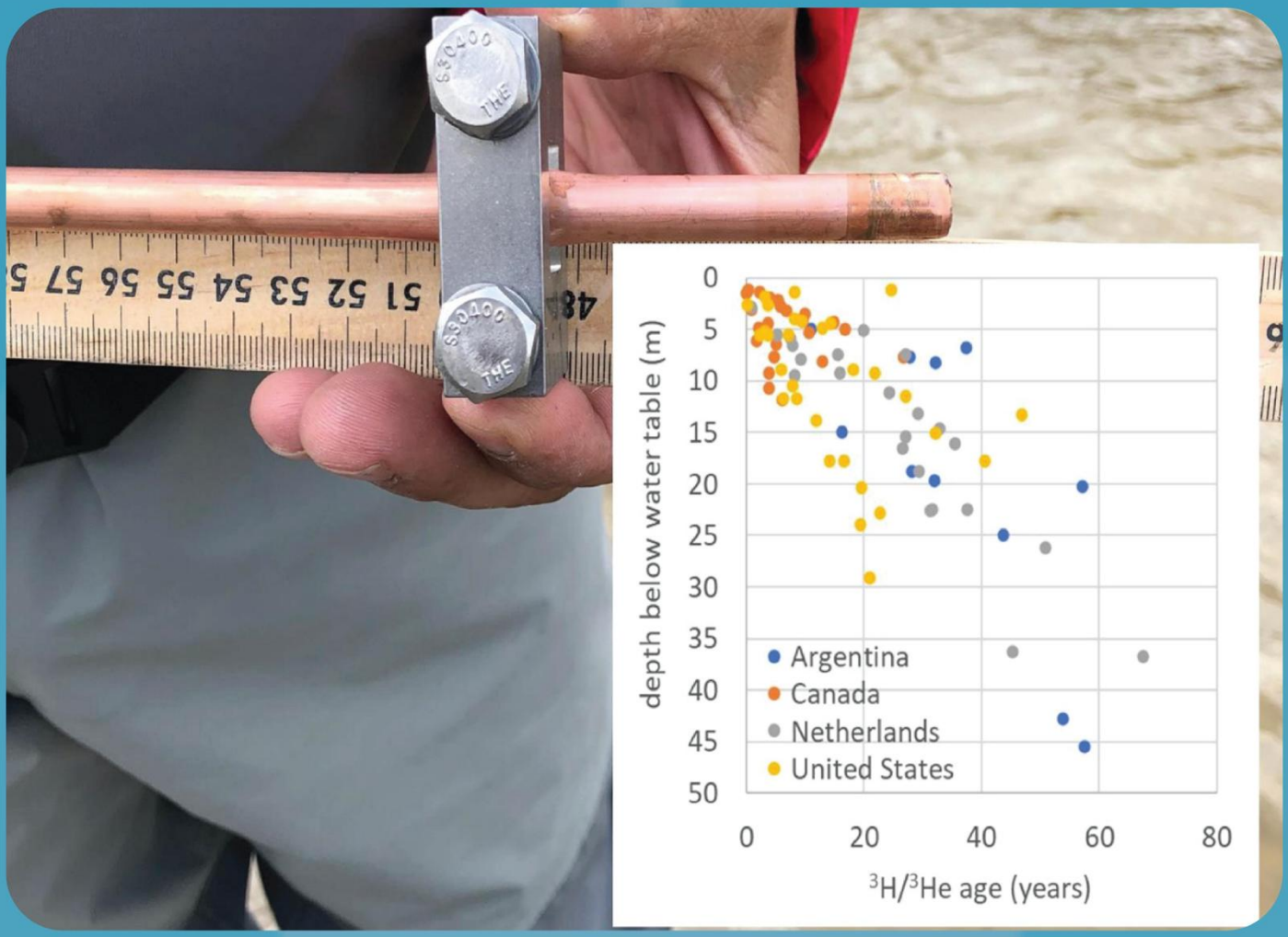

Age Dating Young Groundwater

How to Determine Groundwater Age from Environmental Tracer Data

D. Kip Solomon and Troy E. Gilmore

THE GROUNDWATER PROJECT

Age Dating Young Groundwater:

How to Determine Groundwater Age from Environmental Tracer Data

The Groundwater Project

D. Kip Solomon

Professor
University of Utah
Salt Lake City, Utah, USA

Troy E. Gilmore

Associate Professor
University of Nebraska
Lincoln, Nebraska, USA

Age Dating Young Groundwater:

How to Determine Groundwater Age from Environmental Tracer Data

The Groundwater Project
Guelph, Ontario, Canada
Version 2, March 2026

TDS

Technical Development Solutions

شركة حلول التقنية والتطوير

SUSTAINABLE INNOVATIVE RESOURCES MANAGEMENT

Smart solutions for using resources efficiently, protecting our planet, and securing a prosperous future.

SECTORS

WATER

ENVIRONMENT

MINING

INTEGRATED WATER SERVICES LIFECYCLE

GREEN ENERGY

DIGITIZATION AND AUTOMATION

COMPREHENSIVE MONITORING SOLUTIONS

DISASTER MANAGEMENT SYSTEMS CATEGORY

SERVICES

www.tds.com.sa

The Groundwater Project relies on private funding for book production and management of the Project.

Please consider sponsoring the Groundwater Project so that our books will continue to be freely available. https://gw-project.org/donate/↗

Thank you.

Published by The Groundwater Project, Guelph, Ontario, Canada, 2024.

Age Dating Young Groundwater: How to Determine Groundwater Age from Environmental Tracer Data / D. Kip Solomon and Troy E. Gilmore.

116 pages

DOI: https://doi.org/10.21083/LIIU2727↗.

ISBN: 978-1-77470-058-7

Please consider signing up to the GW-Project mailing list to stay informed about new book releases, events, and ways to participate in the GW-Project. When you sign up to our email list, it helps us build a global groundwater community. Sign up↗.

APA (7th ed.) Citation:

Solomon, D. K., & Gilmore, T. E. (2024). *Age Dating Young Groundwater: How to Determine Groundwater Age from Environmental Tracer Data*↗. The Groundwater Project. https://doi.org/10.21083/LIIU2727↗.

Cover Image: Mikaela Cherry, 2019; inset figure is from Gilmore et al., 2021, and references cited therein

Dedication

This book is dedicated to Robert J. Poreda, University of Rochester retired, who taught D. Kip Solomon the fundamentals of noble gas geochemistry, mass spectroscopy, and critical analysis of field data.

Table of Contents

The Groundwater Project Foreword

The UN-Water Summit on Groundwater, held on 7-8 December 2022, at the UNESCO Headquarters in Paris, France, concluded with a call for Government and other stakeholders to scale up efforts to better manage groundwater. The intent of the call to action was to inform relevant discussions at the UN 2023 Water Conference that was held on 22-24 March 2023 at UN Headquarters in New York City. One of the required actions is *strengthening human and institutional capacity*, to which groundwater education is fundamental.

The 2024 World Water Day theme is '*Water for Peace*', which focuses on the critical role water plays in the stability and prosperity of the world. The UN Water website states that *more than 3 billion people worldwide depend on water that crosses national borders*. There are 592 transboundary aquifers; yet most of these aquifers do not have an intergovernmental cooperation agreement in place for sharing and managing the aquifer. While groundwater plays a key role in global stability and prosperity, it also makes up 99% of all liquid freshwater, so it is at the heart of the freshwater crisis. *Groundwater is an invaluable resource*.

The Groundwater Project (GW-Project) is a registered Canadian charity founded in 2018, committed to the advancement of groundwater education as a means to accelerate action related to our essential groundwater resources. We are committed to *making groundwater understandable* and, with that, enable *building the human capacity for sustainable development and management of groundwater.* To that end, the GW-Project creates and publishes high-quality books about *all-things-groundwater*, for all who want to learn about groundwater. Our books are unique in that they synthesize knowledge, are rigorously peer reviewed, are translated in many languages, and are free of charge. An important tenet of GW-Project books is a strong emphasis on visualization with clear illustrations to stimulate spatial and critical thinking. The GW-Project started publishing books in August 2020, and, by the end of 2023 had published 44 original books and 58 translations. The books are available at gw-project.org↗.

The GW-Project embodies a new type of global educational endeavor made possible through the contributions of a dedicated international group of volunteer professionals from diverse disciplines. Academics, practitioners, and retirees contribute by writing and/or reviewing books aimed at diverse levels of readers including children, teenagers, undergraduate and graduate students, as well as professionals in groundwater fields and the general public. More than 1,000 dedicated volunteers from 70 countries and six continents are involved—and participation is growing. Revised editions of the books are published from time to time. Readers are invited to propose revisions.

We thank our sponsors for their ongoing financial support. Please consider donating to the GW-Project so we can continue the publication of books free of charge.

The GW-Project Board of Directors, January 2024

Foreword

The elapsed time groundwater takes to travel from its recharge area to any point in a groundwater flow domain—such as to a monitoring well—is an important number that results from a combination of physical properties of the flow system. The elapsed time depends on the rate of recharge to the flow path as well as the distribution of hydraulic conductivity and porosity of the geologic media along the flow path between the recharge area and the well.

To determine the values of these parameters would involve much effort and expense and is rarely accomplished. An alternative method involves collecting a water sample from the well and subjecting it to measurements that allow an estimate of the travel time to be calculated. This estimate is known as the *groundwater age* for the well or spring; when these age dating methods are applied in a study area, age determinations are made on several or even many wells.

This book concerns the age dating of groundwater less than 60 years old, adding to the body of knowledge presented in the previously published GW Project book *Introduction to Isotopes and Environmental Tracers as Indicators of Groundwater Flow* (Cook, 2020), which provides an overview of all of the environmental tracers used to estimate groundwater age, including those applied to water much older than 60 years. This book is intended for those who seek to apply age dating methods or who want to understand the nature of and uncertainties in age values reported in the literature, particularly with respect to young groundwater.

Laboratories that conduct age dating measurements on samples as indicated in this book operate in several countries; thus, anyone who seeks these analyses can obtain them on a fee per sample basis. This important advancement means that age dating of groundwater less than 60 years old has moved beyond the experimental stage to being an important tool that can be applied in many types of investigations.

The authors of this book, Dr. Kip Solomon, a professor at the University of Utah, and Dr. Troy Gilmore, an associate professor at the University of Nebraska, are experienced in many different hydrogeologic settings. Over the course of their careers, they have produced a substantial portion of the existing literature concerned with dating methods used on young groundwater.

John Cherry, The Groundwater Project Leader

Guelph, Ontario, Canada, November 2023

Preface

This book provides an overview of common tracer methods that can be used to estimate the age of young groundwater that has recharged since about 1960. The dating tracer methods include tritium (^3He), tritium/helium-3 ($^3He/^3He$), sulfur hexafluoride (SF_6), and chlorofluorocarbons (CFCs). All of these methods except ^3H involve the occurrence and transport of dissolved gases, and thus the basic concepts of dissolved gases are also included. The applications of tracers to address hydrogeologic problems are only mentioned briefly in this book because such problems are the topic of the Groundwater Project book *Introduction to Isotopes and Environmental Tracers as Indicators of Groundwater Flow* (Cook, 2020), which we encourage you to review.

This book is intended for knowledgeable practitioners and/or academics who desire to learn the details of how measured tracer concentrations can be converted to an apparent groundwater age. While we provide an overview of both the analytical methods and the systematics of age dating, the content is most useful for those who wish to implement groundwater age dating in their work.

As hydrogeologists, we are interested in solving both groundwater quality and quantity issues in a world where the availability of high-quality groundwater is diminishing. Our goal is to inform groundwater professionals and policy makers about the concepts and underlying assumptions involved in groundwater dating methods. The ultimate aim is to increase the application of these powerful methods while recognizing their inherent limitations.

By reading this book and completing the exercises, we aim to help readers achieve the following.

1. The ability to describe basic analytical methods used for age-dating tracers.
2. Understanding of the assumptions underlying the use of tracers to estimate groundwater age.
3. Understanding of the specific information needed to convert tracer concentrations to groundwater age.
4. The ability to compute apparent groundwater age given measured tracer concentrations.

Acknowledgments

We deeply appreciate the thorough and useful reviews of and contributions to this book by the following individuals:

- Lorenzo Copia, International Atomic Energy Agency, Vienna, Austria;
- Ramon Aravena, University of Waterloo, Waterloo, Ontario, Canada;
- Peter Cook, Flinders University, Adelaide, South Australia, Australia;
- Ian Clark, University of Ottawa, Ottawa, Ontario, Canada;
- Robert M. Kalin, The Queen's University of Belfast, Belfast, Ireland;
- Craig Jensen, North Carolina State University, Chapel Hill, North Carolina, USA;
- Meg Wolf, University of Utah, Salt Lake City, Utah, USA.

We are grateful for Amanda Sills and the Formatting Team of the Groundwater Project for their oversight and copyediting of this book. We thank Eileen Poeter (Colorado School of Mines, Golden, Colorado, USA) for reviewing, editing, and producing this book.

Where a figure or table was obtained from other sources, a citation appears in the caption. However, where no citation is inserted in the caption, the material is original to this book.

1 Introduction

Groundwater age refers to the elapsed time taken for a parcel of water to move along a groundwater flow path from where it enters as recharge to the point of sample collection. It is often said that groundwater moves slowly so its age may seem irrelevant to our daily lives, but knowing the age of groundwater can help estimate:

- groundwater recharge rates which drive groundwater systems and are useful to municipalities for long-term water resource planning and to know whether they are using more water than is replenished by rain and snow;
- how long it takes for groundwater recharge to reach gaining streams;
- recharge year for groundwater samples which is useful for
    - investigating historical input of contaminants to aquifers, including non-point sources to determine what type and magnitude of contaminants the groundwater might contain based on land use practices at the time, and
    - predicting future discharge of contaminants from aquifers to wells, springs, and streams; and
- calibration constraints to develop more reliable groundwater models of the area.

Because age represents an integration of upstream groundwater velocities, the age at a point in an aquifer potentially contains more information than a point sample taken for a physical property such as porosity or permeability. In this book, we review the basic concepts and systematics of dating methods applicable to groundwater ages younger than about 60 years. The historical development, basic concepts, sample collection and analysis, age calculations, and tracer-specific issues are discussed. The application of age-dating tracers for studying groundwater flow systems—including old water—is the topic of the Groundwater Project book *Introduction to Isotopes and Environmental Tracers as Indicators of Groundwater Flow* (Cook, 2020), which we encourage readers to review.

The focus of this book is on interpreting tracer concentrations from a single discrete sample of groundwater to estimate the *tracer age* of the sample. When a time series of samples and/or a collection of samples that can be interpreted to give a flow-weighted average of the aquifer's water are available, powerful tools such as lumped parameter models (LPM) are available for estimating the mean residence time (Jurgens et al., 2012; Maloszewski & Zuber, 1982). The use of LPMs is beyond the scope of this book; however, understanding the age-dating concepts discussed in this book will help readers implement these models.

The information in this book has been distilled from original research papers—that are cited herein—and is intended to serve as an overview for readers who want to become familiar with dating methods. In this book, we:

1. describe the basic analytical methods used for age-dating tracers,

2. list and explain the assumptions and specific information needed to convert tracer concentrations to ages,
3. provide readers with the ability to compute apparent groundwater age given measured tracer concentration, and
4. describe the uncertainty associated with calculated apparent groundwater ages.

Readers who intend to use tracer data in a study are encouraged to consult the original papers for details and additional explanation.

Use of the age-dating tracers described in this book require specialized analytical equipment and laboratories with this equipment are limited. For example, more than 50 laboratories participated in a recent (2022) proficiency evaluation of ^{3}H conducted by the International Atomic Energy Agency (IAEA). While, only ten laboratories participated in a noble gas intercomparison conducted in 2012 (Visser et al., 2014). Readers seeking contact information for laboratories that offer these specialized analyses are welcome to contact the authors.

The concept of groundwater dating differs from dating as used in geologic studies where age typically refers to the elapsed time since mineral formation. Water molecules continuously associate and dissociate with a hydrogen bond lifetime on the order of one picosecond (Keutsch & Saykally, 2001), so the elapsed time since formation is not meaningful in a hydrologic context. However, the time required for a tracer to move from the recharge location to a collection point can be highly relevant for understanding groundwater flow.

Groundwater tracers can be categorized according to how they function (i.e., how they provide information related to time).

1. *Decaying tracers* use a known rate of radioactive decay along with a known input concentration.
2. *Transient tracers* use a non-constant and known input concentration.
3. *Accumulating tracers* use a known initial concentration and a known rate of production in the subsurface.

Most of the young groundwater tracers discussed in this book are transient tracers, but some make use of radioactive decay and accumulation.

Figure 1 shows groundwater dating methods as a function of the practical time scale over which the tracers are useful. Included in Figure 1 are numerous age-dating tracer methods for evaluating travel times on the order of days to about 60 years. This time scale is relevant to many shallow aquifers that are susceptible to contamination and are often used for residential water supply and irrigation. The methods included in this book are tritium (^{3}H), tritium/helium-3 ($^{3}H/^{3}He$), sulfur hexafluoride (SF_6), and chlorofluoro-carbons (CFCs). Other tracers can be used to qualitatively demonstrate that groundwater is young such as the occurrence of artificial sweeteners and/or pharmaceuticals, elevated

nitrate and chloride, and a time series of stable isotopes. However, the focus of this book is on quantitative age-dating tracers.

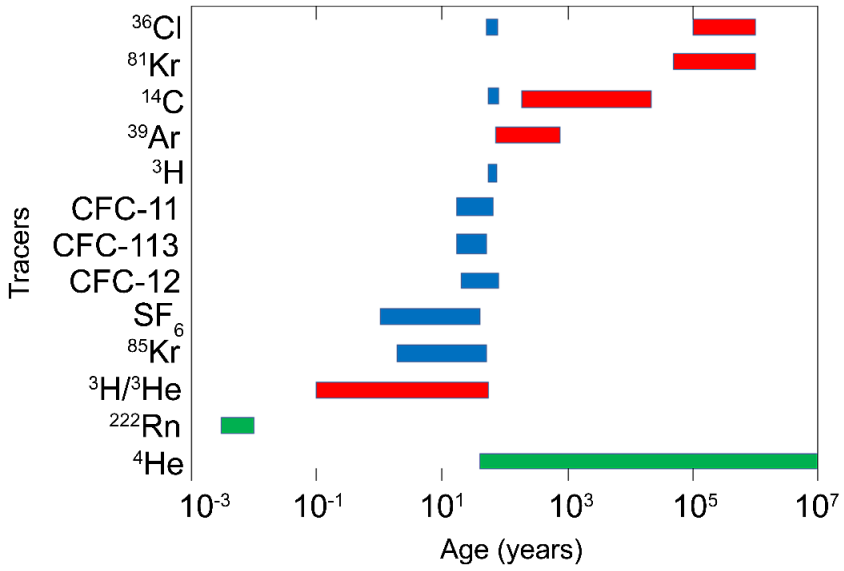

Figure 1 - Approximate age ranges over which different environmental tracers can provide information on groundwater age. Radioactive tracers are indicated in red, transient tracers in blue, and accumulating tracers in green (Cook, 2020).

Except ^{3}H, the young groundwater dating methods discussed in this book utilize dissolved gases and require specialized sample collection techniques to prevent contact between the sample and the atmosphere. Due to laboratory requirements, sample collection methods differ for each of the tracers. While a discussion of the general concepts of sample collection is included in this book, readers are strongly encouraged to contact their specific analytical laboratory for sample collection information and/or to request specialized equipment and sample containers.

The occurrence and solubility of dissolved gases in groundwater is discussed in Section 2 as these concepts are important for most of the young groundwater dating methods. The extent to which a tracer contained within groundwater is transported at the same rate as bulk groundwater largely determines the usefulness of a particular age-dating tracer. Age calculations involve tracer concentrations, and the term *tracer age* or *apparent age* is used throughout this book to emphasize that differences may exist between the movement of a tracer and the bulk movement of groundwater.

Apparent ages are often highly stratified in aquifers; long and even moderate length well screens can result in samples containing mixtures of water that moved along very different flow paths. Figure 2 illustrates (1) how different well depths and screen lengths intercept different flow paths and groundwater age ranges, and (2) how lower recharge rates increase groundwater age gradients; that is, groundwater age increases more rapidly with depth. Also, when wells are aggressively pumped mixing of water from different depths with different ages can occur.

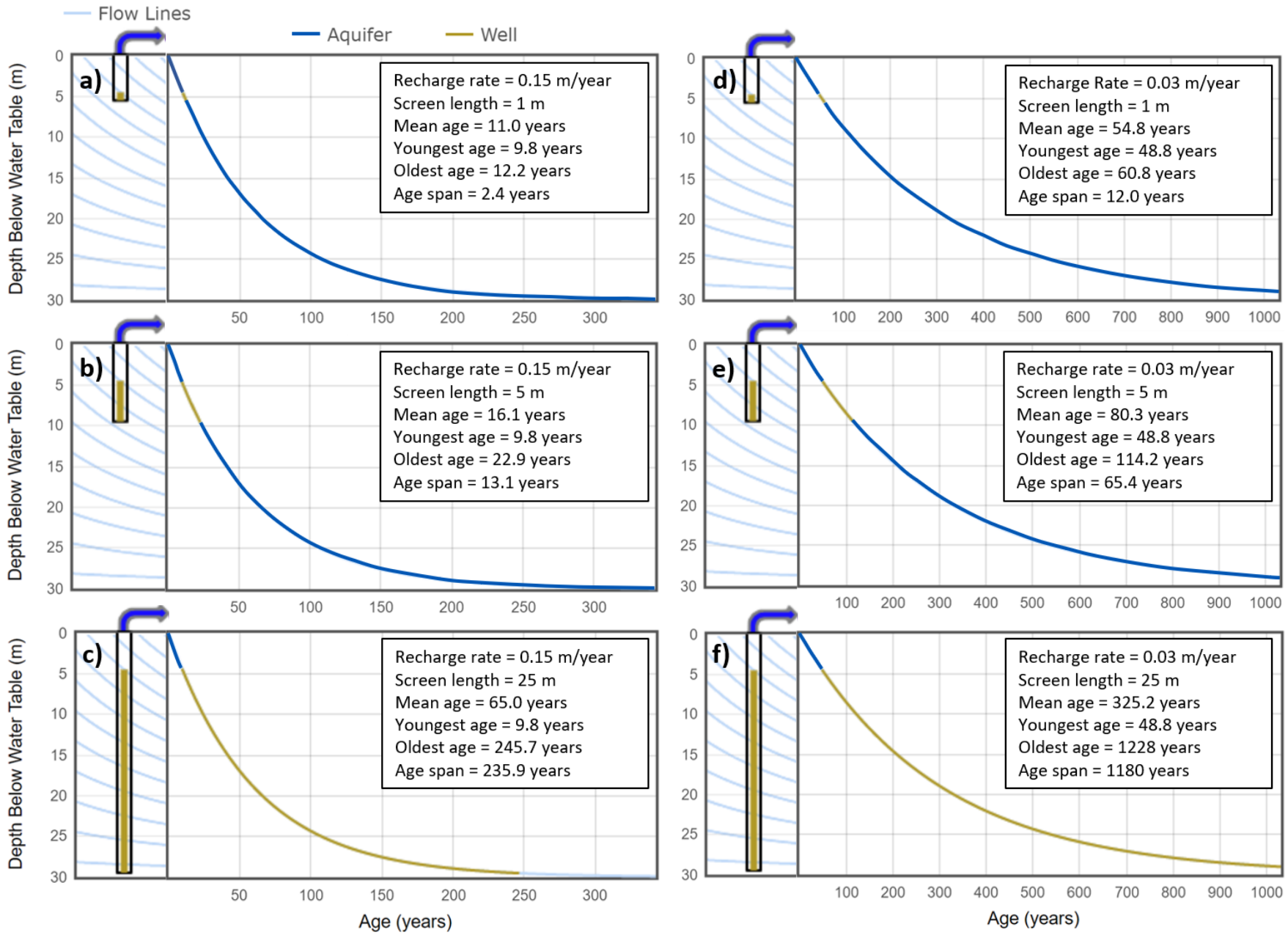

Figure 2 - Groundwater age values for different well depths and screen lengths in a homogeneous aquifer with uniform thickness and uniform porosity. A partial aquifer cross section with groundwater flow lines, well depth, and screen length are depicted on the left side of each panel. Overall mean groundwater age for the aquifer in panels a) through c) is 60 years, while it is 300 years in panels d) through f) because the recharge rate is one-fifth the rate in panels (a) through (c). The gold bar indicates the well screen. Water from all depths along the screen differ in age and enter the well to provide a sample of water with a range of ages. That age range of water entering the well is shown by the gold portion of the age versus depth curve. Modified from the Groundwater Age Mixtures and Contaminant Trends Tool (GAMACTT) provided by Böhlke and others (2014).

We used the web-based Groundwater Age Mixtures and Contaminant Trends Tool (GAMACTT: Böhlke et al., 2014; US Geological Survey, 2016) to develop Figure 2, based on a homogeneous aquifer with uniform thickness (30 m), uniform porosity (0.3), and two different recharge rates (0.15 m/yr and 0.03 m/yr). In these illustrations, a shallow well screen with length of 1 m intercepts young groundwater with an age span of 2.4 years and 12 years respectively in the 0.15 m/year and 0.03 m/year recharge rate scenarios (Figure 2a and Figure 2d). In the low-recharge scenario, even a relatively shallow 5 meter well screen (Figure 2e) intercepts groundwater outside the functional age-dating limitations of tracers discussed in this book because the oldest age intercepted is about 114 years. Both low- and high-recharge scenarios yield a mixture of young and old groundwater from 25 m screens (Figure 2c and Figure 2f) with the low-recharge scenario yielding some groundwater that would be more appropriately age-dated with ^{14}C (Figure 1).

The examples in Figure 2 are based on highly simplified aquifer parameters. In the field, aquifer heterogeneity could lead to the interception of groundwater with even greater age ranges. Also, the estimates of groundwater age discussed in this book utilize solutes dissolved in the water. When advection is the dominate transport mechanism the movement of these solutes and groundwater is similar and so age estimates derived from solute measurements approximate the transit time of groundwater. However, in complex hydrogeologic environments where other transport mechanisms are important, the tracer age of the water may be significantly different than the transit time of water. In bedrock aquifers—where flow is often dominated by discrete fractures and wells intersect multiple fractures—the spectrum of ages can be particularly large, and diffusion of solutes into and out of the matrix (matrix diffusion) complicates the use of age-dating tracers. Further discussion of more complex hydrogeological settings is outside the scope of this book, but we emphasize that it is critical to consider plausible recharge rates and develop appropriate conceptual models for the groundwater system being studied. This groundwork can be used to carefully design or select wells or other sampling points (e.g., streams, springs) that increase the likelihood of successfully sampling, analyzing, and interpreting age tracers in groundwater.

In addition to the convergence of bulk groundwater flow paths (e.g., Figure 2), molecular diffusion and hydrodynamic dispersion contribute to groundwater samples that contain tracer concentrations that represent a spectrum rather than a single age. As discussed by Cook (2020), whether the average tracer concentration associated with this spectrum of ages calculates to the average age of the tracer distribution depends in part on the relationship between tracer concentration and time. When tracer concentration and time are linearly related, the average concentration can be used to map the average age.

While a linear relationship between age and time may approximately exist for some tracers over a narrow range of time, in general, the age calculated using measured (i.e., average) tracer concentrations will be biased—either older or younger (Cook, 2020)—away

from the mean. As a result, some researchers (Turnadge & Smerdon, 2014) have argued against the quantitative use of groundwater ages in favor of reporting raw tracer concentrations.

While rigorous quantitative use of age-dating tracers involves using numerical simulations of groundwater flow and solute transport while adjusting the simulated system to obtain a match between observed and simulated tracer concentrations, it is our view that calculated tracer ages are useful for conceptualizing and understanding groundwater flow systems. Moreover, if the assumptions and equation(s) for calculating the tracer age are clearly defined, the age becomes a transformation of the concentration without loss of raw information or generality. Furthermore, age is a concept that resonates with groundwater practitioners and the general public, offering opportunities to communicate hydrogeologic concepts in ways that—though imperfect—are not possible using only tracer concentrations. Finally, for many tracers, the measured value has to be adjusted or converted to be directly related to transit time and compared with simulations. For example, measured values of ^{3}He must be corrected for non-tritiogenic components as shown in Section 4. Thus, the concepts in this book are useful regardless of whether the goal is a simulated concentration or an estimated age.

2 Dissolved Gases in Groundwater

Except for ^3H, the age-dating tracer methods in this book use dissolved gases. In this section, we discuss the basic concepts of equilibrium gas solubility as a function of temperature and pressure and the occurrence of gas that is not in equilibrium with the fluid due to trapped bubbles. These concepts are illustrated using the noble gases, but they apply to SF_6 and CFCs.

Many gases are relatively inert with respect to geochemical reactions in the subsurface; thus, they behave as conservative tracers. However, when both gas and liquid phases are present, all gases will partition into both phases, which can lead to very different transport behavior than that of conservative ionic tracers in groundwater. As such, the existence of both gas and liquid phases and the solubility of a given gas are important for relating the movement of dissolved gas tracers to the movement of groundwater.

2.1 Henry's Law

Henry's Law describes the equilibrium relationship between the concentration of a gas dissolved in water and the concentration of that gas in the gas phase. The gas phase concentration is a function of both the total gas pressure and the mole fraction of the gas in the gas mixture. Changing either the total gas pressure or the mole fraction can, in turn, change the dissolved concentration. There are many different forms of Henry's Law with some forms describing the solubility of a gas in a liquid, while other forms describe the volatility of a gas. In this section, the volatility forms are described as they are commonly used for noble gases, and they are helpful for describing the effect that bubbles have on dissolved concentrations. When using data from the literature, it is critical that researchers understand exactly which form of Henry's Law is being used, as numerical values and units can differ substantially.

A dimensionless form of Henry's Law is shown in Equation (1).

$$C_i^{gas} = K_{w,i}^{cc} C_i^{water} \quad (1)$$

where:

C_i^{gas} = molar concentration of gas *i* in the gas phase (molL^{-3}, e.g., moles/L)

C_i^{water} = molar concentration of gas *i* in the water phase (molL^{-3}, e.g., moles/L)

$K_{w,i}^{cc}$ = Henry Coefficient for gas *i* (dimensionless)

The dimensioned form of Henry's Law is shown in Equation (2).

$$p_i = K_{w,i} c_i \quad (2)$$

where:

p_i = partial pressure of gas *i* in the gas phase ($ML^{-1}T^{-2}$, typically atm)

c_i = concentration of gas *i* in the water phase ($molL^{-3}$, typically moles/L)

$K_{w,i}$ = Henry Coefficient for gas *i* ($ML^2T^2mol^{-1}$, typically atm−L/mole)

Both the dimensionless and dimensioned forms of Henry Coefficient are specific for each gas and are a function of temperature and salinity, which we subsequently describe.

In noble gas geochemistry, aqueous concentrations are often expressed in units of ccSTP/g. This unit describes the volume of gas in cubic centimeters at standard temperature (0 °C for gases) and pressure (1 atm) per unit mass of water. To visualize this unit, consider 1 gram of water in which the gas is completely removed and placed in a syringe that is then cooled to 0 °C. If the syringe is then compressed until the gas pressure is 1 atm, the gas volume in cubic centimeters within the syringe is ccSTP and the original gas concentration in the water is this volume per 1 g of water. This volume (ccSTP) can be converted to moles using the ideal gas law as shown in Equation (3).

$$n = \frac{PV}{RT} = \frac{(1\text{ atm})(1\text{ ccSTP})}{82.057366\ \frac{\text{cc atm}}{\text{mole °K}}(273.15\text{ °K})} = 0.00004462\text{ mole} \qquad (3)$$

So, 1 cc of gas at standard temperature and pressure is 0.00004462 moles. Therefore, a water having 1 ccSTP of gas per gram of water has a concentration of:

$1\text{ ccSTP/g} = 0.00004462\text{ moles g}^{-1} = 0.004462\text{ moles kg}^{-1}$. Units used in the literature for noble gas concentrations vary (e.g., ccSTP/g, ccSTP/kg, moles/kg). As with all equations, it is important to use consistent units throughout the calculation.

When the aqueous concentration is in units of ccSTP/g, values for $K_{w,i}$ at various temperatures for pure water are shown in Table 1. Also shown in Table 1 are values of $K^{cc}_{w,i}$ (dimensionless). One utility of the dimensionless form of Henry's Law is that the value of $K^{cc}_{w,i}$ represents the preference for a given gas to reside in the gas phase when equal volumes of gas and water are equilibrated. For example, if equal volumes of gas and water are in equilibrium, the amount of He in the gas phase will be more than 100 times the amount in water. In contrast, the amount of xenon (Xe) in the gas phase will be about five times greater (at 0 °C) than in the water phase for equal volumes of gas and water. The values for $K^{cc}_{w,i}$ shown in Table 1 underscore the importance of collecting samples with no headspace.

Table 1 - Henry Coefficient for gases in pure water.

Temp °C	He [1]	Ne [1]	Ar [2]	Kr [3]	Xe [4]	O_2 [5]	N_2 [5]
Dimensioned Henry Coefficient $K_{w,i}$ (atm g / ccSTP)							
0	106	80.3	18.6	9.13	4.49	21.8	42.2
10	111	89.0	23.9	12.4	6.52	26.9	53.2
20	114	96.0	29.3	16.0	8.93	32.6	64.0
30	115	101.0	34.4	19.8	11.6	39.0	74.1
Dimensionless Henry Coefficient $K^{cc}_{w,i}$							
0	106	80.3	18.6	9.13	4.49	21.8	42.2
10	108	85.9	23.1	11.9	6.29	25.9	51.3
20	107	89.4	27.3	14.9	8.32	30.4	59.6
30	104	91.0	31.0	17.8	10.5	35.2	66.7

Values were computed using empirical formulas from the following:

[1] He and Ne: Weiss (1971)

[2] Ar: Weiss (1970)

[3] Kr: Weiss and Kyser (1978)

[4] Xe: Clever (1979)

[5] O_2 and N_2: Sander (1999)

The solubility of a gas in water is inversely proportional to temperature. As the temperature increases, the solubility decreases. Figure 3 shows how the solubility of diverse gases varies as a function of temperature. The variability in solubility that occurs with change in temperature is a function of molecular weight. The heavier the molecule, the greater the sensitivity to temperature. For example, the solubility of He changes by just over ten percent between 0 and 30 °C, whereas Xe solubility varies by more than 60 percent over this temperature range.

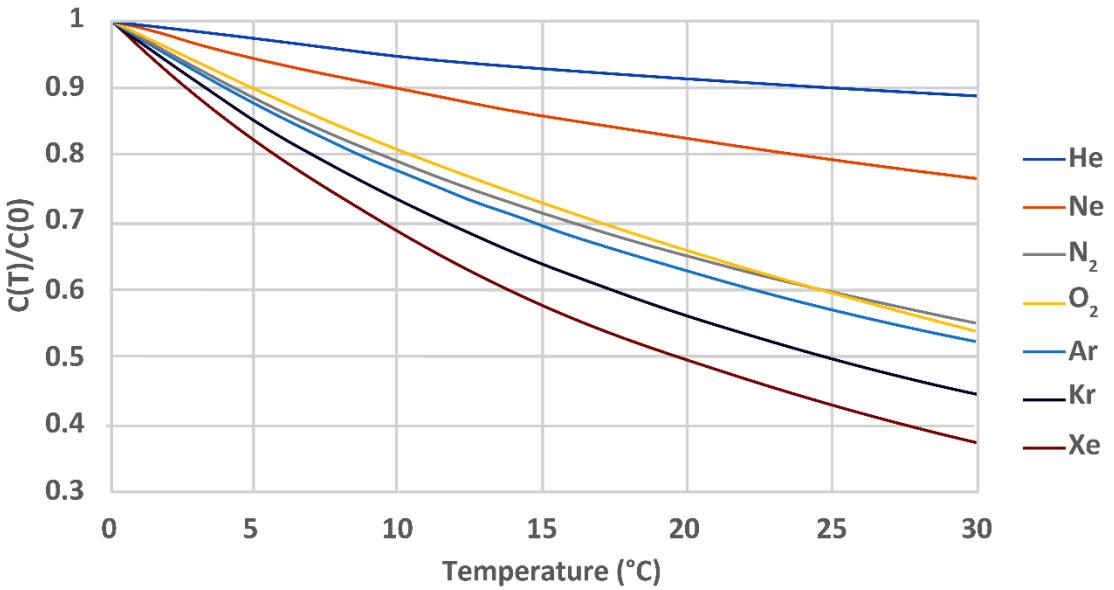

Figure 3 - Dissolved concentration of various gases normalized by the concentration at 0 °C versus temperature. The sensitivity of the concentration to temperature is greater for heavy gases (e.g., Xe) and less for light gases (e.g., He).

The solubility of a gas also depends on salinity. As the salinity of water increases and the thermodynamic activity of water decreases, the concentration of gas dissolved in

water that is in equilibrium with a gas phase is lower. This is known as the salting effect and is generally more significant for high molecular weight gases than for those with low molecular weight. The salting effect for various gases is shown in Figure 4. The solubility of Xe decreases by about 25 percent from freshwater (salinity = 0) to seawater (salinity = 35 g/kg) while the solubility of He decreases by about 20 percent.

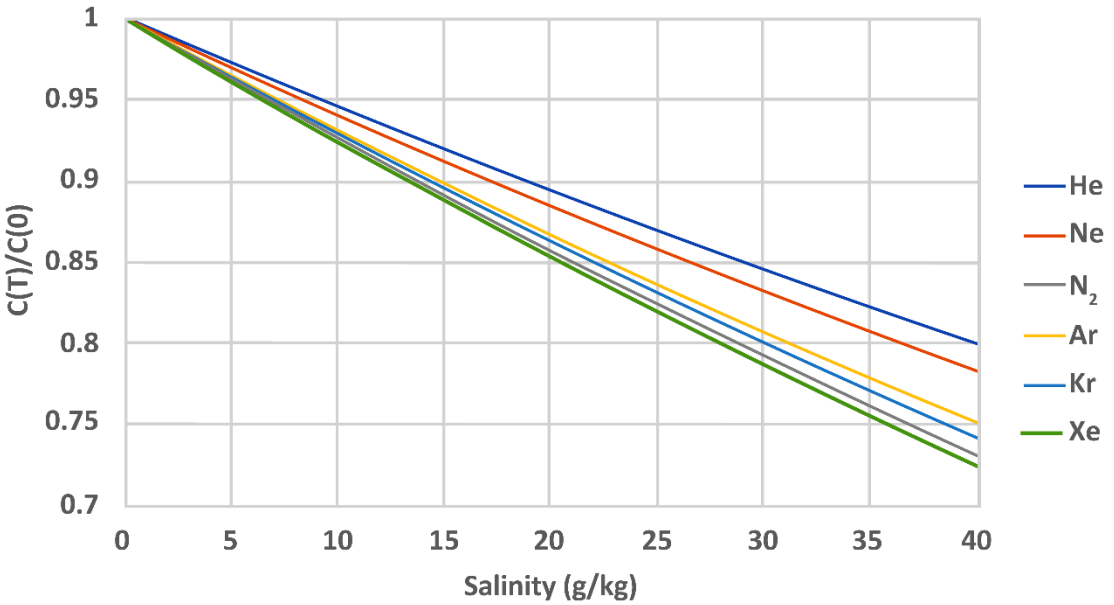

Figure 4 - Dissolved concentration of various gases, normalized by the concentration at 0 salinity, versus salinity. At salinities below about 1 g/kg (i.e., 1,000 ppm), the salting effect is minimal, but it is significant at the salinity of seawater (35 g/kg).

In the subsurface, an important distinction is needed between *open* and *closed* systems. In general, open-system conditions exist in the vadose zone where both gas and liquid phases exist; gas molecules can exchange between phases. Closed system conditions generally occur in the saturated zone such that only dissolved gases exist.

While the solubility of gases is a function of temperature and salinity, it is important to note that below the water table under closed system conditions, the concentration of dissolved gases does not generally change as groundwater warms and/or becomes saltier. Groundwater that equilibrates with the atmosphere at the water table may warm and increase in salinity as it moves deeper into an aquifer. While the increase in temperature and salinity will reduce the equilibrium solubility of a gas—when both gas and liquid phases are present—the increase in fluid pressure is typically sufficient to prevent a gas phase from forming (i.e., bubble formation) and thus the concentration of the gas does not change.

For example, using a very high geothermal gradient of 40 °C/km, the pressure of dissolved N_2 plus O_2 would increase by 0.63 atm/km due to warming, whereas the hydrostatic pressure would increase more than 95 atm/km. Dissolved N_2 plus O_2 are used for this example because these are the dominant gases in infiltrating water, although O_2 can be replaced by CO_2 in the unsaturated zone. Even with a very large geothermal

gradient, the increase in fluid pressure far exceeds the increase in gas pressure due to warming. Thus, the concentration of dissolved gases that is established at the water table does not typically change due to warming along groundwater flow paths.

2.2 Composition of the Atmosphere

The composition of the dry atmosphere is shown in Table 2. Earth's atmosphere differs dramatically from the other terrestrial planets in large part due to biological processes and a balance between production and loss. The dominant atmospheric gases are N_2 and O_2 and these account for more than 99 percent of atmospheric pressure. The composition listed in Table 2 is representative of the troposphere—from sea level to about 12,000 m—where mixing processes are strong. The primary noble gas in the atmosphere is Ar, constituting just under one percent of the total pressure. Gases used for age dating groundwater are present in trace amounts, and their respective partial pressure does not significantly affect the total pressure. Also shown in Table 2 are the major isotopes of each gas with their relative abundances. The composition of major and noble gases in the atmosphere can be considered stable over the time scale of the age-dating tracers that are discussed in this book.

Table 2 - Composition and isotopes of Earth's atmosphere (NOAA, 1976).

Gas	Abundance in dry air (%)	Major isotopes (fraction of natural abundance)
N_2	78.084	^{14}N (0.9964), ^{15}N (0.0036)
O_2	20.946	^{16}O (.9976), ^{17}O (0.0004), ^{18}O (0.0020)
Ar	0.934	^{36}Ar (0.00334), ^{38}Ar (0.00063), ^{40}Ar (0.99604)
CO_2	0.045 (Dec. 2020)	not applicable
Ne	0.001818	^{20}Ne (0.9048), ^{21}Ne (0.0027), ^{22}Ne (0.0925)
He	0.000524	^{3}He (0.00000138), ^{4}He (0.999)
CH_4	0.000189 (Dec. 2020)	not applicable
Kr	0.000114	^{78}Kr (0.00355), ^{80}Kr (0.0229), ^{82}Kr (0.116), ^{83}Kr (0.115), ^{84}Kr (0.570), ^{86}Kr (0.173)
Xe	0.0000087	^{124}Xe (0.000952), ^{126}Xe (0.000890), ^{128}Xe (0.0191), ^{129}Xe (0.264), ^{130}Xe (0.0407), ^{131}Xe (0.212), ^{132}Xe (0.269), ^{134}Xe (0.104), ^{136}Xe (0.0886)

2.3 Atmospheric Equilibrium

When water is in contact with the atmosphere (at a constant pressure, temperature, and humidity) for sufficient time, an equilibrium concentration is reached that can be calculated using Henry's Law. While the Henry Coefficient is a function of both temperature and salinity, it is not a function of the total atmospheric pressure. However, the equilibrium concentration of air in water is a function of the total gas pressure and hence is a function of elevation. Equation (4) is a modification of Henry's Law that gives the concentration of gas x_i in air-saturated water (ASW).

$$C_{i,eq} = \frac{\big(P - e(T)\big)x_i}{K_{w,i}(T,S)} \tag{4}$$

where:

$C_{i,eq}$ = equilibrium concentration of gas i in air-saturated water (L^3M^{-1}, typically in ccSTP/g)

P = atmospheric pressure ($ML^{-1}T^{-2}$, typically in atm)

$e(T)$ = vapor pressure of water at temperature T ($ML^{-1}T^{-2}$, typically in atm)

$K_{w,i}(T,S)$ = Henry Coefficient of gas i at temperature T and salinity S ($M^2L^{-4}T^{-2}$, typically in g-atm/ccSTP)

x_i = fraction of gas i (mixing ratio) in the dry atmosphere (dimensionless)

The atmospheric pressure (P) is a function of elevation (Z) and can be closely approximated by Equation (5).

$$P = P_0 exp\left(-\frac{Z}{Z_s}\right) \tag{5}$$

where:

P = atmospheric pressure ($ML^{-1}T^{-2}$, typically in atm)

P_0 = pressure at elevation (Z) = 0 ($ML^{-1}T^{-2}$, defined as 1 atm)

Z = Elevation (L)

Z_s = scaling factor (L)

Using a value for Z_s of 8,300 m this expression is a very good approximation for Z < 1,800 m. The vapor pressure of water ($e(T)$) in Equation (4) is used because the composition of the atmosphere is typically given without water vapor since the vapor pressure of water is highly variable. For groundwater recharge at the water table, the relative humidity of the soil atmosphere is usually assumed to be 100 percent and then the partial pressure of water vapor depends only on temperature. There are many empirical formulas for computing e as a function of temperature. The simple Antoine equation (Antoine, 1888) states the value of e as shown in Equation (6).

$$\mathrm{e} = 10^{A - \frac{\mathrm{B}}{\mathrm{C+T}}} \tag{6}$$

where:

e = vapor pressure of water in mmHg

A = 8.07131

B = 1,730.63

C = 233.426

T = temperature in °C

In this calculation, e is accurate to better than one percent between 0 °C and 100 °C.

2.4 Total Dissolved Gas Pressure

Henry's Law gives the relationship between the dissolved concentration of a gas and the partial pressure of the gas in contact with the liquid phase. By knowing the dissolved concentration of the dominant gas species, it is possible to compute the partial pressure of each gas. The sum of these partial pressures is known as the *total dissolved gas pressure* (*TDGP*) as shown in Equation (7).

$$TDGP = \sum_{i=1}^{n} p_i = \sum_{i=1}^{n} K_{w,i} c_i \cong K_{w,N_2} c_{N_2} + K_{w,O_2} c_{O_2} + K_{w,Ar} c_{Ar} \quad (7)$$

where:

$TDGP$ = total dissolved gas pressure ($ML^{-1}T^{-2}$, typically in atm)

K_{w,N_2} = dimensioned Henry Coefficient for N_2 ($M^2L^{-4}T^{-2}$, typically in g-atm/ccSTP)

c_{N_2} = concentration of N_2 in water (L^3M^{-1}, typically in ccSTP/g)

K_{w,O_2} = dimensioned Henry Coefficient for O_2 ($M^2L^{-4}T^{-2}$, typically in g-atm/ccSTP)

c_{O_2} = concentration of O_2 in water (L^3M^{-1}, typically in ccSTP/g)

$K_{w,Ar}$ = dimensioned Henry Coefficient for Ar ($M^2L^{-4}T^{-2}$, typically in g-atm/ccSTP)

c_{Ar} = concentration of Ar in water (L^3M^{-1}, typically in ccSTP/g)

For groundwater that equilibrated with the atmosphere, the *TDGP* is essentially the sum of the N_2, O_2 and Ar pressures. Because the Henry Coefficient is a function of temperature and salinity, the *TDGP* will change if the water temperature or salinity changes, even if the dissolved concentration stays constant.

The *TDGP* is a useful quantity for predicting the formation of bubbles (i.e., the exsolution of dissolved gases). If the *TDGP* is less than the fluid pressure, dissolved gases will remain in solution. If the *TDGP* exceeds the fluid pressure, bubbles can theoretically form; however, bubble nucleation is a complex process that can require activation energy. This is particularly important during sampling as a lowering of the fluid pressure via a pump and delivery at the land surface can result in effervescence if the in-situ pressure is not maintained.

When groundwater that has equilibrated at the water table warms and/or becomes saltier, the *TDGP* increases because the Henry Coefficient changes, even though the gas concentration does not change. While the increase in fluid pressure is typically much greater than the increase in *TDGP* in recharge areas—areas of downward flowing groundwater—in discharge areas where warmed groundwater approaches the surface, the *TDGP* can exceed the fluid pressure, potentially leading to gas exsolution. When bubbles do form, the concentrations of both the major and minor components in the dissolved phase can be strongly affected. Low solubility gases such as He and SF_6 will preferentially partition into the gas phase, leaving the water depleted relative to its original concentration.

The *TDGP* can be measured directly using a probe. A *TDGP* probe consists of a length of tubing that is permeable to gases—including water vapor—but not permeable to liquid water (Manning et al., 2003). One end of the tube is connected to a pressure sensor and the other end is plugged. When the tube is placed in water, the gas inside the tube can equilibrate with dissolved gases in the water; the pressure inside the tube will eventually reach the *TDGP*. A *TDGP* probe is particularly useful when collecting samples for dissolved gas analysis. If the fluid pressure is greater than the *TDGP*, the probability of bubble formation is minimal. As described in subsequent sections, the use of sampling containers such as copper tubing that allow the groundwater to be sealed under pressure can effectively eliminate degassing that might otherwise occur. Box 1 provides more details and examples of using a *TDGP* probe for groundwater studies.

2.5 Production of Gas in the Subsurface

In addition to gases derived from the atmosphere, groundwater may contain gases that are produced in the subsurface. The most commonly produced subsurface gases are carbon dioxide (CO_2), methane (CH_4), and nitrogen (N_2). CO_2 is produced in the unsaturated zone by the oxidation, i.e., *decay*, of organic matter and by respiration from organisms including plants and microbes. The concentration of CO_2 in the unsaturated zone can be orders of magnitude higher than in the atmosphere; this, in turn, drives weathering reactions (Drever, 1988; Garrels & Christ, 1965; Solomon & Cerling, 1987). Weathering reactions, decay of organic matter, and fermentation reactions can all produce CO_2 below the water table. While dissolved CO_2 concentrations in groundwater can be significant, the partial pressure of CO_2 often remains at low to moderate levels because of its high solubility in water.

When molecular oxygen is not available, the decay of organic matter continues by a series of reactions that can involve various electron acceptors. Fermentation reactions—in concert with fermentative organisms—can convert organic matter into CH_4, and CO_2. In the deep subsurface, thermal maturation of hydrocarbons can also produce CH_4. Because of its low solubility in water, even modest concentrations of dissolved CH_4 can lead to significant gas pressures. In shallow aquifers that receive recharge from agricultural lands

or human/animal wastes, high concentrations of dissolved nitrate (NO_3^-) can occur. Under appropriate biogeochemical conditions, NO_3^- can be used as an electron acceptor to oxidize carbon to CO_2 and form nitrogen gas (N_2). This process, known as *denitrification*, can result in elevated concentrations of dissolved N_2 which in turn can produce modest partial pressures of N_2.

When gas is produced in the subsurface, it is possible to develop *TDGP* that exceeds the fluid pressure—especially when the fluid pressure is lowered such as near pumping wells. When this happens, it is possible to form bubbles that can be trapped in pore throats. In surface water, buoyant gas bubbles can migrate to the surface and escape to the atmosphere. However, in a porous medium the interaction between interfacial forces, capillary pressures, and the physical size of pore throats makes it difficult for bubbles to migrate. As a result, bubbles tend to accumulate in the porous media.

Although a bubble may form due to excess pressure of just one or several gases, once the bubble is formed, it can strongly influence the concentration of other gases as they can now partition into the bubble as discussed with respect to the dimensionless Henry Coefficient (Section 2.1). This partitioning depends on the solubility of each gas and affects low solubility (high volatility) gases such as He and Ne more than high solubility (low volatility) gases.

2.6 Gases in Groundwater: Excess Air

Groundwater samples frequently have higher dissolved gas concentrations than predicted by equilibrium solubility using Henry's Law (Andrews & Lee, 1979; Herzberg & Mazor, 1979). Groundwater age dating using dissolved gases depends critically on quantifying all processes that lead to measured dissolved gas concentrations. Heaton and Vogel (1981) coined the term *excess air* because the composition of the excess gas was like the composition of the atmosphere. For low solubility gases such as He, Ne, and SF_6, excess air can be greater than equilibrium solubility, and hence must be considered for age dating.

Heaton and Vogel (1981) suggested that small bubbles trapped in recharging groundwater might be transported to depth and then completely dissolve. However, a physically more plausible explanation for excess air is a rising water table that does not completely displace the air in what was—prior to the water table rise—the unsaturated zone. The occurrence of bubbles near the water table is discussed in the soil physics literature (e.g., Peck, 1969) and has been shown to reduce the hydraulic conductivity of unconfined aquifers in a zone near the water table (Ronen et al., 1989).

The concept of a rising water table that traps air bubbles that then either partially or fully dissolve due to the increase in fluid pressure is the basis for the widely used *closed-system equilibration* (CE) model proposed by Aeschbach-Hertig and others (2000). The amount of excess air in groundwater depends on the properties of the porous medium (e.g., pore throat size and distribution) and the magnitude of water table rise. Furthermore, the

impact of excess air on gas concentrations is generally greatest for low-solubility gases, especially if the water table rise is sufficient to completely dissolve trapped air bubbles. Dissolved Ne concentration ranging from 10 to 50 percent above solubility are common; however, values exceeding 400 percent of solubility have been measured and may be associated with artificial recharge (Cey et al., 2008).

Ne's low solubility and its lack of significant subsurface sources makes it a useful indicator of excess air. A common metric of excess air is the deviation of the Ne concentration from the theoretical solubility value, known as ΔNe defined as shown in Equation (8).

$$\Delta\mathrm{Ne} = \frac{C_{m,Ne} - C_{sol,Ne}}{C_{sol,Ne}} \times 100\% \tag{8}$$

where:

$C_{m,\mathrm{Ne}}$ = measured concentration of dissolved Ne (L^3M^{-1}, typically in ccSTP/g)

$C_{sol,\mathrm{Ne}}$ = theoretical concentration of Ne in equilibrium with the atmosphere (L^3M^{-1}, typically in ccSTP/g)

The computation of $C_{sol,\mathrm{Ne}}$ requires assumptions regarding the temperature and atmospheric pressure (elevation) when the sample equilibrated with the atmosphere. Although the temperature may not be known with certainty, the temperature dependence of Ne solubility is relatively small, making ΔNe a relatively robust indicator of excess air. Because the magnitude of excess air is related to the magnitude of water table rise, ΔNe has been used as an indicator of both modern and paleo recharge events, that is, to measure the frequency and magnitude of recharge events (Beyerle et al., 2003).

When the elevation of the water table—where groundwater is last in contact with the atmosphere—is relatively well known (i.e., in non-mountainous terrains), the primary factors affecting the dissolved concentration of atmospheric gases are temperature and the amount of excess air. High solubility gases such as Xe are highly sensitive to temperature but less sensitive to excess air. In contrast, low solubility gases such as Ne are highly sensitive to excess air and less sensitive to temperature. As such, a graphical approach for evaluating temperature and excess air by plotting the dissolved Xe versus Ne concentration is illustrated in Figure 5.

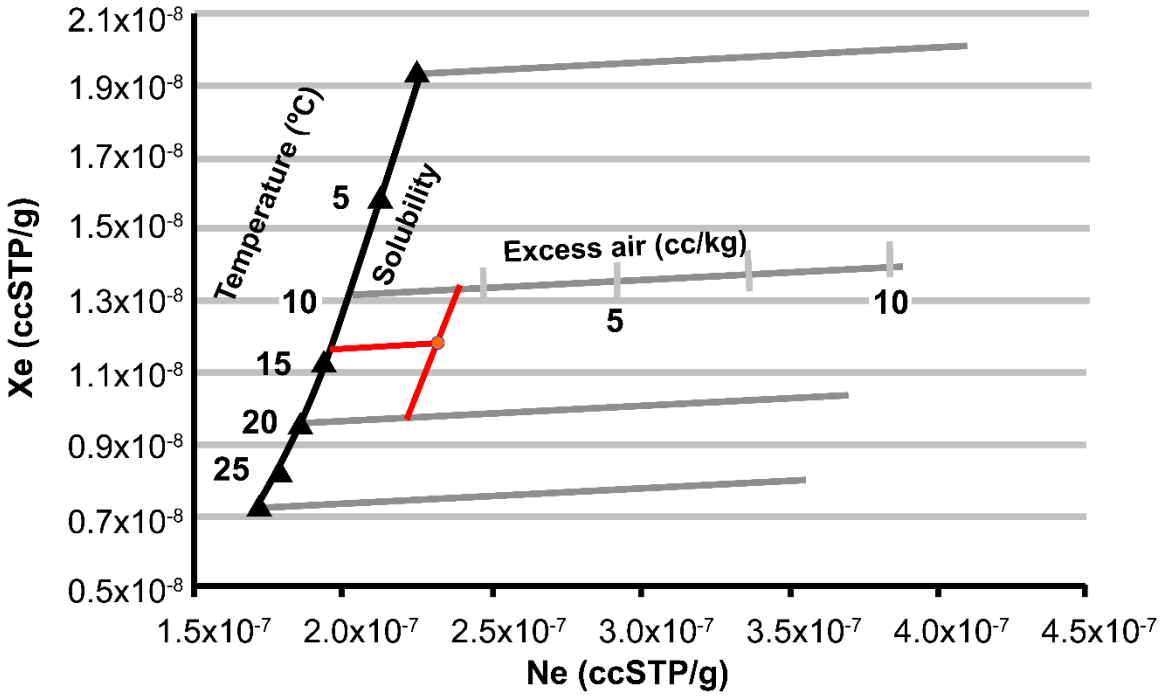

Figure 5 - Graphical approach for evaluating recharge temperature and excess air using Ne and Xe concentration. The solid black line (Solubility) shows the Xe and Ne concentrations expected from solubility equilibrium at various temperatures. The gray lines show expected concentrations if various amounts of excess air are added. The gray lines have been computed for recharge temperatures of 0, 10, 20, and 30 °C. The red circle is a hypothetical sample having Xe and Ne concentrations of 1.18×10^{-8} and 2.30×10^{-7} ccSTP/g. The sample has an approximate recharge temperature of 14 °C that was obtained by extending a line that is parallel to the gray curves to intersect the black solubility curve, and approximately 2 cc/kg excess air that was obtained by extending a line parallel to the black solubility curve to intersect the gray excess air curve (redrawn from Aeschbach-Hertig & Solomon, 2013).

The graph shown in Figure 5 was prepared by calculating the solubility concentrations of Xe and Ne at a given atmospheric pressure (e.g., the pressure at the water table where recharge occurred) at various temperatures to form the black solubility curve. For recharge temperatures of 0, 10, 20, and 30 °C, various amounts of excess air were added. The curves in Figure 5 were calculated using Equation (9).

$$C_i = \frac{\big(P - e(T)\big)\mathrm{x}_i}{K_{w,i}(T,S)} + A' x_i \qquad (9)$$

where:

A' = amount of excess air in units consistent with C_i (e.g., ccSTP/g)

All other parameters are as defined in Equation (4). The first term in Equation (9) is the equilibrium solubility concentration for the *i*th gas and the second term represents the contribution of the *i*th gas from excess air. Figure 5 illustrates how the dissolved concentration of Xe depends mostly on temperature, whereas the dissolved Ne concentration depends mostly on the amount of excess air.

The second term in Equation (9) represents a simple model for excess air and was first proposed by Andrews and Lee (1979). This model is known as the *unfractionated air*

(UA) model as it assumes that bubbles are completely dissolved and hence gas is added in using atmospheric proportions rather than solubility proportions. Exercise 1 provides an opportunity to practice determining the fraction of a gas in air-saturated water.

While the UA model is still widely used and is a useful starting point for evaluating excess air, numerous other models have been proposed. The closed-system equilibration (CE) model introduced by Aeschbach-Hertig and others (2000) describes bubbles trapped from a rising water table that may not fully dissolve if there is insufficient fluid pressure. The partial dissolution of bubbles leads to a fractionation of the dissolved gases between the groundwater and the bubbles according to the solubility of gases. The CE model has two parameters, one that describes the volume of gas trapped per unit mass of water (A) and another for the fractionation factor (F) that describes the fraction of the original gas volume in the porous medium that does not dissolve. The equation for computing the dissolved gas concentration using the CE model is shown in Equation (10).

$$C_i = \frac{\big(P - e(T)\big)x_i}{K_{w,i}(T,S)} + \frac{(1-F)Ax_i}{1 + \dfrac{FAx_i}{\dfrac{\big(P - e(T)\big)x_i}{K_{w,i}(T,S)}}} \qquad (10)$$

where:

A = volume of gas trapped in the porous media per unit mass of water (L^3M^{-1}, typically in ccSTP/g)

F = fractionation factor (dimensionless)

The parameter A in the CE model should not be confused with A' in the UA model, although they both have dimensions of volume of gas per mass of water. In the case of the UA model, A' represents the volume of air that dissolves into the water, whereas A in the CE model is the volume of air per unit mass of water that exists in the porous medium before gas dissolution. When F equals 0 (i.e., none of the original gas volume remains in the porous medium), all the available gas dissolves, in which case A' equals A, and the CE model is the same as the UA model.

The CE model provides a physically more plausible description of gas dissolution than the UA model because very large water table rises are required to produce sufficient pressure to fully dissolve the amount of excess air that is often observed in groundwater samples. However, the CE model has an additional parameter that must be determined, and its evaluation is not possible with the simple graphical approach shown in Figure 5. An optimization procedure for determining both A and F as well as the recharge temperature is discussed later in this section.

Numerous additional models have been proposed to describe the occurrence of excess air in groundwater. These include:

1. a partial re-equilibration (PR) model (Stute et al., 1995),

2. a multi-step partial re-equilibration (MR) model (Kipfer et al., 2002),
3. a partial degassing (PD) model (Lippmann et al., 2003),
4. a negative pressure (NP) model (Mercury et al., 2004),
5. an oxygen depletion (OD) model (Hall et al., 2005), and
6. a gas diffusion relaxation (GR) model (Sun et al., 2008).

These models are discussed in Aeschbach-Hertig and Solomon (2013).

Subsurface processes that lead to excess air are complex and none of the models fully describe these and their associated kinetics. The CE model generally provides a reasonable description of excess air for the purpose of groundwater dating, but site-specific processes may be better described by one of the other models.

The graphical approach (Figure 5) for evaluating recharge temperature and excess air is useful for the UA model when the concentration of two gases (e.g., Xe and Ne) have been measured and there are two unknowns. However, when an excess air model with more parameters is used, more concentration measurements are needed as well as a systematic technique for estimating these parameters. The inverse determination for excess air parameters was simultaneously introduced by Ballentine and Hall (1999) and Aeschbach-Hertig and others (1999) and involves choosing parameters (e.g., *T, A, F*) such that the sum of the error-weighted deviations between measured and simulated gas concentrations, known as chi-squared (X^2), is minimized. The simulated concentrations come from models such as shown in Equation (10) that depend on temperature, salinity, pressure or elevation, and excess air parameters. Mathematically, X^2 is expressed as shown in Equation (11).

$$X^2 = \sum_{\mathrm{i}=1}^{\mathrm{n}} \left(\frac{C_{m,i} - C_{s,i}}{\sigma_i} \right)^2 \qquad (11)$$

where:

$C_{m,i}$ = measured concentration of the *i*th gas (L^3M^{-1}, typically in ccSTP/g)

$C_{s,i}$ = simulated concentration of the *i*th gas (L^3M^{-1}, typically in ccSTP/g)

σ_i = measurement error of the *i*th gas (L^3M^{-1}, typically in ccSTP/g)

The inverse approach uses powerful optimization algorithms to iteratively select values of unknown parameters in an excess air model until X^2 reaches a minimum value—that is, when the average deviation between simulated and measured values is minimized. By weighting the deviations by the measurement errors (σ_i), it is possible to evaluate the probability that the chosen excess air model provides an adequate representation of the solubility and excess air processes. For example, if four gases are measured (i.e., $i = 4$ in Equation (11)) and the difference between each measured gas concentration ($C_{m,i}$) and the concentration computed ($C_{s,i}$) using an excess air model was equal to the measurement error (σ_i), then X^2 would equal 4.

If our excess air model included three unknown parameters (e.g., *T, A, F*), then the degrees of freedom (DF) would be 1 (DF = constraints = free parameters = number of gases measured − number of unknown parameters = 4 − 3 = 1). The probability (*p*-value) for a X^2 of 4 can be computed to be 0.046 (from standard X^2 probability calculators or tables). High X^2 values give low *p*-values. This means there is approximately a five percent chance that the X^2 value results from random measurement errors.

In general, *p*-values of less than 0.01 have been used for rejecting a given excess air model, and thus we cannot reject the possibility that the model itself in our example is inappropriate. On the other hand, a X^2 value of 7 with 1 DF would have a *p*-value of 0.008. Since there is less than a one percent chance that this X^2 value results from random measurement errors, it is probably not an adequate description of the physical processes for that sample—if the measurement error used for calculating X^2 is correct.

The X^2 probability distribution was developed for hypothesis testing and is best used for *rejecting* a given model rather than finding the "best" model. In other words, if two models are compared, the one with the highest X^2 is not necessarily "worse" than the model with a lower X^2 if both have p-values that are greater than 0.01. In such a case, the choice between models should rely on which model provides a better physical description of subsurface processes at a given site. Exercise 2 provides further practice with the X^2 concept.

The inverse approach for noble gases has been implemented into several computer programs. Several of these use Excel workbooks with solubility equations as a function of temperature and pressure and excess air models programmed into worksheets. Table 3 shows known programs along with their availability.

While excess air in groundwater can clearly result from natural processes such as water table fluctuations, it is important to be aware that it can also be an artifact of drilling operations such as using air as a drilling fluid or well development using compressed air. If air bubbles are forced into the formation many borehole volumes must be purged to eliminate this artifact (Manning et. al., 2003; Poulsen et al., 2020).

Table 3 - Software available for interpreting dissolved gases.

Program name	Description	Availability	Comments
NOBLEBOOK	Excel workbook for inverse modeling of dissolved noble gas concentration	https://www.iup.uni-heidelberg.de/de/research/hydrotrap/noblebook↗	Uses Solver™ in Excel for optimization.
PANGA	Computer program for the analysis of noble gas data.	https://www.iup.uni-heidelberg.de/de/research/hydrotrap/panga↗	Includes uncertainty analysis. Versions available for both Windows and Mac OS
DGMETA	Excel based computer program for dissolved gas modeling and environmental tracer analysis	https://pubs.er.usgs.gov/publication/tm4F5↗	Includes uncertainty analysis and SF_6 and CFCs

2.7 Noble Gas Thermometry

Noble gas thermometry is an application of the solubility and excess air concepts discussed in this section. The objective is to utilize the temperature dependence of the solubility of atmospherically derived gases to estimate the temperature at the water table when groundwater was last in contact with the atmosphere (i.e., an open system). The general idea is to collect a sample for dissolved gases, analyze the sample for a suite of noble gases (typically Ne, Ar, Kr, and Xe), select an excess air model, and use the inverse approach to find a temperature and excess air parameters that best fit the suite of noble gas concentrations. He is not normally used in noble gas thermometry because of subsurface sources. While there are also subsurface sources of Ar, its retention by most minerals makes it suitable for all but very old—and typically deep—groundwater samples.

Noble gas thermometry has been particularly useful for examining the recharge temperature of old groundwater to help reconstruct past climates (e.g., Stute et al., 1995), and the derived excess air parameters have been used to deduce paleo humidity as large water table fluctuations lead to large amounts of excess air (e.g., Aeschbach-Hertig et al., 2002). Noble gas results are also useful for dating methods such as CFCs when the equilibrium concentration of a tracer is highly sensitive to the recharge temperature, and SF_6 when the dissolved concentration is sensitive to excess air.

The subsurface temperature recorded by noble gas thermometry is related to the mean annual temperature at the recharge location but can also depend on the depth of the water table and the seasonality of recharge. Figure 6 shows simulated temperatures in the subsurface for a region in which the mean annual temperature is 10 °C but fluctuates seasonally between 0 °C and 20 °C. The annual temperature fluctuations diminish with depth being about ±4 °C at a depth of 2 m and ±1 °C at 6 m. At a depth of 10 m, the annual temperature fluctuations at the surface are nearly completely damped. Thus, in areas where the depth to the water table is greater than about 10 m, the recharge temperature is likely to be similar to the mean annual temperature—the influence of the geothermal gradient is

minimal at this depth—but the recharge temperature could vary significantly when the water table is shallow.

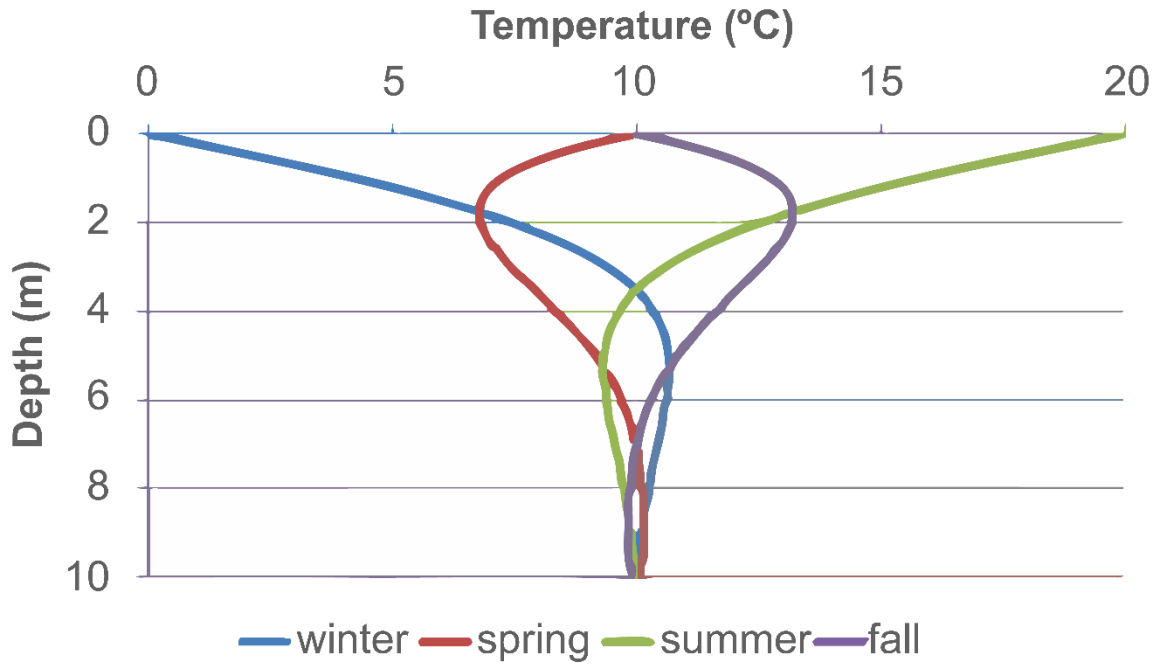

Figure 6 - Simulated soil temperatures in a temperate climate. The mean annual temperature is 10 °C and the air temperature varies from 0 to 20 °C. The dampening of the surface temperature with depth is controlled mostly by thermal diffusivity of the surficial material, which in turn is a function of its water content and to a lesser extent its mineralogy. When the water table is more than 10 m below land surface, the annual temperature variations are nearly completely damped for a typical thermal diffusivity of 0.005 cm^2/s (redrawn from Aeschbach-Hertig & Solomon, 2013).

Noble gas concentrations are a function of four factors: temperature, pressure—which is a function of elevation, salinity, and excess air. In principle, the inverse approach can be used to solve for any of these parameters as long as more noble gas concentrations are available than unknown parameters; that is, the system of equations being inverted needs to be over determined. However, temperature and pressure are correlated, and experience has shown that it is difficult to use the inverse approach to accurately solve for both recharge temperature and pressure (i.e., elevation). In mountainous terrains, where neither recharge temperature nor elevation are typically known, additional information is needed to estimate both parameters. For example, Manning and Solomon (2003) used the relationship between mean annual temperature and elevations, known as the *atmospheric lapse rate*, to help constrain the recharge location of groundwater in a basin-fill aquifer beneath Salt Lake City, Utah, USA.

3 Tritium Dating Method

Tritium (^{3}H, T) is a radioactive isotope of hydrogen (H) that is produced naturally in both the atmosphere and subsurface and is also produced by various nuclear activities including nuclear reactors, weapons testing, and nuclear fuel reprocessing facilities (Michel et al., 2018). In the atmosphere, ^{3}H readily oxidizes to form tritiated water—typically HTO—and has a half-life of 12.32 years (Lucas & Unterweger, 2000).

Because it is a part of the water molecule, ^{3}H is nearly an ideal tracer for water. The ^{3}H content of water is typically expressed in tritium units (TU) which is 1 atom of ^{3}H in 10^{18} atoms of hydrogen (^{1}H, ^{2}H, and ^{3}H). One TU has an approximate activity of 0.118 Becquerels per kilogram (Bq kg^{-1}; Stonestrom et al., 2013). A Becquerel is 1 disintegration per second, which is equal to 3.19 picocuries per kilogram (pCi/kg). The use of ^{3}H as a tracer in groundwater was summarized by Solomon and Cook (2000).

3.1 Background and Historical Development

Prior to the nuclear era, the primary source of ^{3}H in the hydrosphere was the result of cosmic rays interacting with nitrogen and oxygen (Kaufman & Libby, 1954). Because the cosmic ray flux depends on latitude, the natural production of ^{3}H also depends on latitude, with production being greatest at the poles. Prior to 1950, the ^{3}H content of precipitation ranged from 3 to 6 TU in Europe and North America (Kaufman & Libby, 1954), 1 to 3 TU in Australia (Allison & Hughes, 1977), and approximately 15 TU in Antarctica (Begemann & Libby, 1957; Taylor, 1968). The global inventory of ^{3}H prior to 1950 was estimated to be 3.5 kg (O'Brien, 1979).

Numerous nuclear reactions can produce ^{3}H in the subsurface (Davis & Murphy, 1987), but the most significant for hydrologic studies is the fission of lithium-6 (^{6}Li) by neutrons that are mostly generated by the decay of uranium- (U) and thorium-series (Th) nuclides (Andrews & Kay, 1982). Average concentrations of U, Th, and Li in crustal rocks suggest that the subsurface production of ^{3}H should generally be 0.2 TU or less (Lehmann et al., 1993).

Beginning in the early 1950s, atmospheric ^{3}H values rose sharply as the result of above-ground testing of thermonuclear weapons. As shown in Figure 7, ^{3}H values in precipitation rose to more than 5,000 TU in Canada in 1963 and then declined as a result of a ban on above-ground testing. Peak values in the southern hemisphere were much lower and lagged in time because weapons testing primarily occurred in the northern hemisphere and interhemispheric mixing is slow. For example, the maximum ^{3}H observed in Kaitoke, New Zealand, was about 75 TU in 1966.

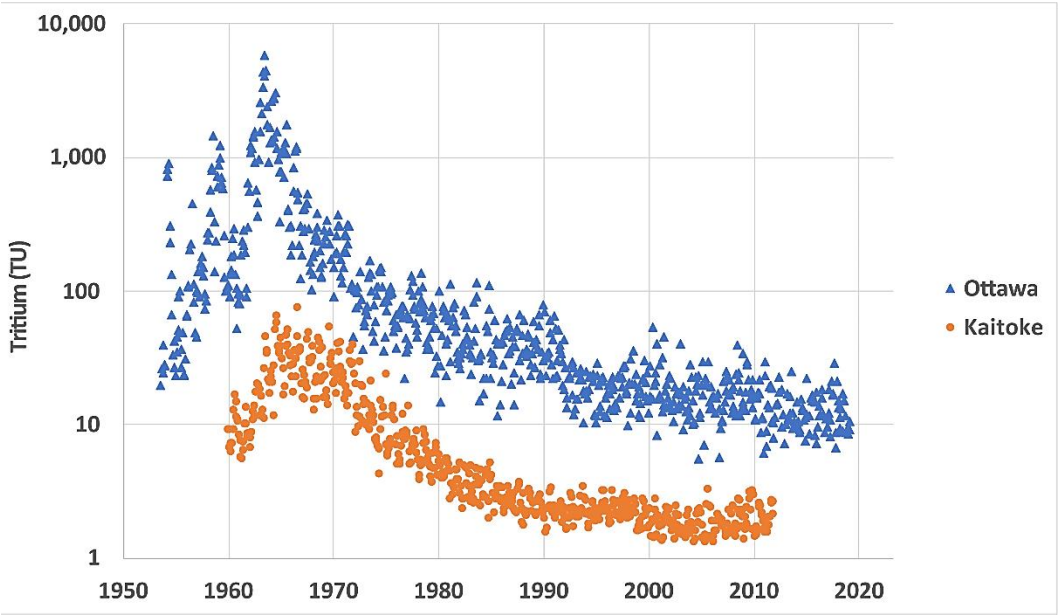

Figure 7 - Tritium in precipitation in Ottawa, Canada, in the northern hemisphere and Kaitoke, New Zealand, in the southern hemisphere (IAEA/WMO, 2020).

Between 1952 and 1953, approximately 600 kg of ^{3}H was injected into the atmosphere (Rozanski et al., 1991). The beta decay energy of ^{3}H is low (18.6 keV) and the recommended limit in drinking water by the World Health Organization (WHO) is about 85,000 TU (WHO, 2008), which is far greater than peak concentrations in the 1960s.

The spike-like injection of ^{3}H into the atmosphere created an event marker for hydrologic studies. Historically, a common use of ^{3}H in groundwater studies was to distinguish pre- from post-bomb water. In 1990, it was possible to distinguish pre- and post-bomb water with a ^{3}H detection limit of 0.6 TU—a typical value for analytical laboratories at that time; current detection limits are lower. This distinction is no longer possible in some areas with a detection limit of 0.6 TU (Eastoe et al., 2012). However, as is discussed subsequently, it is possible to estimate a minimum age for a given detection limit and natural background value.

In addition to spatial variations resulting from variations in the flux of cosmic rays and the location of nuclear weapons testing, temporal variation also exists in atmospheric ^{3}H values. From the mid-1960s to the mid-1990s, the most prominent temporal change was an exponential decrease as bomb ^{3}H decayed and rained out of the atmosphere. Since about 1990 in the southern hemisphere and 2000 in the northern hemisphere, atmospheric ^{3}H values appear to have reached steady-state levels. Most naturally produced and bomb-derived ^{3}H in the atmosphere resides in the stratosphere (Rozanski et al., 1991). Transfer of ^{3}H from the stratosphere to troposphere results from eddy diffusion and injections by the jet stream, and by the so-called *spring leak*. The latter results from a seasonal rise in the tropopause at high latitudes that occurs in the spring. In the northern hemisphere, ^{3}H values are typically at a maximum from May to July and in the southern

hemisphere from August to September (Rozanski et al., 1991). An example of temporal variations in atmospheric ^3H in Vienna, Austria, is shown in Figure 8. The average ^3H value in Vienna for the period from 2000 to 2021 is 10.5 TU with a standard deviation of 2.8 TU (coefficient of variation = 26 percent).

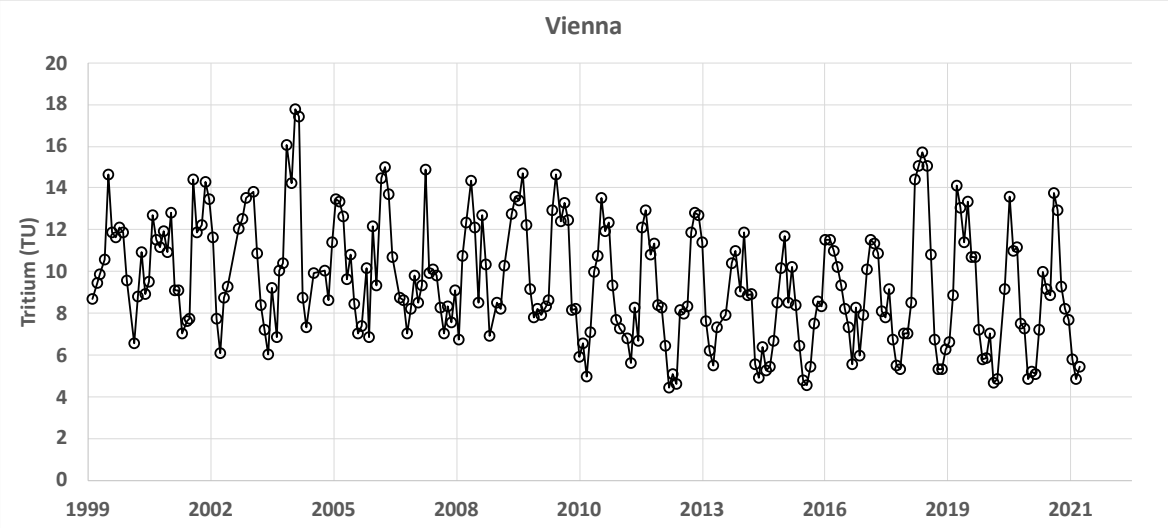

Figure 8 - Temporal variations in ^3H in precipitation in Vienna, Austria (IAEA/WMO, 2020).

Local sources of ^3H exist in the vicinity of nuclear reactors and nuclear processing facilities. A variety of reactions in nuclear power plants produce ^3H; it is ultimately transferred to cooling water and then discharged to the environment. Such releases are often episodic, leading to short-term spikes in rivers in the vicinity of power plants. In continental precipitation, ^3H values are higher than ocean precipitation due to factors including cyclical neutron fluxes, stratospheric inputs, distance from tropospheric moisture sources (Terzer-Wassmuth et al., 2022), and the location of anthropogenic nuclear sources.

When surface water evaporates, a modest fractionation of dissolved gas occurs as the vapor pressure for the light isotopes of water is larger than that of the heavier isotopes. At equilibrium, the ratio of the ^3H concentration in the vapor phase to that of the liquid phase is about 0.86 at 0 °C and 0.96 at 70 °C (Sepall & Mason, 1960). This results in some surface water bodies being modestly enriched in ^3H over local precipitation (Brown & Barry, 1979) with greater enrichment in colder climes.

The Global Network of Isotopes in Precipitation (GNIP) database is maintained by the International Atomic Energy Agency (International Atomic Energy Agency/World Meteorological Organization (IAEA/MO), 2020). Terzer-Wassmuth and others (2022) used it to modify a cluster-based water isotope model for stable isotopes to predict annual average ^3H values in modern (i.e., post-2000) precipitation. The global distribution of contemporary ^3H in precipitation has also been simulated with atmospheric, general-circulation models (Cauquoin et al., 2015) to evaluate inputs to both the oceans and continents. (Oms et al., 2019). These models reveal spatially variable ^3H values in

contemporary precipitation ranging from 1 to 25 TU that are sufficiently predictable for practical hydrological applications (Terzer-Wassmuth et al., 2022). Key variables in the global model of Terzer-Wassmuth and others (2022) for predicting the spatial patters of ^3H in precipitation include air temperature, latitude, land mass fraction, and distance from the sea coast.

3.2 Basic Concepts and Systematics

As a groundwater dating method, ^3H is both a transient and radioactive tracer. Figure 9 illustrates the general concept of using a transient radioactive tracer to estimate the recharge year (age = sample year − recharge year). When the recharge concentration is either increasing or constant, the measured concentration can be uniquely related to the recharge year by extending the measured concentration backward in time along a decay curve until the extended value intersects the recharge concentration curve (Figure 9).

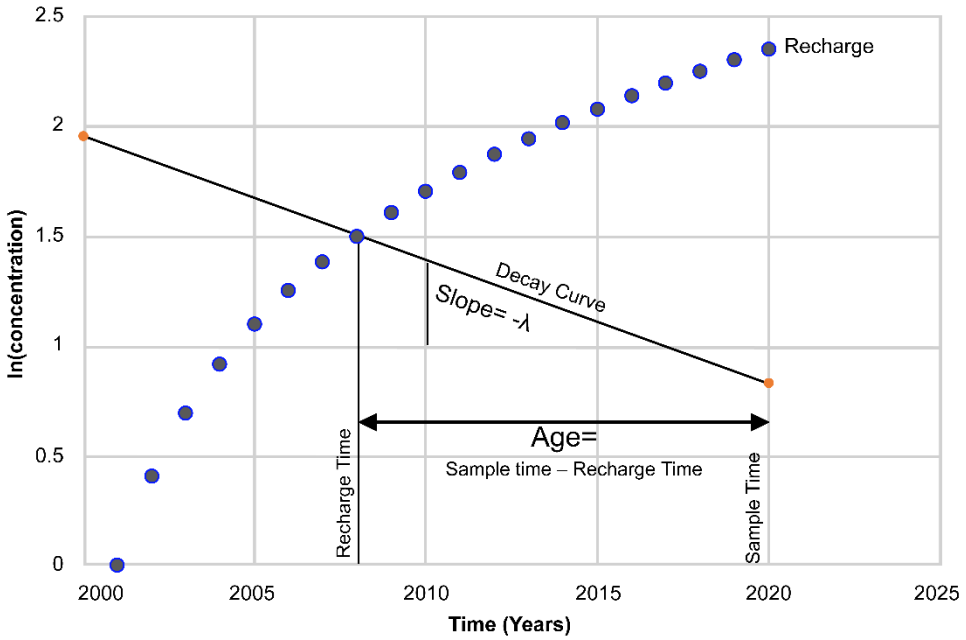

Figure 9 - General concept of using a radioactive transient tracer for groundwater dating. The solid circles represent the concentration of recharge as a function time. The vertical axis is the natural logarithm of the tracer concentration. A decay curve having a slope of $-\lambda$ (where λ is the decay constant (T^{-1})) is drawn through the point corresponding to the concentration of the sample and the time it was collected to intersect the recharge curve. The intersection of the line and the curve gives the recharge time of the sample. The age is given by the sample time minus the recharge time.

Using this approach to determine a tracer age for groundwater assumes that the amount of tracer decay in the unsaturated zone—prior to recharge—is small relative to the decay that occurred during groundwater transport prior to sampling—that is, an age determined using ^3H includes the transit time in the unsaturated zone. The slope of the decay curve on a semi-log plot is given by the decay constant of the tracer. An alternative to the approach illustrated in Figure 9 is to *decay-correct* the atmospheric curve to the time

of sampling, in which case the age can be read directly from a plot (Cook & Dogramaci, 2019).

While tritium data are available from GNIP↗ which is managed by the IAEA in the USA, spatial and temporal interpolations of ^3H in precipitation are available from Michel and others (2018).

3.3 Sample Collection and Analysis

Samples for ^3H analysis should ideally be collected in glass bottles with minimal headspace and a tight-fitting cap (e.g., a polyseal cap). However, when samples will be shipped to the laboratory, the use of high-density polyethylene bottles—or other plastic that has a low permeability to water vapor—is generally acceptable as it avoids breakage issues associated with glass bottles. Typically, 1 L is sufficient volume, but readers are encouraged to contact their chosen laboratory for specific requirements.

Because the modern atmosphere may contain a ^3H concentration much higher than the sample, it is important to avoid contact between the sample and the atmosphere. However, extreme care to avoid contact such as submerging the collection bottle in a larger container that is filled with sample water is generally not required. Historically, some watches had luminescent dials that utilized ^3H gas and these should not be worn during sample collection. There are many different luminescent technologies used in modern watches, but, as ^3H gas is still used by several manufacturers, it is best to avoid wearing a watch during sample collection. When ^3H analyses are to be performed in the unsaturated zone, water must be first extracted using a suction lysimeter in situ or distillation from a core sample.

Tritium analyses are usually performed using *liquid scintillation counting* (LSC), *gas proportional counting* (GPC), or ^3He in-growth. In a recent comparison of 78 international ^3H laboratories, 70 used LSC, seven used ^3He in-growth, and one used GPC (Copia et al., 2020).

A pre-treatment using electrolytic enrichment of samples is commonly done for both the LSC and GPC methods for samples having ^3H values less than several TU. The electrolytic enrichment process decomposes water to oxygen ($O_2(g)$) and hydrogen ($H_2(g)$) gas that is depleted in ^3H relative to the remaining liquid phase. Typically, between 2,000 to 250 ml of sample is reduced to a volume of about 10 to 15 ml. The electrolysis process highly favors the formation of $^1H_2(g)$ at the cathode over $^2H_2(g)$ and $^3H_2(g)$, leaving the remaining solution enriched in ^2H (deuterium) and ^3H (Copia et al., 2021). A ^3H enrichment factor of about 16 to 32 is common, but a factor as great as 175 can be obtained (Morgenstern & Taylor, 2009).

The enrichment process involves five steps:

1. predistillation to remove dissolved ions that might interfere with the electrolysis process,
2. the addition of an electrolyte to facilitate electrolysis,
3. electrolysis to enrich the sample in ^{2}H and ^{3}H,
4. alkalinity neutralization to lower the pH of the solution after electrolysis, and
5. final distillation to quantitatively recover the enriched water.

For the GPC method, methane is synthesized (e.g., reaction of water with aluminum carbide at 150 °C; Horvatinčić, 1980) from either the raw water sample or from the residual solution following electrolytic enrichment. The produced methane is then placed into a counting cell along with quenching gas at pressures that are typically 5 to 7 atm.

For the LSC method, about 10 ml of either the raw sample or the residual solution following electrolytic enrichment is added to a scintillation cocktail. The function of the scintillation cocktail is to absorb energy from radioactive decay and convert it into light pulses that can then be detected by a photomultiplier tube. Low background LSC are commercially available that employ both shielding and anti-coincidence detection combined with sample blanks to reduce and correct for background radiation. The tritium detection limit for LSC of raw samples is typically between 2 to 10 TU and between 0.05 to 0.6 TU for enriched samples.

The ^{3}He in-growth method utilizes the child of ^{3}H decay: ^{3}He. A sample is first placed into a container having low He permeability and degassed to remove dissolved He from the sample. The container is then sealed and stored for one to 12 months during which time ^{3}He is produced from ^{3}H decay. After the in-growth period, the evolved He is let into a final clean-up line and then a sector-field mass spectrometer where ^{3}He and ^{4}He are measured using peak-height manometry. The purpose of the ^{4}He measurement is to correct for He leakage, outgassing, or insufficient degassing of the sample. While the ^{3}He in-growth method is conceptually straight forward, several important factors affect the method's implementation:

- The sample must be 99.9995 percent degassed of its dissolved He content in a container that will not leak or outgas more than about 10,000 atoms of ^{3}He during the in-growth period. Special glass with a high aluminum content that is stored at -20 °C to reduce helium diffusion, or an all-metal flask is used.
- The sector-field mass spectrometer must have a resolving power greater than about one in 400 amu to separate the $^{3}He^{+}$ peak from the hydrogen deuterium (HD) peak.

The detection limit for the ^{3}He in-growth method depends on the sample size, holding time, and residual helium from the degassing procedure or leakage during storage. For a sample volume of 500 ml and in-growth period of six weeks, detection limits of 0.05 TU are common. For larger volumes (up to 3,000 ml) and/or longer holding times (up to one year) a detection limit of 0.003 TU has been reported (Jenkins, 1981). A significant

advantage to the ^{3}He in-growth method is that time and sample amount are interchangeable in terms of the detection limit. For example, Marston and others (2012) measured the ^{3}He content of structural waters in clay minerals on typical volumes of 20 to 30 ml with a detection limit of 0.5 TU by using an in-growth time of 24 weeks compared with six weeks typically used for 500 ml samples.

3.4 Calculation of Tracer Age

When the recharge concentration increases monotonically with time or is stable, the age of a radioactive transient tracer can be calculated as previously discussed by correcting the measured concentration for decay and projecting the decay-corrected value back to its intersection with the recharge versus time curve. However, when the recharge concentration declines with time, a unique determination of age is not always possible. If the recharge concentration declines at the same rate as the tracer decays, an infinite number of possible ages can explain the measured value. The non-uniqueness in age is illustrated in Figure 10 which shows the atmospheric ^{3}H values for Vienna, Austria, along with decay curves for three hypothetical samples collected in 2015.

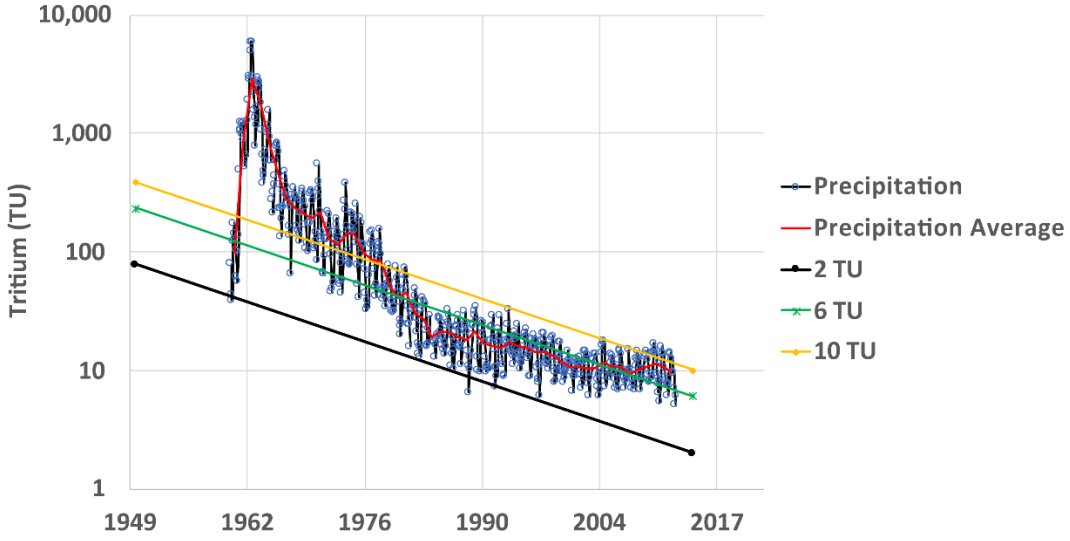

Figure 10 - Example of groundwater dating with ^{3}H with three hypothetical samples collected in 2015 in the vicinity of Vienna, Austria, where the precipitation data were collected. The 2 TU sample can be reasonably assigned a recharge year of 1961. The decay curve for the 6 TU sample intersects the average precipitation curve (solid red line) in 1961 and a few times between 1982 and 2009, so only a minimum age of six years (2015 – 2009 = 6) can be assigned by using the latest time at which the decay curve crosses the average precipitation curve. The 10 TU sample is likely modern (age = 0), but recharge years of 1962 and 1978 cannot be ruled out.

The red curve in Figure 10 represents annual average values and may be a more representative value for recharge at the water table with dispersion in the unsaturated zone smoothing annual variations. Sample 1 has a measured concentration of 2 TU, and this sample can reasonably be interpreted as being recharged prior to the bomb peak, most likely in the early 1960s. Although the decay curve for this sample intersects the

precipitation curve for one sample on October 15th, 1988, it is unlikely this single value was representative of recharge in 1988; it is more likely that the average value was around 14 TU in 1988. If the pre-bomb recharge concentration is assumed to be 10 TU for this location, then the most probable recharge year for this sample is about 1960 for an age of 2015 – 1960 = 55 years.

Hypothetical sample 2 has a concentration of 6 TU, and its decay curve intersects the average precipitation curve in 1961 and a few times between 1982 and 2002. With the assumption that unsaturated zone transport has smoothed the annual variations in precipitation, it is reasonable to conclude that this sample has a minimum age of 6 years (2015 – 2009 = 6), but it could be as old at 55 years (2015 – 1960 = 55).

The third sample is likely modern with an age of zero, but its decay curve intersects the average precipitation curve in 1962 and 1978, so older ages cannot be ruled out.

The procedure used for the previous example can be summarized in the following four steps:

1. Obtain an atmospheric ^{3}H input function for the area of interest, which can be challenging. For study sites near a GNIP station, missing data points—a common occurrence—can be filled in using a linear regression with one of the complete stations such as Vienna, Austria, or Ottawa, Canada. For study sites not near a GNIP station, the input function might be reconstructed by triangulation or inverse distance weighting of the correlation parameters of nearby stations (Harms et al., 2016; Michel et al., 2018). For sites located in the USA, the correlation and spatial interpolation of Michel and others (2018) might be used. The global model of Terzer-Wassmuth and others (2022) may be especially useful for estimating the contemporary value.
2. Compute annual average concentrations. If precipitation amount data are available, the monthly values should be weighted by precipitation.
3. Calculate the decay curve for a given sample. The sample date and measured concentration represent one point for this curve and only one additional point is needed. The additional point can be calculated using Equation (12).

$$C_o = C_m \exp(\lambda \Delta t) \tag{12}$$

where:

C_o = concentration at an arbitrary time; a convenient choice is 1950 as the precipitation ^{3}H record begins after 1950 (e.g., TU)

Δt = sample time – C_o time (T)

C_m = sample concentration (e.g., TU)

λ = tritium decay constant (T^{-1}, 0.05626 yr^{-1})

4. Plot the raw ^{3}H in precipitation data, the average (precipitation weighted) data, the sample concentration (C_{m}) and the arbitrary C_{o} data, with a line connecting C_{o} and C_{m}.

The previous example illustrates the variable degree to which a unique age can be assigned to a sample. Even if a unique age cannot be assigned, it may be possible to calculate a minimum age using Equation (13).

$$Age_{min} = \frac{-\ln\left(\frac{C_{meas}}{C_{background}}\right)}{\lambda} \tag{13}$$

where:

Age_{min} = minimum age of the sample (T)

$C_{background}$ = ^{3}H concentration in precipitation at the time the sample was collected (e.g., TU)

C_{meas} = sample concentration (e.g., TU)

λ = tritium decay constant (T^{-1}, 0.05626 yr^{-1})

$C_{background}$ in Equation (13) is the ^{3}H concentration in precipitation at the time the sample was collected and assumes that previous atmospheric ^{3}H values were greater than or equal to $C_{\mathrm{background}}$. Furthermore, C_{meas} must be less than $C_{\mathrm{background}}$. In practice, Equation (13) generally applies only to samples collected after about the year 2000 and in areas with no significant local ^{3}H sources. Exercise 3 provides an opportunity to practice estimating sample age.

When a vertical profile of ^{3}H values is available, it is sometimes possible to identify the mid-1960s bomb peak as an event marker, although decay and dispersion are making it harder to locate the peak as time goes on. This technique has more commonly been used in the unsaturated zone but has also been used in the saturated zone. Figure 11 shows a vertical profile of ^{3}H values from a shallow unconfined aquifer near Sturgeon Falls, Ontario, Canada (Solomon et al., 1993). The 1963 bomb peak is clearly delineated in the profile and defines the age of groundwater at the depth and location of the peak.

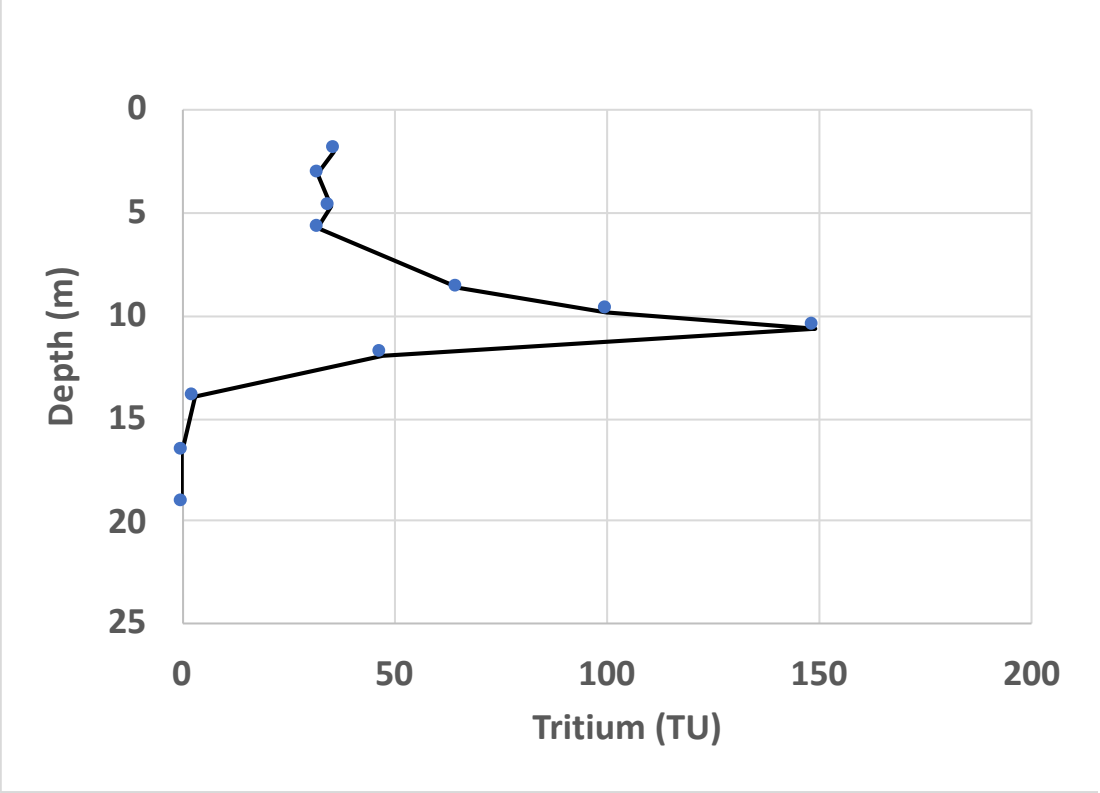

Figure 11 - Vertical profile of ^{3}H values from an unconfined aquifer near Sturgeon Falls, Ontario, Canada (redrawn from Solomon et al., 1993). Peak ^{3}H concentration at a depth of 10.6 meters marks the location of water that recharged in 1963.

While the determination of groundwater age from a single discrete sample using ^{3}H can be non-unique as described previously, a unique determination of the mean residence time may be possible using a *lumped parameter model* (LPM; Maloszewski & Zuber, 1982). The details of LPMs are beyond the scope of this book, but as shown by Morgenstern and Taylor (2009), if a sample can be collected that contains a flow-weighted mixture of all aquifer flow paths—using a fully-screened well or at a major spring where flow paths converge—and if the residence time distribution is known, it may be possible to uniquely define the mean residence time from this single, or *mixed*, sample. Prior understanding of site conditions and conceptual models are required for this approach to be successful.

3.5 Sensitivity of Age to Input Parameters

The primary uncertainty associated with applying Equation (13) is the background ^{3}H concentration ($C_{background}$) due both to temporal variations at a given location and spatial variation between measurement stations. Hydrodynamic dispersion in the unsaturated zone may effectively smooth intra-annual variations and hence reduce the age uncertainty. However, hydrodynamic dispersion is complex and depends on many factors (variation in hydraulic conductivity, water content, temporal variations in precipitation, scale, among others), making it difficult to generalize the degree to which average ^{3}H values are representative of recharge conditions.

One way to assess the uncertainty in age due to uncertainty in the background concentration is to compute the standard deviation of the background concentration and then construct mean plus standard deviation and mean minus standard deviation curves as shown in Figure 12. The example in Figure 12 uses the Vienna atmospheric curve and a hypothetical sample having 5.5 TU that was collected on January 1st, 2015. The decay curve intersects the mean minus one standard deviation curve in 2009 and the mean plus one standard deviation in 2001. The decay curve intersects the average precipitation curve in 2003 for this example. The age and associated uncertainty are thus calculated in years as 12 years with an uncertainty of +2 to -6 years. However, it is important to point out that the 5.5 TU decay curve for this example also intersects the average precipitation curve in the early 1980s, so a much older age of 35 years cannot be ruled out by the ^{3}H data alone. Exercise 4 provides an opportunity to practice using the ^{3}H dating method.

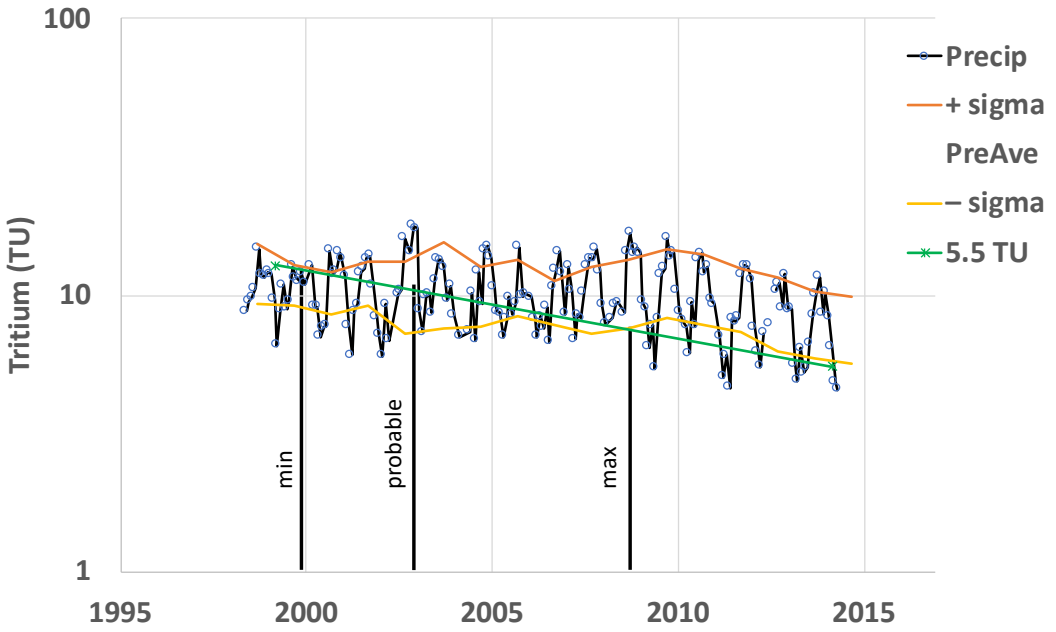

Figure 12 - Example of computing the most probable age and uncertainty for a hypothetical sample containing 5.5 TU that was collected near Vienna, Austria, on January 1st, 2015. Section 3.5 provides further discussion. The average precipitation value (PreAve), plus (+ sigma) or minus (- sigma) are plotted to constrain age estimates.

3.6 Discussion of Tracer-Specific Issues

Because it is part of the water molecule, ^{3}H is nearly an ideal tracer for groundwater, and advection and dispersion will have essentially the same effects on tritiated water (HTO) as H_2O. As previously discussed, a small fractionation between water vapor and liquid results in the vapor phase being depleted in ^{3}H relative to the liquid. Nevertheless, ^{3}H can be transported in the vapor phase and this results in important differences between ^{3}H transport and dissolved ions in the unsaturated zone. For example, Phillips and others (1988) showed that ^{3}H in the unsaturated zone in arid regions was transported at a faster rate than ^{36}Cl because ^{3}H was transported in both vapor and liquid

phases, while ^{36}Cl was only transported in liquid phase. Significant ^{3}H transport in the vapor phase has also been observed in the vicinity of nuclear reactors (Noguchi et al., 2001).

3.7 Summary

Tritium is part of the water molecule and is a widely used tracer in groundwater studies. While ^{3}H occurs naturally, concentrations in precipitation rose dramatically beginning in the 1950s due to nuclear weapons testing. Historically, ^{3}H has been used to distinguish pre- from post-bomb water.

As a groundwater dating method, ^{3}H is both a radioactive and transient tracer. Absolute dating is done by extending a decay curve from the measured concentration back in time to its intersection with the curve representing the measured concentration of ^{3}H in precipitation through time. However, in the northern hemisphere from about 1980 to 2000, the precipitation and decay curves are approximately parallel, leading to large ranges of possible ages. From about 2000 to present, the precipitation curve has been approximately flat—constant average concentration—making absolute dating possible for recharge years beyond 2000. For waters that fell as precipitation after 2000, the primary uncertainty in absolute dating with ^{3}H is the spatial and temporal variability in the input concentration. Age uncertainties on the order of ± 5 years are typical but depend on factors such as the magnitude of annual variations.

4 Tritium/Helium-3 Dating Method

The *tritium-helium age-dating method* relies on the measurement of tritium (^3H, as discussed in Section 3) and noble gases in groundwater samples. Because the method relies on measurement of a parent (tritium: ^3H) and child product (tritiogenic helium: $^3He_{trit}$) of radioactive decay, the $^3H/^3He$ age dating is not reliant on a historical record of atmospheric concentrations or activities. Measured noble gases—He and Ne, at a minimum, but preferably Ne, He, Ar, Kr, and Xe—are used to determine the amount of ^3He produced from decay of ^3H during transport in the aquifer: tritiogenic helium, $^3He_{trit}$. Given ^3H and $^3He_{trit}$ for a groundwater sample, it is possible to use the known half-life of ^3H (12.32 years; Lucas & Unterweger, 2000) to calculate groundwater tracer age.

Because groundwater age involves both time (recharge year, or *age*) and space (the location of sampling relative to the water table), the concept is well suited for many applications related to aquifer resilience and groundwater quality issues. For example, recharge rates (dimensions of LT^{-1}) based on $^3H/^3He$ ages were first reported by Solomon and Sudicky (1991), and this technique has been used broadly (e.g., Table 1 in McMahon et al., 2011, which includes studies based on SF_6 and CFC tracers).

Similarly, estimation of recharge year for groundwater samples is useful for investigating historical input of contaminants to aquifers, including non-point sources (e.g., Böhlke, 2002; Puckett et al., 2011) and point sources (Shapiro et al., 1999). Knowledge of historical contaminant inputs to aquifers can then be useful for predicting future discharge of contaminants from aquifers, including discharge from wells—for interactive examples, see Böhlke and others (2014) and related web interface—and groundwater discharge to streams (Gilmore, Genereux, Solomon, Farrell, et al., 2016; Gilmore, Genereux, Solomon, & Solder, 2016).

$^3H/^3He$ age dating has been used to constrain and/or calibrate groundwater models. One example is McMahon and others (2010), where six $^3H/^3He$ age estimates—out of 2,574 total field observations including other parameters—had a major influence on refining the numerical model. Similarly, in a groundwater quality study, Wells and others (2021) used existing $^3H/^3He$ groundwater age estimates (Böhlke et al., 2007; Wells et al., 2018) in a machine-learning framework to constrain the range of groundwater and vadose zone transport rates. Additional examples of $^3H/^3He$ applications can be found in Gilmore and others (2021).

4.1 Background and Historical Development

Tolstikhin and Kamensky (1969) first reported on the concept of using the $^3H/^3He$ parent-child concentrations to determine an age of water. The method was used to investigate circulation of ocean waters (Jenkins & Clarke, 1976) and later applied to lakes

(Torgerson et al., 1979). About a decade later, the first use of tritium-helium age dating for groundwater was reported by Schlosser and others (1988) and Poreda and others (1988).

Helium has two naturally occurring and stable isotopes. Most natural He is ^{4}He with an abundance that is nearly a million times greater than ^{3}He in the atmosphere. The ^{3}He found in groundwater can be derived from the following:

1. the atmosphere,
2. subsurface production in the Earth's crust,
3. primordial He (e.g., degassing from mantle rocks), or
4. the decay of ^{3}H.

The He isotopic composition of each of these sources is vastly different. The atmosphere contains about 5.24 ppmv (ppm volume) He with a ^{3}He/^{4}He ratio of $1.382 \pm 0.005 \times 10^{-6}$ (Sano et al., 2013). In the subsurface, ^{4}He is a radioactive decay product of U and Th and a small amount of ^{3}He is produced from the fission of ^{6}Li, which produces ^{3}H that then decays to ^{3}He.

The ^{3}He/^{4}He ratio produced by the Earth's crust ranges from about 10^{-8} to 10^{-7} and depends on many factors including neutron production and the Li content of crustal rocks (Solomon, 2000). Primordial He that degasses from the mantle is relatively rich in ^{3}He with a ^{3}He/^{4}He ratio that ranges from about 1×10^{-5} to 2×10^{-5}. When produced from ^{3}H decay, ^{3}He is called $^3\mathrm{He}_{\mathrm{trit}}$ and is used for ^{3}H/^{3}He dating. As is discussed later in this section, separating $^3\mathrm{He}_{\mathrm{trit}}$ from other components is an essential task for dating.

4.2 Basic Concepts and Systematics

Tritium decays via beta emission to stable ^{3}He. ^{3}H/^{3}He age dating relies on measurement of both parent (^{3}H) and child (^{3}He) products that occur during groundwater transport. The physical process starts with

1. infiltration of water at the land surface,
2. transport through the vadose zone, and finally
3. recharge to the groundwater system.

During processes (1) and (2), the water is exposed to a gas phase. The gas phase is atmospheric air at the land surface and often a close approximation to atmospheric air at the water table. Thus, any $^3\mathrm{He}_{\mathrm{trit}}$ produced during infiltration and vadose zone transport is generally lost as the dissolved gases in water equilibrate with atmospheric air. Once recharge occurs, process (3), the groundwater is no longer in contact with an atmospheric gas phase.

As a result, and assuming the recharge rate is sufficiently high—nominally, > 3 mm yr^{-1}, (Gilmore et al., 2021; Solomon et al., 1993)—the $^3\mathrm{He}_{\mathrm{trit}}$ begins to accumulate in the groundwater. Accumulation of $^3\mathrm{He}_{\mathrm{trit}}$ continues until groundwater is sampled or

exposed again to a gas phase such as when the groundwater discharges to a stream or spring or is pumped out of a well.

Figure 13 illustrates the accumulation of $^3He_{trit}$ over time as the initial ^3H in groundwater recharge decays. The horizontal axis illustrates the relevant timescale of the $^3H/\,^3He$ age-dating method, where 2.6 percent of initial ^3H remains after 65 years and 1.4 percent remains after 75 years.

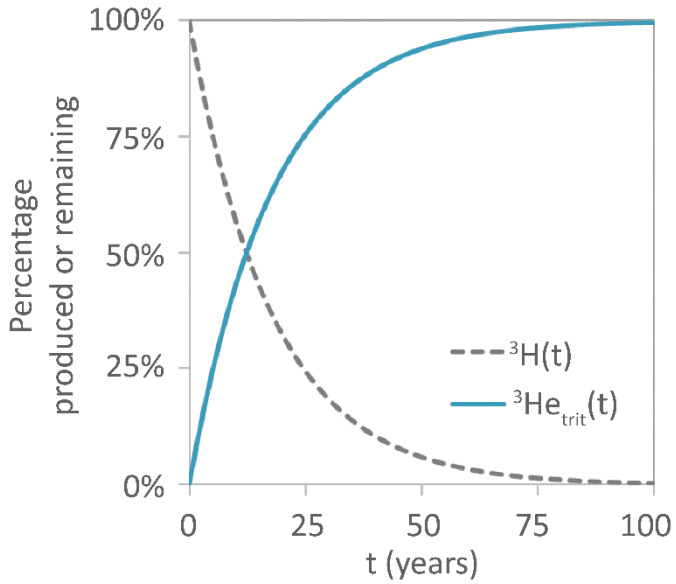

Figure 13 - ^3H remaining and $^3He_{trit}$ produced over time due to radioactive decay. A ^3H half-life of 12.32 years was used.

To determine the groundwater age from $^3H(t)$ and $^3He_{trit}(t)$, the age equation shown in Equation (14) is used.

$$Age = \frac{\ln\left(1 + \frac{^3He_{trit}(t)}{^3H(t)}\right)}{\lambda} \qquad (14)$$

where:

Age = elapsed time since groundwater recharge, i.e., since exposure to atmosphere (T)

λ = decay constant (T^{-1})

t = time of sampling

Concentration units for both $^3He_{trit}$ and ^3H in Equation (14) are in TU. The age equation assumes that groundwater tracer transport can be described as *piston flow* (Maloszewski & Zuber, 1996). Practically speaking, this assumption means that ^3H and produced $^3He_{trit}$ travel together without mixing across other groundwater flowlines. Exercise 5 provides an opportunity to practice calculating estimated groundwater age.

The age equation is based on the decay of tritium to tritiogenic helium shown in Equation (15).

$$^3H_{trit}(t) = {}^3H(t_0)(1 - e^{-\lambda t}) \quad (15)$$

Initial ^3H ($^3H(t_0)$) is equal to the $^3H(t)$ plus $^3He_{trit}$ determined from the groundwater sample as shown in Equation (16).

$$^3H(t_0) = {}^3H(t) + {}^3He_{trit}(t) \quad (16)$$

The decay constant (λ) is calculated as shown in Equation (17), based on the half-life of tritium (12.32 years; Lucas & Unterweger, 2000).

$$\lambda = \frac{\ln 2}{12.32 \text{ years}} = 0.05626 \text{ yr}^{-1} \quad (17)$$

4.3 Sample Collection and Analysis

Collection of groundwater for ^3H samples is straightforward and described in Section 3. Glass or high-density polyethylene bottles are preferable and a sample volume of about one liter is typically sufficient for ^3H analysis, although this can vary according to the tritium laboratory.

Collection of groundwater samples for determination of $^3He_{trit}$ is more challenging but very feasible with good communication with the noble gas laboratory where the samples will be analyzed. Detailed descriptions of sampling procedures can be found in Aeschbach-Hertig and Solomon (2013), which is summarized subsequently. Additional details are provided in Box 2 and Box 3. Practical considerations for selecting appropriate sampling sites (i.e., vadose zone thickness, well depth, screen length, among others) and a similar summary of sampling procedures can be found in Gilmore and others (2021).

Sampling containers and techniques may vary between noble gas labs (Aeschbach-Hertig & Solomon, 2013), so it is important to coordinate with the lab to obtain materials from the labs and/or the detailed specifications of required equipment. Water samples are commonly collected in refrigeration-grade copper tubes (Figure 14 and Boxes 2 and 3) for analysis of dissolved gases, but gas samples may also be collected directly in the field using diffusion samplers (Figure 14). In all cases, it is critical to avoid exposure of the groundwater sample or dissolved gas samples to air because dissolved noble gases can quickly equilibrate with the atmosphere as discussed in Section 2.

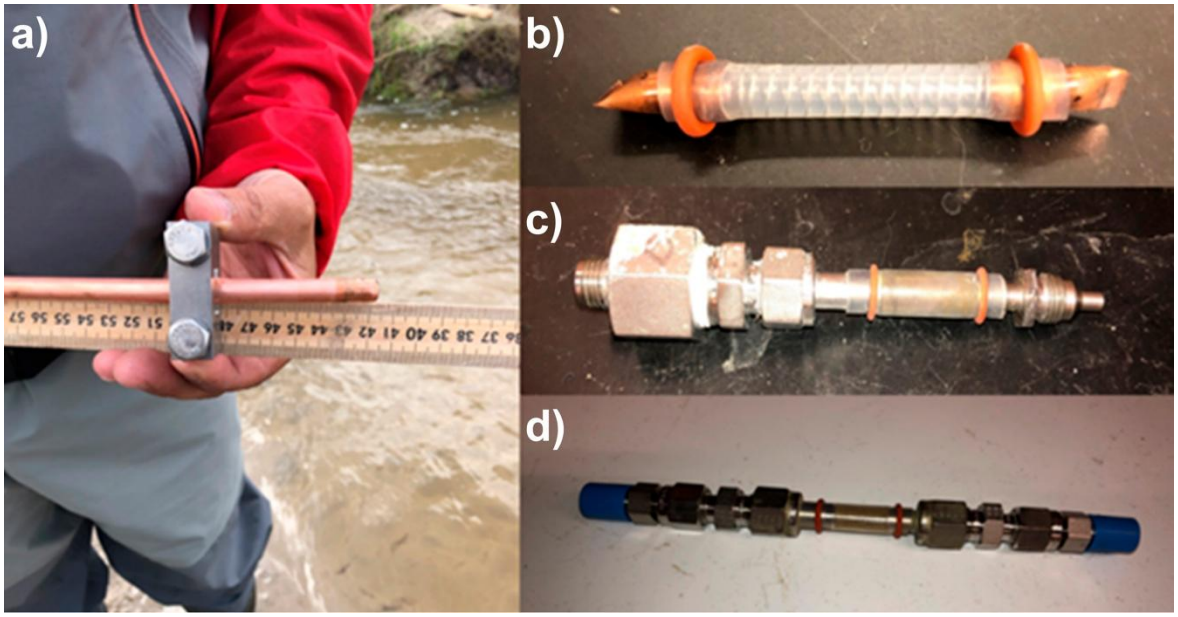

Figure 14 - Noble gas sampling details including a) refrigeration clamp attached to the end of a copper tube and b) permeable tubing used for the standard diffusion sampler. The copper tubing shown is what remains after the gas samples have been collected in the field. Panels c) and d) show an advanced diffusion sampler (used with permission of Gilmore et al., 2021).

Parameters that are especially useful for dissolved gas sampling include temperature and conductivity because gas solubility is dependent on these two parameters. Dissolved oxygen and *TDGP* (Manning et al., 2003) are also useful measurements because they can indicate potential for loss of dissolved gases (degassing) due to high gas concentrations that can occur due to generation of biogenic gases in the subsurface. The potential for loss of dissolved gases from groundwater samples is especially high when sampling in hot weather, when gas solubility is lower. Pumping at a higher rate and/or shortening or insulating pump tubing can be helpful during hot weather. Similarly, elevating the overflow tubing to increase head pressure on the sample in the copper tube can also help to keep gases in solution. Box 2 and 3 discuss procedures for sampling from wells and streambeds respectively. Section 2 provides additional discussion of these field parameters along with the process of degassing and their relationship to noble gas concentrations in groundwater samples.

For noble gases, a diffusion-based sampling method is available to passively extract dissolved gases from groundwater as an alternative to the copper tube method. A more detailed treatment of these methods is provided by Aeschbach-Hertig and Solomon (2013). Standard diffusion samplers (e.g., Figure 14b) use a short piece of permeable tubing (e.g., a 10 cm length of silicone) attached to short pieces of copper tubing (8 cm) on each end. The outer ends of the copper tubing are sealed with a tungsten carbide pinch-off tool to prevent water from entering the sampler and gas exchange once samples are collected. The sampler is submerged in a groundwater well for about 24 hours, allowing gases in the groundwater to equilibrate with the air in the permeable tubing and attached copper tubing (Sanford et al., 1996).

The sampler is then removed from the well and the pinch-off tool is used to seal the copper tubes near the attachment point with the permeable membrane (e.g., Figure 14b). The process of sealing the sample gases in the copper tube must be completed quickly to avoid gas exchange with the atmosphere. This method requires in situ measurement of temperature and *TDGP* of the sampled groundwater (Aeschbach-Hertig & Solomon, 2013).

An advanced diffusion sampler (Figure 14c, d) can be used to eliminate gas exchange with the atmosphere instead of collecting and sealing the standard diffusion sampler shown in Figure 14b (Gardner & Solomon, 2009). An added benefit of using an advanced sampler is that *TDGP* does not need to be measured in the field (Aeschbach-Hertig & Solomon, 2013). There are four main components of advanced diffusion samplers:

1. the volume where gas sample is collected and stored,
2. the gas exchange membrane,
3. a piston, and
4. a hydraulic activation mechanism (Gardner & Solomon, 2009).

Like the passive sampler, the equilibration time for the advanced diffusion sampler is about 24 hours. A hand-operated pump closes the sampler in-situ to temporarily seal off the sample from further gas exchange. The sampler is then withdrawn from the well and the sample tubing is clamped shut for long-term storage (Gardner & Solomon, 2009).

Lab analysis of groundwater for ^{3}H activity is achieved using the helium in-growth method as described in Section 3.3, which includes a description of ^{3}He and ^{4}He measurement in gas extracted from groundwater. The analytical approach for measuring ^{3}He and ^{4}He contained in sampled groundwater (i.e., the copper tube method) or gases in diffusion samplers is the same as for ^{3}He and ^{4}He extracted for the helium in-growth method. These isotopes are measured by peak-height manometry using large-radius *sector-field mass spectrometry* (SFMS).

Precise measurement of ^{3}He is complicated because of its very low abundance in groundwater samples and because of its low abundance relative to ^{4}He. The SFMS needs a high resolving power to separate ^{3}He (mass = 3.016) from the hydrogen deuterium ion (HD; mass = 3.021) and is present in all metal vacuum systems, and to assure that the ^{3}He peak has no interference from the tail of the ^{4}He peak. Either SFMS or quadrupole mass spectrometry is used for other noble gases needed for the ^{3}H/ ^{3}He age-dating method. Ideally, a full suite of noble gases is measured in addition to ^{3}He, including Ne, Ar, Kr, and Xe (Stanley et al., 2009). In some cases, only Ar and/or Ne are measured to decrease the cost of analysis.

4.4 Calculation of Tracer Age

Figure 15 shows five to six typical steps that can be followed to determine $^3H/^3He$ age from noble gas and tritium data. Step 1 is a data triage step to evaluate whether the groundwater sample is likely to be in the applicable age range for the $^3H/^3He$ method and evaluate whether the sample may be a mixture of old and young groundwater (Step 1d). A key variable in step 1 is R/R_a, which is the ratio of ^3He to ^4He measured in the sample (R) and the $^3He/^4He$ of air (R_a) as shown in Figure 15, steps 1a, b, and d. Either R/R_a or the R measured for each groundwater sample should be included in the results reported by the noble gas laboratory analyzing the samples.

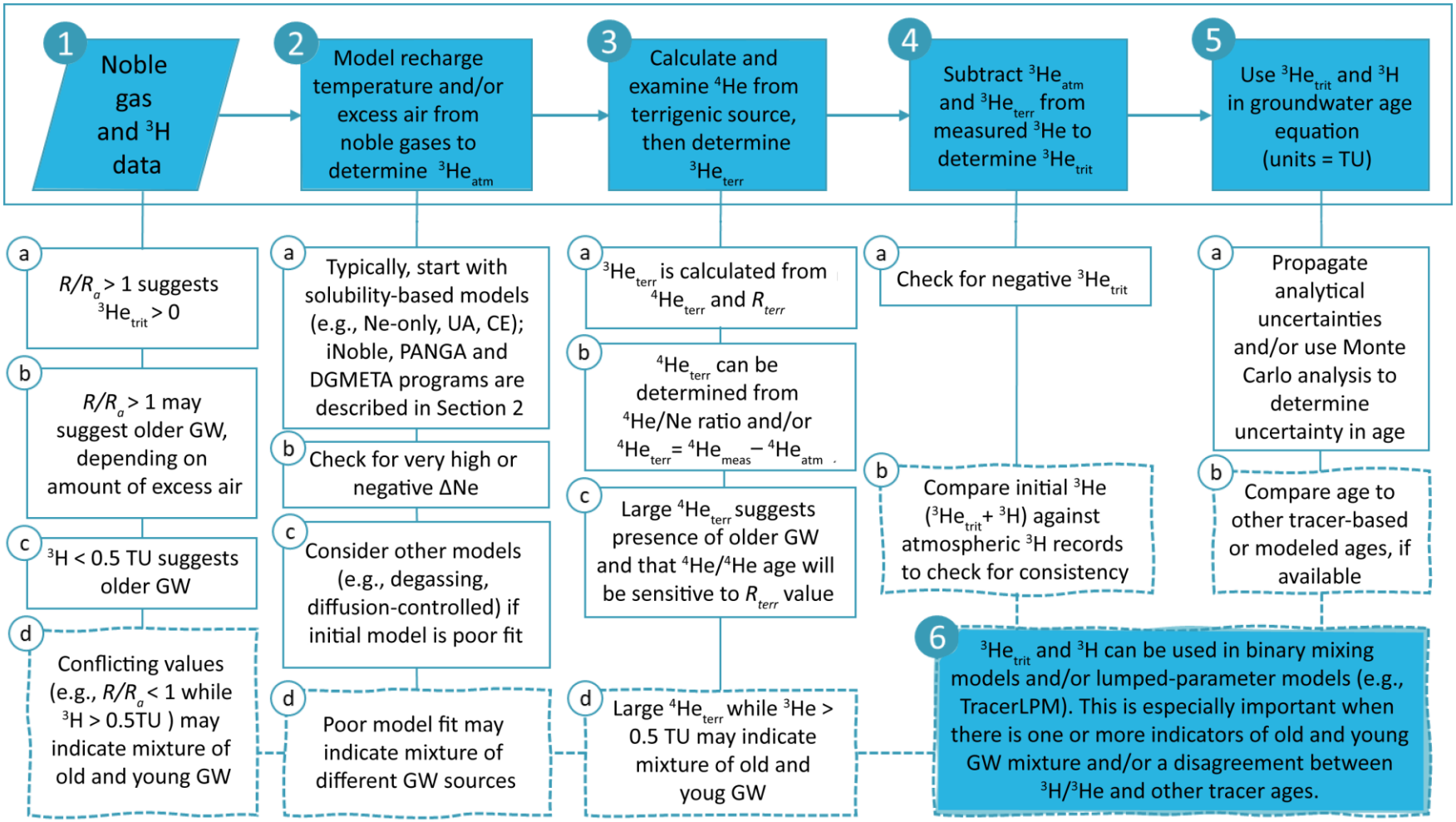

Figure 15 – The process for interpreting ^{3}H and noble gas data for tritium-helium age dating. Shaded and numbered boxes are major steps of the process. Text boxes below the first five steps show key criteria to consider while interpreting noble gas and ^{3}H data. Dashed lines and outlines indicate special consideration for samples that may be mixtures of old and young groundwater (modified from Gilmore et al., 2021).

Inspection of the tritium-helium age calculation shown in Equation (14) reveals the need to determine $^3He_{trit}$, which is just one component of the overall ^3He budget in any groundwater sample. The complete budget for ^3He in groundwater, rearranged to solve for $^3He_{trit}$, is shown in Equation (18).

$$^3He_{trit} = {}^3He_m - {}^3He_{atm} - {}^3He_{terr} \quad (18)$$

where:

^3He_m = ^3He measured in the groundwater sample

$^3He_{atm}$ = portion of dissolved ^3He derived from atmospheric sources

$^3He_{terr}$ = portion of dissolved ^3He derived from terrigenic sources, including crustal ^3He ($^3He_{crust}$) and mantle ^3He ($^3He_{man}$)

Units for concentrations in Equation (18) are typically expressed in ccSTP/g. ^3He_m may be reported as $\delta\ ^3He$, which is equivalent to $(R/R_a - 1)100\%$, and can therefore be converted to ccSTP/g based on the definitions of R and R_a and the measured concentration of ^4He in ccSTP/g. The age calculated by Equation (14) requires that ^3H and $^3He_{trit}$ be in the same units. Equation (19) expresses a conversion factor (*CF*) used to convert from ccSTP/g to TU.

$$CF = \left(\frac{4.021 \times 10^{14}}{1 - \frac{S}{1000}} \right) \quad (19)$$

where:

S = salinity of the sample in parts per thousand (i.e., ‰)

Determination of the atmospheric component ($^3He_{atm}$) of the ^3He budget is addressed in Figure 15 (step 2). $^3He_{atm}$ can be broken into two components as shown in Equation (20).

$$^3He_{atm} = {}^3He_{sol} + {}^3He_{EA} \quad (20)$$

where:

$^3He_{sol}$ = ^3He concentration at solubility equilibrium with the atmosphere at recharge temperature and elevation

$^3He_{EA}$ = the portion of dissolved ^3He derived from excess air

$^3He_{EA}$ describes dissolved ^3He attributed to an atmospheric source but in excess of solubility equilibrium at recharge temperature and elevation. Excess air is due to vadose zone processes and/or water table dynamics (i.e., dissolution of air that is trapped in pore spaces as described in Section 2). Selection of a noble gas model as described in Section 2 (e.g., the CE model or graphical method shown in Figure 5) or in Aeschbach-Hertig and

Solomon (2013) is necessary to determine the solubility and excess air components of the $^3He_{atm}$ budget.

ΔNe—defined in Equation (8) of Section 2—is an important variable mentioned in Figure 15 (step 2b) because it is sensitive to excess air (Figure 5). When ΔNe is negative, it is likely that noble gases have been lost from the sample (Figure 6: steps 2b and c) and noble gas modeling becomes more complex (Aeschbach-Hertig et al., 2008; Aeschbach-Hertig & Solomon, 2013; Gilmore et al., 2021; Gilmore, Genereux, Solomon, Farrell, et al., 2016; Gilmore, Genereux, Solomon, & Solder, 2016; Visser et al., 2007; Visser et al., 2009), as described in the discussion of tracer-specific issues in Section 4.6.

Step 3 in Figure 15 addresses the $^3He_{terr}$ component of the ^3He budget, which is based on an estimate or assumption of R_{terr} (Figure 15: steps 3a and c), the $^3He/^4He$ of terrigenic He. The typical assumed value for R_{terr} is 2×10^{-8} (Mamyrin & Tolstikhin, 1984), with a range of 10^{-9} to 10^{-7} (Solomon, 2000), based on values associated with a crustal source (R_{crust} in Table 4). If a mantle source (R_{man}, Table 4) of He is present, age dating becomes very difficult because the R_{man} is an order of magnitude greater than R_a for atmospheric He.

Table 4 - $^3He/^4He$ ratios (R_x) for different ^3He reservoirs (i.e., sources).

^3He reservoir	Variable	Typical Value	Notes
Atmosphere	R_a	1.382×10^{-6}	Considered a constant for all practical purposes, based on ^4He outgassing from the earth, production of ^3He from cosmic rays, and loss of ^3He to atmosphere.
Atmosphere, adjusted for fractionation	R_{sol}	1.357×10^{-6}	Because there is a slight fractionation of ^4He and ^3He when dissolved, R for water in equilibrium with the atmospheric air is $0.98 \times R$.
Crustal source of R_{terr}	R_{crust}	2×10^{-8}, theoretically, although in practice may reach 2×10^{-7}	Theoretical value based on production of ^3He by hitting ^6Li with a neutron. Actual values based on old (^3H below detection) groundwater range from 2×10^{-8} to 2×10^{-7}.
Mantle source of R_{terr}	R_{man}	1.1×10^{-5} to 1.4×10^{-5}	Given the magnitude of R_{man}, $^3H/^3He$ age dating becomes very difficult.

Step 4 in Figure 15 is trivial if the calculated $^3He_{trit}$ is positive and initial tritium, $^3He(t_0)$ as determined using Equation (16) is reasonable compared to historical atmospheric ^3H records. Similarly, Step 5 is a simple calculation of groundwater tracer age based on Equation (14). However, it is important to perform the checks a and b for Steps 4 and 5 to confirm that the calculated age is reasonable. An example of a graph used for Step 4b is shown in Figure 16. Samples that plot below the precipitation curve are likely to be mixtures of young and old water. When appropriate, tracer results need to be modeled as mixtures of groundwater with different ages, as described in Step 6 of Figure 15.

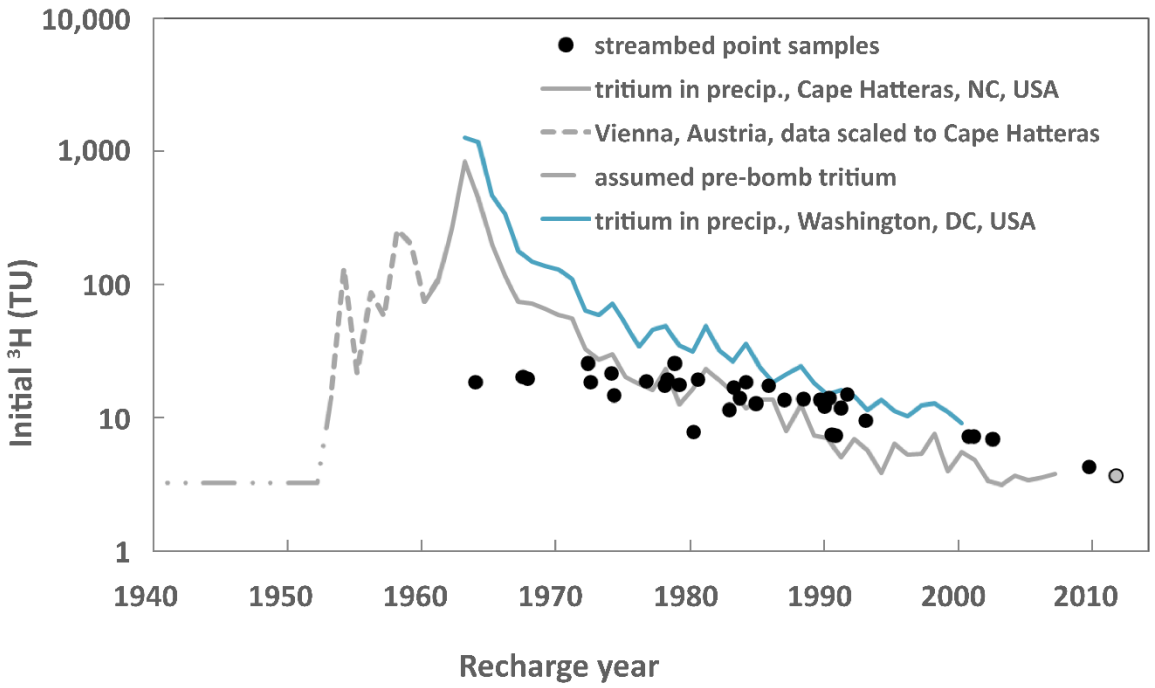

Figure 16 – Graph showing initial tritium ($^3H(t_0)$, calculated from measured ^3H plus ^3H equivalent of tritiogenic helium from the sample) for groundwater samples collected in the streambed of a gaining stream in North Carolina (NC), USA, in July 2012 (modified from Gilmore, Genereux, Solomon, & Solder, 2016). Black dots are streambed samples with the initial ^3H on the y-axis and recharge year determined from tracer age using the $^3H/^3He$ method on the x-axis.

4.5 Sensitivity of Age to Input Parameters

Based on low solubility and sensitivity to excess air, the behavior of He is like Ne as shown in Figure 5. Early $^3H/^3He$ age-dating studies relied solely on Ne and He measurements, and some noble gas labs continue to use this approach. Step 2a in Figure 15 refers to the Ne-only model. It is instructive to carefully review the Ne-only model formulation shown in Equation (21) because

1. $^3He_{trit}$ can be determined manually using just two gas concentrations with simplifying assumptions,
2. therefore, the equation can be used to develop an intuition about the sensitivity of $^3H/^3He$ ages of different variables required for calculation of $^3He_{trit}$.

$$^3\mathrm{He}_{trit} = {}^4\mathrm{He}_m(R_m - R_{terr}) - {}^4\mathrm{He}_{sol}(R_{sol} - R_{terr}) - \left(\frac{^4\mathrm{He}}{\mathrm{Ne}}\right)_{EA}(\mathrm{Ne}_m - \mathrm{Ne}_{sol})(R_a - R_{terr}) \quad (21)$$

where:

^4He_m = measured concentration of ^4He

R_m = measured $^3He/^4He$ ratio; commonly referred to simply as R as in the notation R/R_a

R_{terr} = $^3He/^4He$ ratio for terrigenic He (Table 4)

R_{sol} = $^3He/\ ^4He$ ratio for water in solubility equilibrium with air at assumed recharge temperature and elevation; R_{sol} is equal to αR_a, where α is the air-water fractionation factor (0.98)

$\left(\frac{^4He}{Ne}\right)_{EA}$ = $^4He/Ne$ ratio of excess air dissolved in the sample; 0.288 for complete dissolution (unfractionated excess air)

Ne_m = measured Ne concentration in water

Ne_{sol} = Ne concentration for water in solubility equilibrium with air at assumed recharge temperature and elevation

R_a = $^3He/\ ^4He$ ratio of atmospheric air

Exercise 6 provides an opportunity to practice calculating estimated groundwater age including the additional calculations needed to determine tritium-helium age such as the Ne-only formulation.

Only ^4He and Ne concentrations explicitly appear on the right-hand side of Equation (18), so it is worth noting that $^4He\ R_x = {}^4He\ (\ ^3He/\ ^4He)_x$ where x is, for example, a subscript as shown in Equation (21). This simplifies to a ^3He concentration.

The first term in Equation (21), i.e. the $^4He_m(R_m - R_{terr})$, is equivalent to the first term in Equation (18), i.e. the ^3He_m minus a $^3He_{terr}$ component. The second and third terms in Equation (21)—which represent solubility equilibrium and excess air components at an assumed recharge temperature—are equivalent to the second term in Equation (18), i.e. $^3He_{atm}$ minus a $^3He_{terr}$ component.

Relative to other noble gases, He is least sensitive to recharge temperature (as shown in Figure 3 of Section 2) and salinity (as shown in Figure 4 of Section 2). Similarly, $^3H/\ ^3He$ age is mildly sensitive to recharge temperature and elevation, as shown in Figure 17a and Figure 17b, respectively.

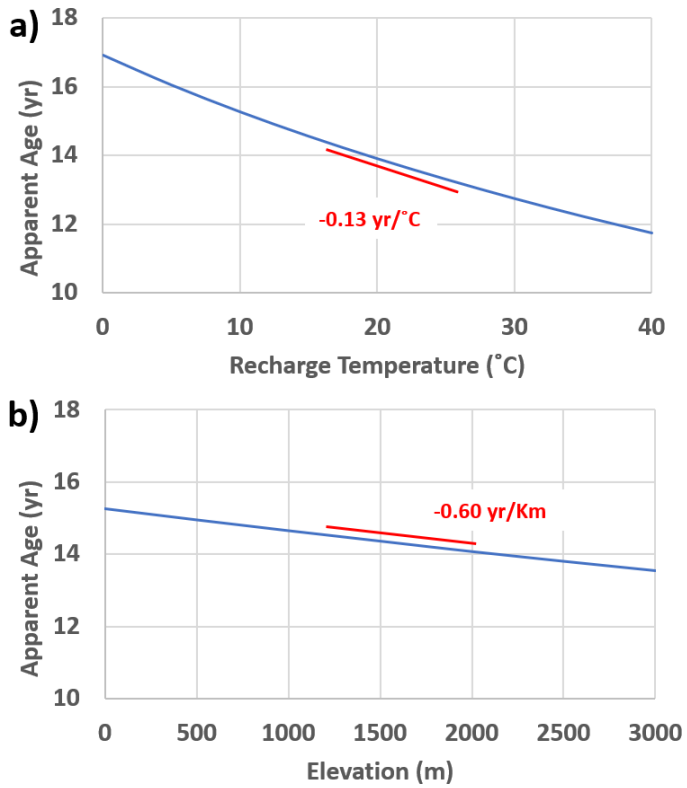

Figure 17 - Sensitivity of $^{3}H/^{3}He$ tracer age for a) recharge temperature and b) elevation. The recharge temperature and elevation sensitivity examples were calculated from a hypothetical base case with $^{3}H = 10$ TU, $R/R_a = 1.5$, recharge temperature of 10 °C, and recharge elevation of 0 m. Recharge temperature or elevation were then varied over the range shown in the respective plots. While curves shown are non-linear, approximate slopes (red lines) for portions of the curves are annotated for illustration of relative sensitivity.

In contrast to recharge temperature, recharge elevation, and salinity, $^{3}H/\,^{3}He$ age is sensitive to excess air. The sensitivity to excess air is twofold, based on the total amount of excess air (Figure 18a) and the extent of dissolution of air bubbles during the formation of excess air measured in the groundwater sample (Figure 18b). In the context of Equation (21), this sensitivity is based on the $(Ne_m - Ne_{sol})$ term (where excess Ne indicates excess air) and the value of the $^{4}He/\,Ne$ term.

In the case where R/R_a is small—suggesting relatively little $^{3}He_{trit}$ in the sample—a very modest overestimation of excess air (> 0.6 ccSTP/kg) can yield a negative tracer age. The $^{4}He/Ne$ term can range from the value for atmospheric air (0.288; using this value assumes complete dissolution of air at the time excess air is formed, i.e., UA) to 0.8 for partial dissolution.

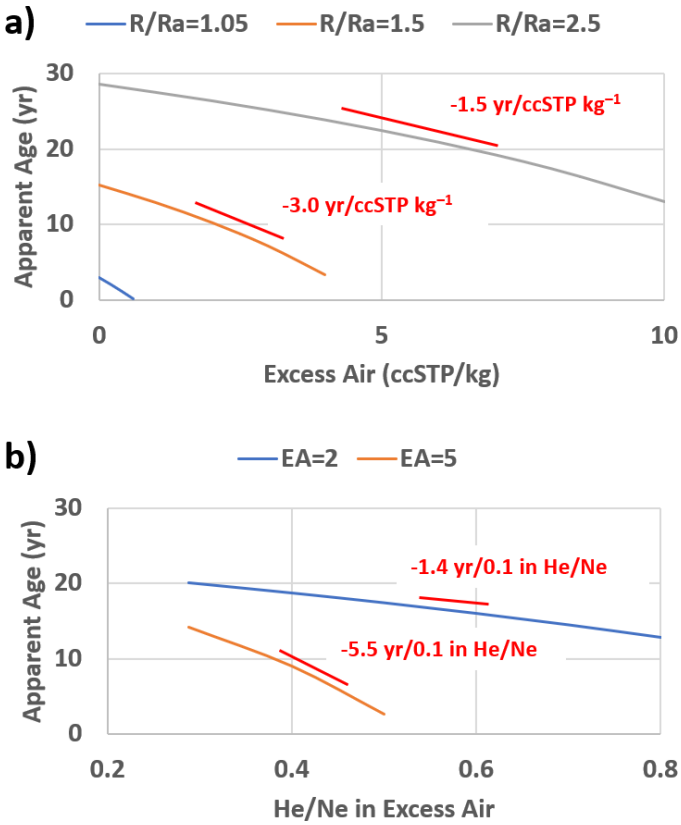

Figure 18 - Sensitivity of $^{3}H/^{3}He$ tracer age to excess air. Graph a) is based on a hypothetical sample with ^{3}H = 10 TU, recharge temperature of 10 °C, and recharge elevation of 0 m. For a sample with "true" excess air = 0 ccSTPkg^{-1}, adding 4 ccSTPkg^{-1} excess air reduces the tracer age from 12.9 years to 3.3 years when $R/R_a = 1.5$. In graph b), tracer age was calculated for two samples with moderate excess air (2 or 5 ccSTP/kg), but with different $^{4}He/Ne$ ratios as shown in Equation (21) ranging from 0.288 (atmospheric air) to 0.8 (the ratio of air that is fractionated by the ratio of Ne to He solubilities). While curves shown are non-linear, approximate slopes (short red lines) for portions of the curves are annotated to illustrate relative sensitivity.

Inspection of the Ne-only formulation in Equation (21) shows how the $^{4}He/Ne$ ratio could impact the determination of $^{3}He_{trit}$ and therefore tracer age. More complex model formulations such as the closed-system equilibration (CE) model and the partial re-equilibration (PR) model (Stute et al., 1995), are also based on different assumptions about fractionation of gases, particularly for excess air. The CE model in its simplest form is equivalent to the UA model, while the PR model yields very different estimates of He content when compared with other noble gases. While it is advisable to seek the simplest model(s) that reasonably fit the noble gas data (i.e., start first with Ne-only and/or UA model as shown in Figure 15, Step 2a), it is also important to consider other noble gas models as warranted by the data and/or conceptual models of the sampled system. Comprehensive discussion of excess air models can be found in Aeschbach-Hertig & Solomon (2013).

The prevalence of the R_{terr} variable in Equation (21) illustrates how $^3H/^3He$ ages may be sensitive to assumptions about terrigenic He. Similarly, other methods for determination of $^4He_{terr}$ (Figure 15, Step 3) can be used to evaluate the magnitude of $^4He_{terr}$. If $^4He_{terr}$ is $< 10^9$ ccSTP/g, then $^3He_{trit}$ is not sensitive to the selection of R_{terr} (Figure 19). $^3He_{terr}$ may be present due to production of helium in the Earth's crust and/or derived from the Earth's mantle (Table 4). However, mantle sources are negligible (< 0.2 TU) in many cases and typically not considered (Schlosser et al., 1989). However, if present, mantle He may preclude calculation of groundwater age due to the magnitude of R_{man}.

Last, the ^4He_m variable in Equation (21) is key to calculating $^3He_{trit}$. Figure 19b shows how the tracer age is sensitive to the measurement accuracy for ^4He. For the illustrative example, we observe that the tracer age would be negative if ^4He were severely underestimated (< 65 percent of solubility at the assumed recharge temperature and elevation).

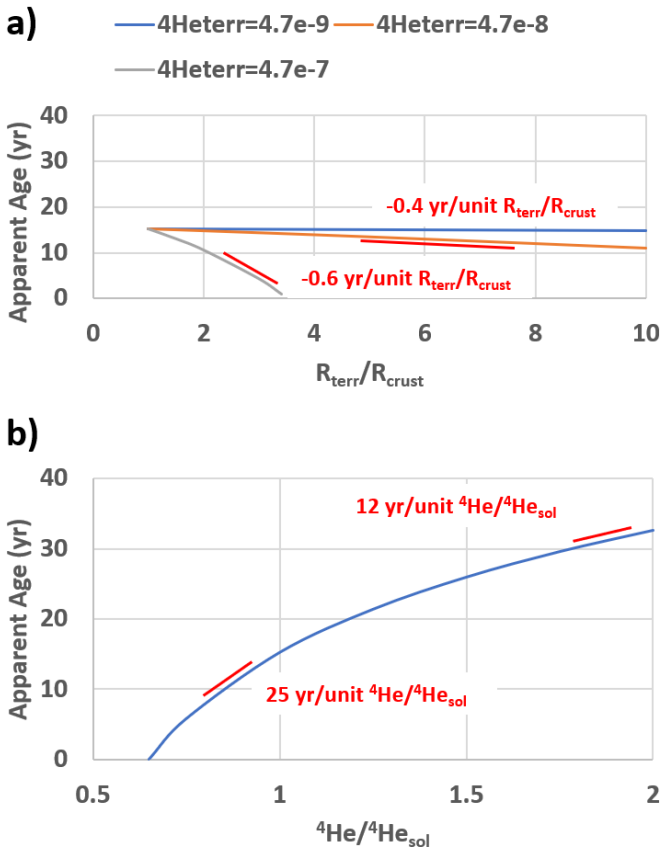

Figure 19 - Sensitivity of $^3H/^3He$ tracer (apparent) age to variation in a) R_{terr} and b) ^4He. Simulations were based on a hypothetical sample with ^3H = 10 TU, recharge temperature of 10 °C, and recharge elevation of 0 m. An R/R_a of 1.5 was assumed for the R_{terr} illustration. While curves shown are non-linear, approximate slopes (short red lines) for portions of the curves are annotated to illustrate relative sensitivity.

4.6 Discussion of Tracer-Specific Issues

The $^3H/^3He$ age-dating method has some advantages over other transient tracers for young groundwater. For instance, the $^3H/^3He$ age from Equation (14) is theoretically independent of a transient historical record of atmospheric concentrations, unlike the SF_6, CFC, or ^3H-only methods. However, the extreme variation of ^3H in the mid-twentieth century—the bomb peak, as shown in Figure 7—can lead to high $^3He_{trit}$ values that are more conducive to diffusion and dispersive mixing of $^3He_{trit}$ during transport through the aquifer (Scanlon et al., 2002; Solomon & Sudicky, 1991). These effects are much more likely in the northern hemisphere than in the southern hemisphere where the bomb peak was much lower.

Compared to transient tracers like SF_6, where more recent atmospheric concentrations are much higher than background concentrations—as discussed in Section 5—the $^3He_{trit}$ signal in very young groundwater is quite small. This can be observed on the left-hand side of Figure 13 where $^3He_{trit}$ values are much lower than ^3H. The analytical detection limit for ^3H is very low, but the small $^3He_{trit}$ is modeled from noble gas data and determined by subtraction as shown in Equation (18). Modeled $^3He_{trit}$ that is slightly negative (e.g., negative, with absolute value of < 0.5 TU) is occasionally calculated when groundwater is very young. However, large negative values could indicate an issue with sampling, analysis, or noble gas modeling. Extreme cases are shown in Figure 18 and Figure 19.

Mixing of old and young groundwater sources may also affect $^3H/^3He$ tracer age. While groundwater mixtures are a complex topic that may be best evaluated with numerical models, $^3H/^3He$ ages tend to be biased toward the younger groundwater source. The bias may be minor for moderate mixing. For example, a binary mixture of Source 1 (3.2 years) and Source 2 (25 years) in equal proportions would appear to have a $^3H/^3He$ age of 11 years, while the average age is 14 years (Table 5). An extreme case is a binary mixture of pre-bomb peak groundwater with very young groundwater. In this case, a mixture of 50 percent 3.2-year-old groundwater and 50 percent 73-year-old groundwater would appear to have a $^3H/^3He$ age of about ten years, which is much younger than the average age of the two sources (38.2 years; Table 5).

Table 5 - $^3H/^3He$ tracer age based on hypothetical binary mixtures.

	Source 1	Source 2	Source 3	50/50 mixture of Sources 1 and 2	50/50 mixture of Sources 1 and 3
^3H (TU)	10.0	3.0	0.1	6.5	5.1
$^3He_{trit}$ (TU)	2.0	9.0	6.0	5.5	4.0
Age (years)	3.2	25.0	73.0	11.0	10.0

As discussed previously, the solubilities of He and Ne are low and similar. If ΔNe is negative—which indicates degassing, as illustrated in Figure 15, Step 2b—noble gas

modeling for the determination of $^3He_{trit}$ becomes more complex. Since ^3He is a decay product, it is important to know when the degassing occurred. If degassing occurs near the point of recharge, then very little $^3He_{trit}$ would be lost—it has not been produced yet at the time of degassing—and only $^3He_{atm}$ would be lost from the sample. Correcting $^3He_{trit}$ for degassing (e.g., with the CE model) would lead to an older groundwater age estimate than the actual groundwater age. If degassing occurs near the point of discharge or during sampling, then $^3He_{trit}$ would be lost from the sample. In this case, correction of $^3He_{trit}$ for degassing is necessary to achieve the best estimate of groundwater age. However, these corrections are complicated because the original recharge temperature and excess air are also uncertain due to the degassing. One approach that has been used to reduce the number of unknowns is to assume a reasonable recharge temperature and excess air value—based on other groundwater samples collected in the area—and then apply the CE model to correct for degassing (Gilmore, Genereux, Solomon, & Solder, 2016).

Two additional conditions may cause challenges when using the $^3H/^3He$ method: very deep water tables (i.e., thick vadose zone) and/or very low recharge rates. A research site with a deep water table and low recharge rate may preclude the use of $^3H/^3He$ if the bulk of atmospheric ^3He has decayed prior to recharge. The vadose zone transport time is calculated as shown by Equation (22).

$$t_{vz} = \frac{L_{vz}\theta_{vz}}{q} \tag{22}$$

where:

t_{vz} = vadose zone transport time (T)

q = recharge rate (LT^{-1})

θ_{vz} = mobile water content (dimensionless)

L_{vz} = vertical distance from land surface to the water table (L)

Equation (22) can be used in many cases for a rough estimate of whether vadose zone transport is likely to exceed the applicable range for nearly complete decay of atmospheric levels of ^3H. Or, in the case of a shallower water table where recharge rate is very low, diffusion of $^3He_{trit}$ from groundwater to the gas phase in the vadose zone may dominate over the advection of $^3He_{trit}$ into the groundwater system. The $^3He_{trit}$ signal can be lost if recharge rates are about 3 mm yr^{-1} or lower. In contrast, ^3He loss is likely less than 20 percent when the recharge rate is 30 mm yr^{-1} or higher (Gilmore et al., 2021, and references in their Table 2; Solomon et al., 1993). In dual porosity settings including fractured porous rock aquifers, differential transport of ^3H and ^3He may occur due to differences in aqueous diffusion coefficients (LaBolle et al., 2006). Because ^3H and ^3He have

different diffusion coefficients, they can be separated during transport. In such system, the tracer age may not have a simple relationship to the fluid velocity.

4.7 Summary

The tritium-helium-3 age-dating method is a robust method for estimating the age of groundwater that was recharged after the mid-1900s. Because the method relies on measurement of a parent (^3H) and child product ($^3He_{trit}$) of radioactive decay, $^3H/^3He$ age dating is not reliant on a historical record of atmospheric concentrations or activities.

The process for determining groundwater tracer age (Figure 15) includes determination of $^3He_{trit}$ by first measuring ^3He in a water sample and then subtracting the ^3He components from atmospheric and terrigenic reservoirs, including ^3He from the solubility equilibrium concentration at recharge temperature and elevation, ^3He from excess air, and ^3He from terrigenic production. The method is especially sensitive to the choice of noble gas model—particularly regarding excess air—and parameters related to different reservoirs of ^3He such as the signature of terrigenic He. Measurement of ^3H is also required. For young waters without significant amounts of radiogenic He and small amounts of excess air, age uncertainties of ± 2 years are typical, but large amounts of excess air (e.g., > 10 ccSTP/kg) and uncertainty in the appropriate excess air model can lead to uncertainties greater than ten years.

Although the basic age equation for the $^3H/^3He$ method is straightforward, its application is sometimes complicated by the need to determine a relatively small value ($^3He_{trit}$) by taking the difference of two or more large values (^3He_m, $^3He_{sol}$). Thus, it is important to choose an appropriate noble gas model for the available data. Furthermore, uncertainty in very young groundwater—age less than a few years—can be large on a percentage basis. The $^3H/^3He$ age-dating method is well suited for determination of groundwater recharge rates greater than about 30 mm yr^{-1}; lower recharge rates may not allow confinement of produced $^3He_{trit}$ in the groundwater. Groundwater tracer ages from samples containing mixtures of young and old groundwater will be biased (sometimes strongly) toward the $^3H/^3He$ age of the young groundwater.

5 Sulfur Hexafluoride Dating Method

Sulfur hexafluoride (SF_6) is a relatively stable gas whose concentration in the atmosphere has been steadily increasing since the mid-1970s. Its low solubility in water combined with parts per trillion (ppt) level concentration in the atmosphere result in low, but measurable, concentrations in young groundwater. Its monotonic increase in the atmosphere makes it suitable as a transient age-tracer for waters that recharged after about 1975.

Although local sources of SF_6 do not appear to be as common as for CFCs, naturally produced SF_6 can limit the dating range of this tracer in some hydrogeologic environments. Sample collection is relatively simple and the measurement of SF_6 is less complex than ^3H and noble gases. A significant theoretical advantage of the SF_6 dating method is that since about 1980 the increase in atmospheric concentration has been nearly linear with time. As a result, the computed tracer age represents the flow-weighted average age of the mixture (i.e., there is minimal bias toward one end member).

In addition to groundwater dating, SF_6 has been used as an injected tracer in surface and groundwater systems. The very low detection limit of SF_6 combined with its inertness, availability, and low cost make it an attractive injected tracer. It has been used in streams to evaluate gas exchange in support of using radon as a tracer of groundwater seepage (Cook, Lamontage, et al., 2006; Wanninkhof et al., 1990). Because the injected concentrations typically exceed concentrations derived from the atmosphere by many orders of magnitude, groundwater dating in the vicinity of an injected SF_6 tracer test is usually problematic. An excellent summary of SF_6 dating including sampling and analytical methods and natural sources of SF_6 is provided by Busenberg and Plummer (2000).

5.1 Background and Historical Development

SF_6 is a colorless, odorless, and nonflammable gas that is commonly used as an electrical insulator and blanket gas in high-temperature metal working operations. It has an octahedral geometry and is relatively stable in the atmosphere with an estimated lifetime of more than 1,000 years (Kovács et al., 2017). Industrial production of SF_6 began in 1953 with a reported production of 9.04 Gg/yr in 2018, most of which was from the electrical power industry (Simmonds et al., 2020). Natural sources of SF_6 to the atmosphere appear to be small but may be significant for groundwater as discussed in Section 6.6 (Harnisch & Eisenhauer, 1998; Busenberg & Plummer, 2000).

SF_6 is a potent greenhouse gas with warming potential that is 23,900 times that of CO_2 (Intergovernmental Panel on Climate Change, 1995). Although SF_6 was included in the Kyoto Protocol to the UN Framework Convention on Climate Change (UN, 1998), controls on releases apply only to developed countries. As of 2018, atmospheric concentrations continue to rise with no sign of a decline in the annual rate of rise.

The natural background concentration (i.e., atmospheric concentration prior to 1953) of SF_6 has been estimated to be between 0.001 and 0.04 parts per trillion by volume (pptv) (Harnisch & Eisenhauer, 1998; Maiss & Brenninkmeijer, 1998). The earliest measurements of atmospheric SF_6 in the 1970s reported values of less than 1 ppt (Krey et al., 1977; Lovelock, 1971). Watson and Liddicoat (1985) reconstructed the atmospheric history of SF_6 for the 1970s and early 1980s using depth profiles from the ocean.

Routine measurements of atmospheric SF_6 began in 1995 as part of the Global Monitoring Laboratory (GML) of the National Oceanic and Atmospheric Administration (NOAA) in the USA. The atmospheric mixing ratio[1] for SF_6 in both the northern and southern hemispheres is shown in Figure 20. The southern hemisphere curve lags the northern hemisphere by about 1.5 years because more SF_6 sources are in the northern hemisphere and interhemispheric mixing is slow. Since the mid-1980s the atmospheric concentration has increased by seven to eight percent each year.

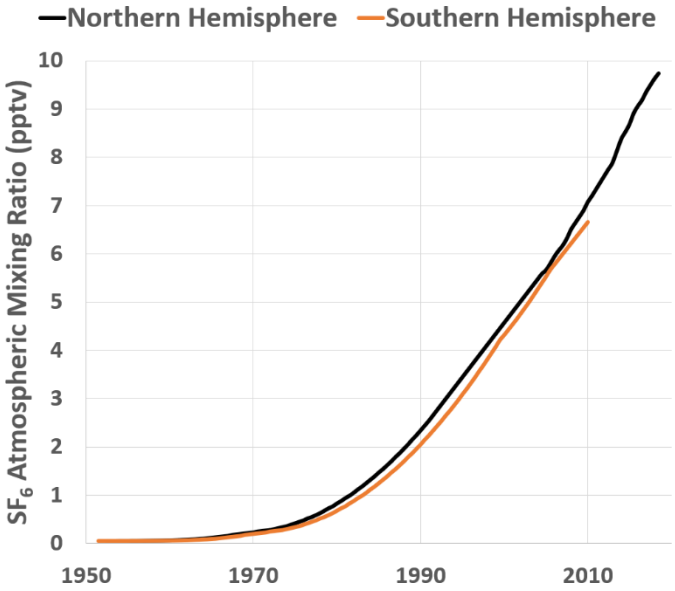

Figure 20 - SF_6 atmospheric mixing ratio for northern and southern hemispheres. Since the mid-1980s, the annual increase has been approximately seven to eight percent.

Biodegradation and sorption of SF_6 in the subsurface do not appear to be significant (Wilson & Mackay, 1996) and, as SF_6 is not used in common household products, neither is contamination of groundwater in urban regions (Busenberg & Plummer, 2000).

[1] In atmospheric science, it is common to express gas concentrations as a mixing ratio, which is the moles of a given gas divided by the moles of all other gases in a mixture. The mole fraction is the moles of a given gas divided by the moles of all gases—including the given gas—in the mixture. When the moles of a given gas are much less than the total (i.e., for trace gases), the mixing ratio and mole fraction are essentially equivalent.

5.2 Basic Concepts and Systematics

Lovelock (1971) was the first to recognize the potential of SF_6 as a tracer in the atmosphere and oceans. Busenberg and Plummer (2000) reported SF_6 measurements in groundwater and described its use as a dating tool. The basic concept of SF_6 dating is shown in Figure 21. Samples are collected such that they do not contact the atmosphere. The aqueous concentration is measured by gas chromatography after the SF_6 has been extracted (stripped) from the water sample. The aqueous concentration is then converted into an air concentration using Henry's Law (i.e., the air concentration that is in equilibrium with the measured aqueous concentration at assumed temperature, pressure, and salinity at recharge). The equivalent air concentration is then compared to the atmospheric concentration curve to estimate the year the sample was last in contact with the atmosphere (the recharge year). The tracer age is simply the sample collection date minus the recharge year. The conversion from an aqueous concentration to an equivalent air concentration, or *mixing ratio*, utilizes Henry's Law with a coefficient that is temperature dependent.

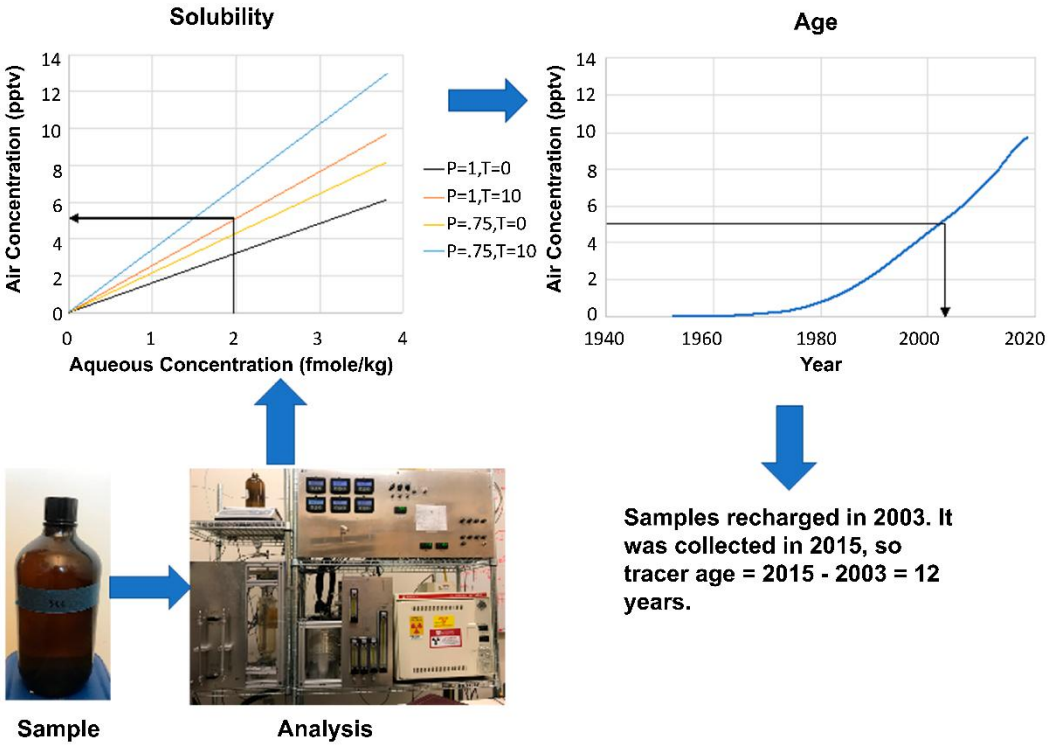

Figure 21 - General concept of groundwater dating with SF_6. The aqueous concentration of SF_6 is measured by gas chromatography. Using estimates of the recharge temperature and pressure (elevation) the aqueous concentration is converted to the air concentration (i.e., the concentration in air that would be in equilibrium with the measured aqueous concentration at the temperature and pressure when the sample was at the water table). Using the atmospheric concentration curve, the air concentration is converted into a recharge year. For a water sample with an aqueous concentration of 2 femtomole/kg that recharged at a pressure of 1 atm (i.e., sea level) with a water table temperature of 10 °C—and assuming no excess air—the equivalent air concentration would be about 5.1 pptv. The atmosphere had a concentration of 5.1 pptv in 2003 and the sample was collected in 2015. Thus, the tracer age is 2015 − 2003 = 12 years.

The example solubility curves shown in Figure 21 were computed for two recharge temperatures and two recharge pressures (elevations). In practice, a solubility curve is computed for the exact recharge temperature and pressure conditions for a sample. Also, the measured concentration can include excess air, as discussed in Section 2, that needs to be removed from the measured concentration before an equivalent air concentration is computed as presented in Section 5.4.

5.3 Sample Collection and Analysis

Like all dissolved gas tracers, samples for SF_6 must be collected such that gas exchange with the atmosphere does not occur and bubbles are not trapped within the sample container. Numerous sample containers have been used including custom-made metal cylinders with valves on each end (Figure 22). A simple and effective sampling method uses a one-liter glass bottle with a narrow mouth as shown in Figure 22. The bottles are filled using a submersible pump with the discharge tube extending to near the bottom of the bottle. The bottle is purged with 3 to 4 L of water before slowly removing the discharge tube such that the bottle is totally filled—no headspace is left. A polyethylene cone-shaped liner inside a cap (i.e., a *polyseal* cap), is then installed onto the bottle. The cone-shaped liner displaces a small amount of water that was at the water–atmosphere interface upon installation, resulting in minimal contamination of the remaining water by the modern atmosphere.

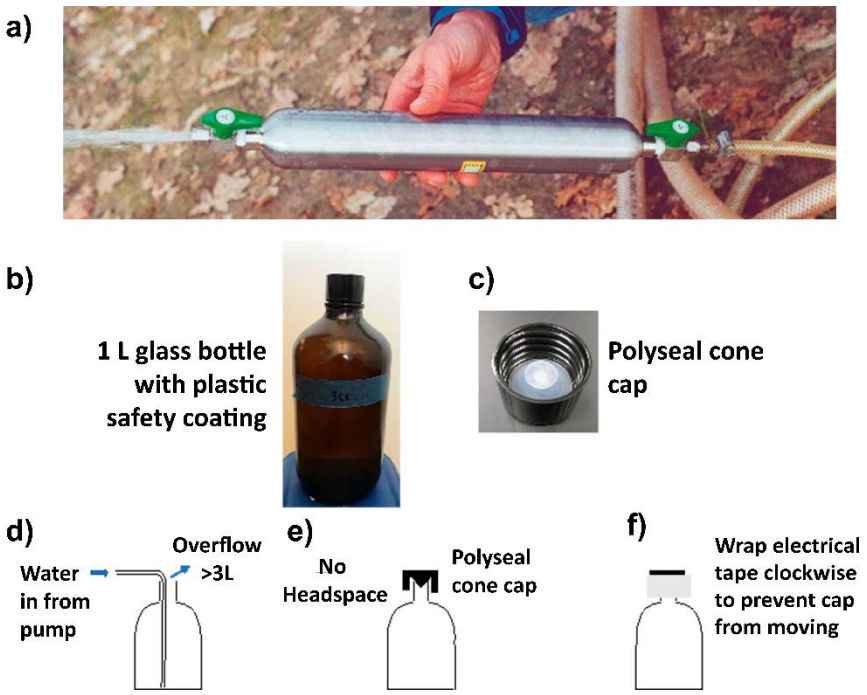

Figure 22 - Sampling SF_6 a) stainless steel cylinder for SF_6 samples and b) glass narrow-mouth bottle with c) *polyseal* cone-shaped cap. Samples for the bottles should be filled by d) inserting a tube to the bottom and flushing more than 3L, then e) installing the cap with no headspace and f) wrapping electrical tape counterclockwise around the cap to prevent it from moving,

Headspace and purge-and-trap are the two primary analytical methods used for SF_6 age dating. The headspace technique introduces a known amount of SF_6 free gas into a sample container of known volume. The container is shaken resulting in a partitioning of SF_6 between the water and gas headspace. Because of its low solubility, there is a strong preference for SF_6 to reside in the gas phase. After equilibration, the headspace gas is subsampled with a syringe or gas sampling valve and then quantified with a *gas chromatograph* (GC) using an electron capture detector.

With the purge-and-trap technique, a known amount of water is introduced into a sparging chamber. SF_6-free carrier gas—typically N_2 or He—is bubbled through the water inside the sparging chamber and then through a trap that retains SF_6 but not the carrier gas or oxygen. Traps are typically filled with a porous polymer (e.g., Porapak™ Q) and are held at −70 to −80 °C. After sufficient stripping, the trap is warmed to release SF_6, which is then routed into a GC for analysis.

Both the headspace and purge-and-trap methods have been used for low-level SF_6 analyses (Bullister & Wisegarver, 2008; Busenberg & Plummer, 2000; Busenberg & Plummer, 2010; Wanninkhof et al., 1987; Wanninkhof et al., 1991). The headspace method is particularly useful for higher concentrations that exist in injected tracer studies (Clark et al., 1994; Cook, Lamontagne, et al., 2006; Wanninkhof et al., 1990).

5.4 Calculation of Tracer Age

As a transient tracer, the general concept of SF_6 dating involves comparing a measured concentration in a water sample with historical concentrations in the atmosphere. Henry's Law is used to relate the measured aqueous concentration of a sample to the equilibrium gas-phase concentration. Because the Henry Coefficient is temperature dependent, and because the partial pressure of SF_6 in the atmosphere depends on total pressure, both the recharge temperature and pressure (i.e., elevation) are needed for age dating. Furthermore, if groundwater contains excess air, and therefore some excess SF_6 above equilibrium solubility, the amount of excess air is also required.

The temperature and salinity dependence of the Henry Coefficient was investigated by Bullister and others (2002), who provided an empirical equation for calculating the equilibrium constant (K_h) for the solubility form of Henry's Law as shown by Equation (23).

$$C = K_h(T,S)\big(P - e(T)\big) \tag{23}$$

where:

C = aqueous concentration ($molM^{-1}$, typically in moles/kg)

K_h = temperature- and salinity-dependent equilibrium constant ($molM^{-2}LT^2$ typically in moles kg^{-1} atm^{-1})

x = dry air mole fraction (dimensionless)

P = atmospheric pressure ($ML^{-1}T^{-2}$, typically in atm)

e = temperature dependent vapor pressure of water ($ML^{-1}T^{-2}$, typically in atm)

Values for K_h and e at various temperatures for fresh water are shown in Table **6**. If the recharge temperature (T), salinity (S), and elevation (and hence P) are known, Equation (23) can be solved for the dry air mole fraction (x) and then x can be computed for a measured aqueous concentration. The dry air mole fraction can then be compared to the history of SF_6 in the atmosphere to obtain a recharge date as illustrated in Figure 21.

Table 6 - Values of K_h for SF_6 and water vapor (e) at various temperatures for fresh water (salinity = 0).

Temperature (°C)	K_h [mole kg^{-1} atm^{-1}]	e [atm]
0	0.0006216	0.0060
10	0.0003969	0.0121
20	0.0002739	0.0230
30	0.0002023	0.0418
40	0.0001587	0.0726

K_h from Bullister and others (2002)
e from Antoine (1888) and Section 2.3 of this book

Equation (23) represents equilibrium conditions and does not include the effects of excess air. Solomon and others (2010) derived an expression for the dry-air mole fraction—which is essentially equivalent to the mixing ratio—that includes excess air as given by the CE model presented in Section 2.2 and Equation (24).

$$x = \frac{C}{K_h(P-e) + \dfrac{(1-F)A}{1 + \dfrac{FA}{K_h(P-e)}}} \tag{24}$$

where:

x = dry air mole fraction (dimensionless)

C = aqueous concentration ($molM^{-1}$, typically in mole/kg)

K_h = temperature- and salinity-dependent equilibrium constant ($molM^{-2}LT^2$ typically in moles $kg^{-1}atm^{-1}$)

P = atmospheric pressure ($ML^{-1}T^{-2}$, typically in atm)

e = temperature-dependent vapor pressure of water ($ML^{-1}T^{-2}$, typically in atm)

A = volume of gas trapped in the porous media per unit mass of water ($molM^{-1}$, typically in moles/kg)

F = fractionation factor (dimensionless)

As discussed in Section 2, when gas bubbles completely dissolve, the fractionation factor (F) is 0 and the CE model reverts to the UA model; such that Equation (20) becomes Equation (25).

$$x = \frac{C}{K_h(P - e) + A'} \tag{25}$$

where:

A' = amount of excess air dissolved per unit mass of water (molM^{-1}, typically in moles/kg)

As discussed in Section 2.6, A in Equation (24) and A' in Equation (25) are not generally equivalent except when air bubbles are fully dissolved as represented by $F = 0$.

A general procedure for calculating a tracer age using SF_6 is as follows:

1. Measure the aqueous concentration (C) of SF_6 in a groundwater sample.
2. Estimate the recharge elevation (Z) of the sample.
3. Compute the recharge pressure (P) using Equation (5): $P = P_0 \exp\left(-\frac{Z}{Z_s}\right)$ where P_0 is the pressure at $Z = 0$ (1 atm) and Z_s is a scaling factor (Z_s = 8,300 m for Z < 1,800 m).
4. Estimate the recharge temperature for the sample. This could utilize noble gas thermometry, if available, or could be taken as the average annual temperature of the recharge zone for the sample.
5. Estimate the recharge salinity for the sample. In many cases this is assumed to be zero for fresh water in the recharge area.
6. Compute the equilibrium constant (K_h) for the temperature and salinity of the recharge area. This could be computed using the equations of Bullister and others (2002) or could be approximated from the values given in Table **6**.
7. Compute the vapor pressure of water (e) at the recharge temperature. This could be computed using empirical equations such as Antoine (1888; Section 2.3) or could be interpolated from the values given in Table **6**.
8. Estimate the amount of excess air in the sample. If noble gas data are available, the values of A and F for the CE model or A' for the UA model can be obtained by fitting theoretical values to measured values as discussed in Section 2.6. The units for A or A' must match those of C. If a noble gas model provides A or A' in units of ccSTP/g, these can be converted to mole/g by dividing by the molar volume of an ideal gas (22414 ml/mole).
9. Compute the mole fraction (x) of SF_6 in the atmosphere that would have resulted in the measured aqueous concentration using (24) for the CE model or Equation (25) for the UA model.

10. Compare the computed mole fraction—which is essentially equivalent to the mixing ratio—to the atmospheric history (Figure 20) to derive the estimated year the sample recharged.
11. Compute the age as sample date minus recharge year.

Exercise 7 provides an opportunity to practice calculating tracer age using SF_6.

5.5 Sensitivity of Age to Input Parameters

The procedure outlined in Section 5.4 for calculating a tracer age from a measured concentration of SF_6 involves numerous parameters—recharge temperature, salinity, elevation, and excess air—that are uncertain to some degree. In this section, we summarize the sensitivity of the computed age to uncertainty in some of these parameters.

Figure 23 shows the relationship between the SF_6 tracer age and various input parameters for a water sample having an aqueous concentration of 1.0 fmole/kg SF_6. An fmole is a femtomole which is an amount of substance equal to 10^{-15} moles. The sample was assumed to have been collected in the year 2015, and the age was calculated as 2015 minus the computed recharge year. The recharge temperature, recharge elevation, and amount of UA were varied to illustrate the sensitivity of the computed age to these parameters. The sensitivity of the tracer age to recharge temperature is about -0.5 year/°C between recharge temperatures ranging from 0 to 40 °C. In other words, if the assumed recharge temperature was 1 °C warmer than the true value, the tracer age would be 0.5 years younger than the true age. The sensitivity to recharge elevation is about -0.3 year/100 m; thus, using a recharge elevation that is 100 m greater than the true elevation results in an age that is 0.3 years younger. The sensitivity of the age to excess air is not constant but instead is about 2 year/(ml kg^{-1}) for smaller amounts of excess air and decreases to about 0.3 year/(ml kg^{-1}) for excess air greater than 20 ml/kg.

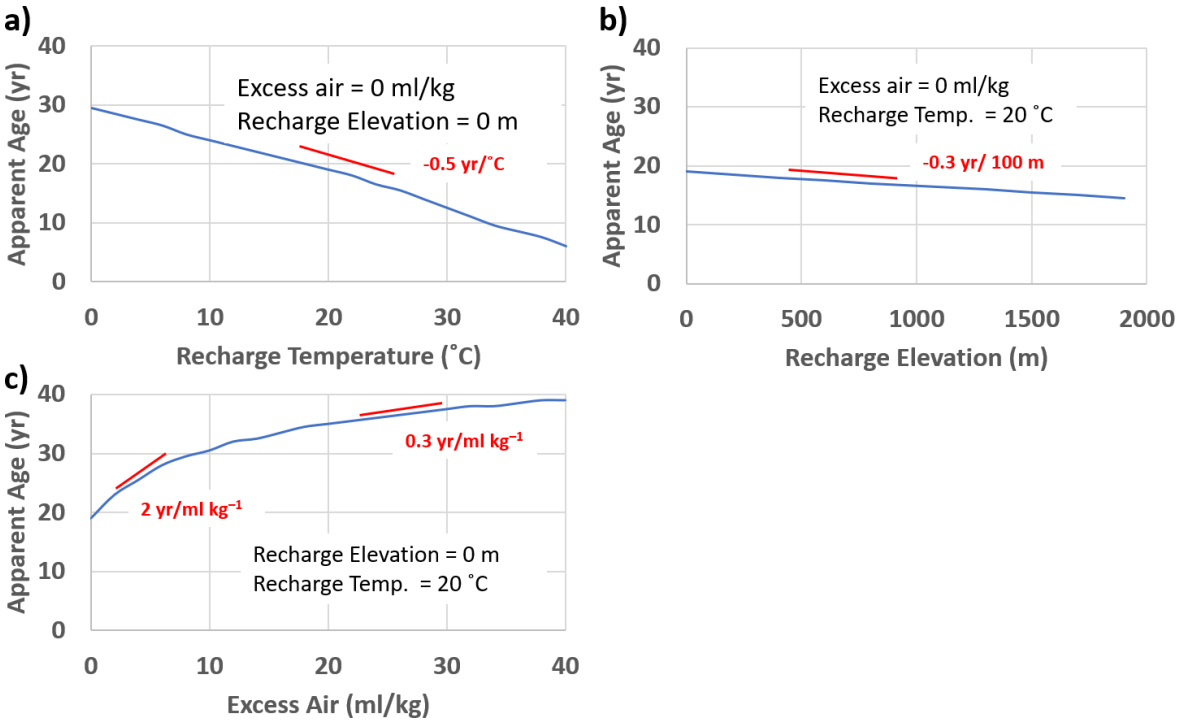

Figure 23 - Sensitivity of SF_6 tracer age (i.e., apparent age) to input parameters. The tracer age of a hypothetical sample collected in 2015 and having a SF_6 concentration of 1.0 fmole/kg was computed for various values of recharge temperature, recharge elevation, and excess air as indicated. The sensitivities (change in age per change in parameter) are shown in red.

The considerable sensitivity of SF_6 tracer ages to excess air suggests that precise dating with this method requires an actual measurement of excess air. As discussed in Section 2.6, the dissolved Ne concentration, expressed as ΔNe, is a sensitive indicator of excess air. For UA, a ΔNe of ten percent is equal to about 1 ml/kg of excess air. ΔNe values between 20 and 50 percent are common in groundwater (Aeschbach-Hertig & Solomon, 2013), and values greater than 200 percent have been reported (Solomon et al., 2011). For the water sample illustrated in Figure 21, a ΔNe of 50 percent, if not accounted for, would lead to an error of more than 30 percent in the calculated age. If a direct measure of excess air is not available, SF_6 dating can still be useful, but it is important to include the uncertainty in the estimated age that results from the uncertainty in excess air, along with the uncertainty in all other assumed parameters and measurement errors.

5.6 Discussion of Tracer-Specific Issues

Aside from the uncertainty in age discussed in Section 5.5, a significant limitation of the SF_6 dating method results from subsurface sources referred to as *terrigenic* SF_6. For example, Harnisch and Eisenhauer (1998) found SF_6 in naturally occurring fluorite and igneous rocks containing fluorite. Busenberg and Plummer (2000) measured SF_6 concentrations in excess of atmospheric solubility in hot springs located in volcanic areas that indicated the existence of a natural subsurface source. Busenberg and Plummer (2000) extracted SF_6 from fluid inclusions in crushed rocks and minerals and found detectible

amounts in most of the samples tested, especially those from igneous rocks. Koh and others (2007) found evidence for terrigenic SF_6 on Jeju Island, Korea (which is of volcanic origin), by comparing SF_6 tracer ages with ages from CFC-12. They found that SF_6 ages were biased young relative to CFC-12 ages by typically 20 years but as much as 30 years.

The presence of terrigenic SF_6 is obvious when aqueous concentrations exceed the solubility plus excess air concentration for modern water. Small additions of terrigenic SF_6 that bias age are much harder to discern. As a practical matter, an SF_6 tracer age should be considered a minimum age unless the presence of terrigenic SF_6 can be ruled out. Potential ways to evaluate the existence of terrigenic SF_6 include the following.

- Use of multiple age-dating tracers (e.g., Koh et al., 2007).
- Collection of a spectrum of SF_6 concentrations from a specific hydrogeologic system in which the distribution trends to less than 0.04 pptv (atmospheric equivalent value) for the oldest samples.
- Observation of a favorable comparison between quantities such as recharge rate derived from SF_6 and physical methods (e.g., water balance; Solomon et al., 2015).
- Ruling out the existence of volcanic and/or igneous rocks along groundwater flow paths.

5.7 Summary

SF_6 is a relatively stable gas and the atmospheric concentration has been monotonically increasing since the mid-1950s. As a transient age-dating tracer, SF_6 benefits from nearly linear increase in the atmosphere of seven to eight percent per year since about 1980. Its low solubility in water combined with ppt-level concentration in the atmosphere result in low but measurable concentrations in young groundwater.

Further, measurement of SF_6, while still somewhat specialized, is less complicated than with tracers such as ^3H and noble gases. The process of calculating a tracer age involves measuring an aqueous concentration, calculating the atmospheric (gas-phase) concentration that would be in equilibrium—after correcting for excess air—with the aqueous concentration, and comparing the atmospheric-equivalent value with the history of SF_6 in the atmosphere.

The primary limitation to SF_6 dating is uncertainty that results from the amount of excess air in a sample, and from the existence of terrigenic SF_6. Despite these limitations, excellent agreement between SF_6 ages and CFC ages (e.g., Busenberg & Plummer, 2000) and $^3H/^3He$ ages (e.g., Solomon et al., 2015) have been reported. When samples contain less than about 2 ml/kg of excess air and no terrigenic sources, age uncertainties of $\pm$ 5 years are typical for SF_6 dating.

While SF_6 is a potent greenhouse gas and was included in the Kyoto Protocol, there is currently no indication that the rate of atmospheric growth is declining. From a

groundwater-dating point of view, higher atmospheric values are 1) easier to measure, and 2) tend to minimize complications due to terrigenic sources. As such, SF_6 is likely to become an increasingly common dating method in the future.

6 Chlorofluorocarbon Dating Method

Chlorofluorocarbons (CFCs) are compounds that were first synthesized in the late 1920s as refrigerants to replace more toxic compounds such as ammonia and methyl chloride. The term CFCs is used for a range of compounds containing carbon, chlorine, and fluorine. The most-used CFCs for groundwater dating have been dichlorodifluoromethane (CF_2Cl_2, known as CFC-12), trichlorofluoromethane ($CFCl_3$, known as CFC-11), and trichlorotrifluoroethane ($C_2F_3Cl_3$, known as CFC-113).

Atmospheric concentrations of CFCs began rising in the 1940s and received considerable attention in the 1970s as agents of ozone depletion (Molina & Rowland, 1974). Beginning in 1987, many industrial countries agreed to phase out the use of CFCs as part of the Montreal Protocol on Substances that Deplete the Ozone Layer (United Nations Environmental Programme, 1987). As a result, the atmospheric concentrations of CFC-11, CFC-12, and CFC-113 peaked in 1994, 2001, and 1996, respectively (Montzka et al., 1999; Plummer & Busenberg, 2006).

The rise in atmospheric CFC concentrations through the second half of the twentieth century created an opportunity for groundwater dating (Busenberg & Plummer, 1992). Although the decline in atmospheric concentrations in the twenty-first century has created a non-uniqueness in relationship between age versus concentration, CFCs continue to be a useful dating tool for waters that recharged between about 1940 to 1990.

A comprehensive guide book on the use of CFCs for groundwater dating↗ is available from the IAEA. In addition to covering the basic concepts of CFC groundwater dating (Plummer, Busenberg, & Cook, 2006), this guidebook covers effects and processes that can modify CFC tracer ages (Cook, Plummer, et al., 2006), binary mixtures of young and old waters (Plummer, Busenberg, & Han, 2006), models of groundwater age and residence times (Solomon, Cook, & Plummer, 2006), applications of CFCs in groundwater studies (Solomon, Plummer, et al., 2006), case studies (Plummer, Busenberg, Cook, Oster, et al., 2006), comparison with other dating methods (Han et al., 2006), and sampling and analytical methods (Busenberg et al., 2006). Because of the existence and availability of this guidebook, only a summary of the basic concepts, sample collection/analysis, and interpretations is included in this section. Readers who intend to use CFCs in their research are strongly advised to review the guidebook.

6.1 Background and Historical Development

Chlorofluorocarbons are synthetic gases that are relatively stable in both the atmosphere and subsurface. Industrial production of CFCs began in the 1930s as refrigerants for cooling devices; in the 1940s, they were widely used as propellants, solvents, degreasers, and blowing agents for plastic foam. Atmospheric lifetimes of CFC-11, CFC-12, and CFC-113 are 45 ±7, 87 ±17, and 100 ±32 years respectively (Volk et al, 1997).

As a result of widespread production and long atmospheric lifetimes, CFC concentration in the atmosphere began to rise in the 1940s.

The first measurements of CFCs in the atmosphere were reported in 1971 after the invention of the *electron capture detector* (ECD; Lovelock, 1971). Atmospheric concentrations prior to 1971 have been reconstructed. This is possible because

1. CFCs are synthetic compounds without natural sources (i.e., concentrations prior to 1920 were zero),
2. records exist of CFCs produced,
3. concentrations in firn (i.e., granular snow on a glacier) air from glaciers have been measured, and
4. numerical simulations have been performed (Plummer & Busenberg, 2006, and the references cited in their chapter).

Lovelock and others (1973) reported CFC-11 concentrations in both air and seawater and suggested that CFCs could be used as a tracer in ocean circulation studies. The continued production of CFCs through the mid-1980s led to a monotonic increase in atmospheric concentrations and thus recharging water was imprinted with a unique CFC concentration each year. However, the realization that CFCs were a primary contributor to stratospheric ozone depletion (Molina & Rowland, 1974) resulted in an agreement among many industrialized nations to limit the release of CFCs, which ultimately resulted in a peaking and subsequent decline in atmospheric CFC concentrations (Figure 24).

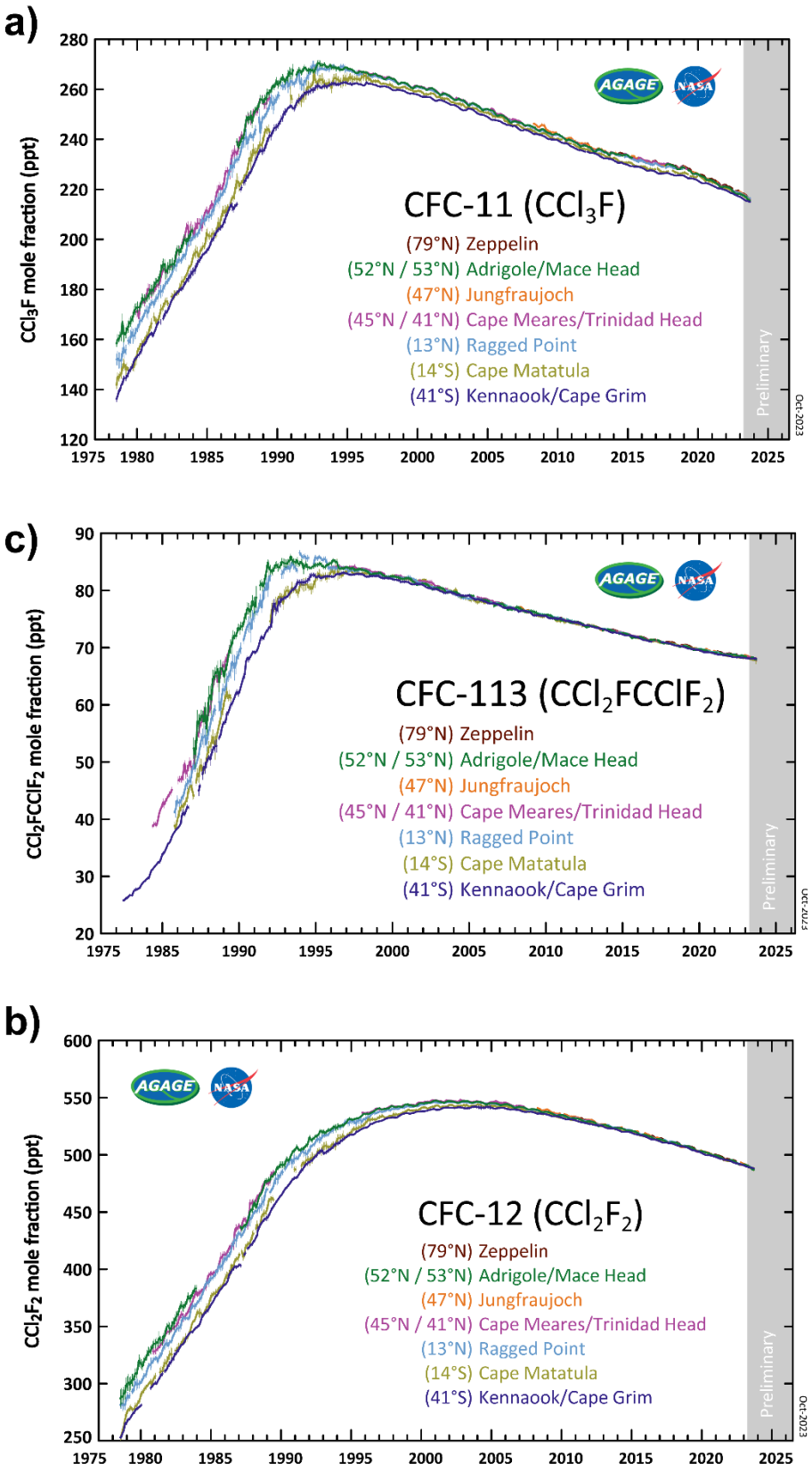

Figure 24 - Measured CFC atmospheric mixing ratio for northern and southern hemispheres for the period between 1975 and the early 2020s. Earlier, atmospheric concentrations have been reconstructed using production records and ocean samples (redrawn from http://agage.mit.edu/).

The production of CFCs occurred mostly in the northern hemisphere between 30° N and 70° N (Hartley et al, 1996). This resulted in higher atmospheric concentrations in the northern versus southern hemisphere from the 1940s to 2000. However, because atmospheric lifetimes are much longer than interhemispheric mixing, these differences are much less than tritium, and declining production has resulted in an essentially negligible difference since about 2000. In urban areas, however, CFC concentrations in air are often elevated due to local sources. For example, CFC-11 and CFC-12 were elevated by 125 percent and 62 percent above the northern hemisphere average in Heidelberg, Germany (Oster et al., 1996). Ho and others (1998) observed enrichments of between six and 13 percent in the air of New York City, New York, USA.

6.2 Basic Concepts and Systematics

The potential for CFCs to function as groundwater tracers was first demonstrated in the 1970s. For example, Thompson and others (1974) injected CFC-11 into a sand and gravel aquifer and detected its arrival at monitoring wells in accord with expected groundwater travel times. Similarly, Shultz and others (1976) showed that CFCs were a useful tracer of groundwater recharge from sewage effluent.

Starting in the early 1980s, CFCs were used as tracers of ocean circulation and dynamics (e.g., Bullister, 1989). New analytical methods for water samples were developed for the simultaneous analysis of multiple CFCs (e.g., Bullister & Weiss, 1988), and the solubilities of CFC-11 and CFC-12 were measured with high precision (Warner & Weiss, 1985). Advances in sample collection procedures and evaluations of the usefulness of CFCs as a groundwater dating tracer followed in the 1990s (Busenberg & Plummer, 1992; Cook et al., 1995; Ekwurzel et al. 1994). Further applications of CFC dating for constraining groundwater flow models (e.g., Reilly et al., 1994), tracing nitrate contamination (Böhlke & Denver, 1995) and tracing leakage from sinkholes in karst systems (Katz et al., 1995) helped to further refine and articulate the usefulness of the CFC method.

The basic concept for CFC dating is like SF_6 and is shown in Figure 25. Samples are collected such that they do not contact the atmosphere. The aqueous concentration is measured by gas chromatography after the CFCs have been extracted (stripped) from the water sample. The aqueous concentration is then converted into an air concentration using Henry's Law (i.e., the air concentration that is in equilibrium with the measured aqueous concentration at an assumed temperature, pressure, and salinity at recharge). The equivalent air concentration is then compared to the atmospheric concentration curve to estimate the year the sample was last in contact with the atmosphere (i.e., the recharge year). The tracer age is then the sample collection date minus the recharge year.

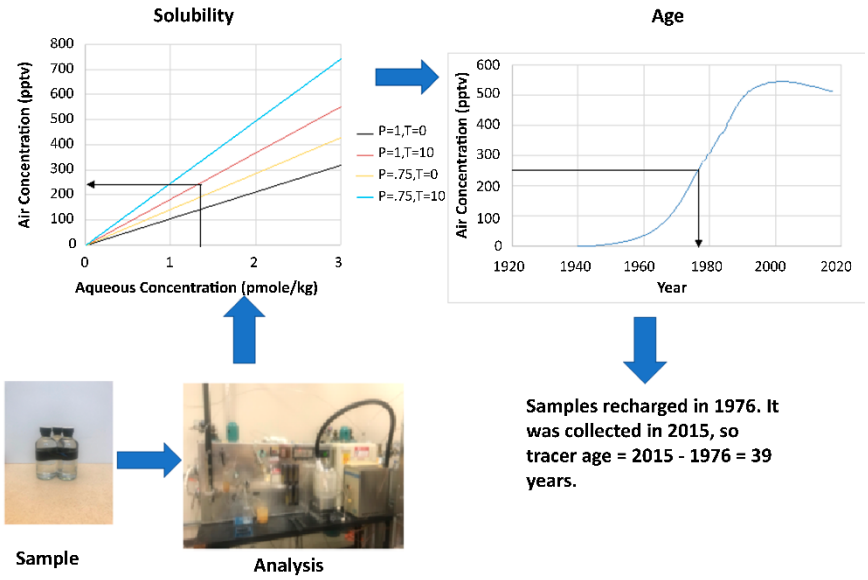

Figure 25 - General concept of groundwater dating with CFCs. The aqueous concentration of CFCs (above examples are for CFC-12) is measured by gas chromatography. Using estimates of the recharge temperature and pressure (i.e., elevation) the aqueous concentration is converted to the air concentration (i.e., the concentration in air that would be in equilibrium with the measured aqueous concentration at the temperature and pressure when the sample was at the water table). Using the atmospheric concentration curve for CFC-12, the air concentration is converted into a recharge year. For a water sample with an aqueous concentration of 1.3 pmole/kg (i.e., picomoles per kg) that recharged at a pressure of 1 atm (i.e., sea level) with a water table temperature of 10 °C—and assuming no excess air—the equivalent air concentration would be about 250 pptv. The atmosphere had a concentration of 250 pptv in 1976, and the sample was collected in 2015. Thus, the tracer age is 2015 − 1976 = 39 years.

The conversion from an aqueous concentration to an equivalent air concentration (mixing ratio) utilizes Henry's Law with a coefficient that is temperature dependent. The example solubility curves shown in Figure 25 were computed for two recharge temperatures and two recharge pressures (i.e., elevations). In practice, a solubility curve is computed for the exact recharge temperature and pressure conditions for a sample. Also, the measured concentration can include excess air (Section 2.6) that theoretically should be removed from the measured concentration before an equivalent air concentration is computed. However, because CFCs are much more soluble than SF_6 and light noble gases, this correction is usually minor and is often neglected.

6.3 Sample Collection and Analysis

The primary source of CFCs in groundwater is the atmosphere, so care must be taken to eliminate contact between the sample and the atmosphere. Furthermore, CFCs from the atmosphere tend to sorb onto sampling equipment—especially items made of plastic—and desorption can artificially elevate CFC concentrations. Non-porous materials such as metal and glass are recommended over plastic materials whenever possible. A simple and effective sampling method uses a 125 mL glass bottle with a narrow mouth as shown in Figure 26. The bottles and foil-lined caps are placed inside a secondary beaker—

approximately 2L in volume—and both the bottle, and the beaker are filled using a submersible pump with the discharge tube extending to near the bottom of the bottle as shown in Figure 26. The sample bottle and beaker are purged with 3 to 4L of water before removing the discharge tube. The foil-lined cap is installed underwater to eliminate any contact with the atmosphere.

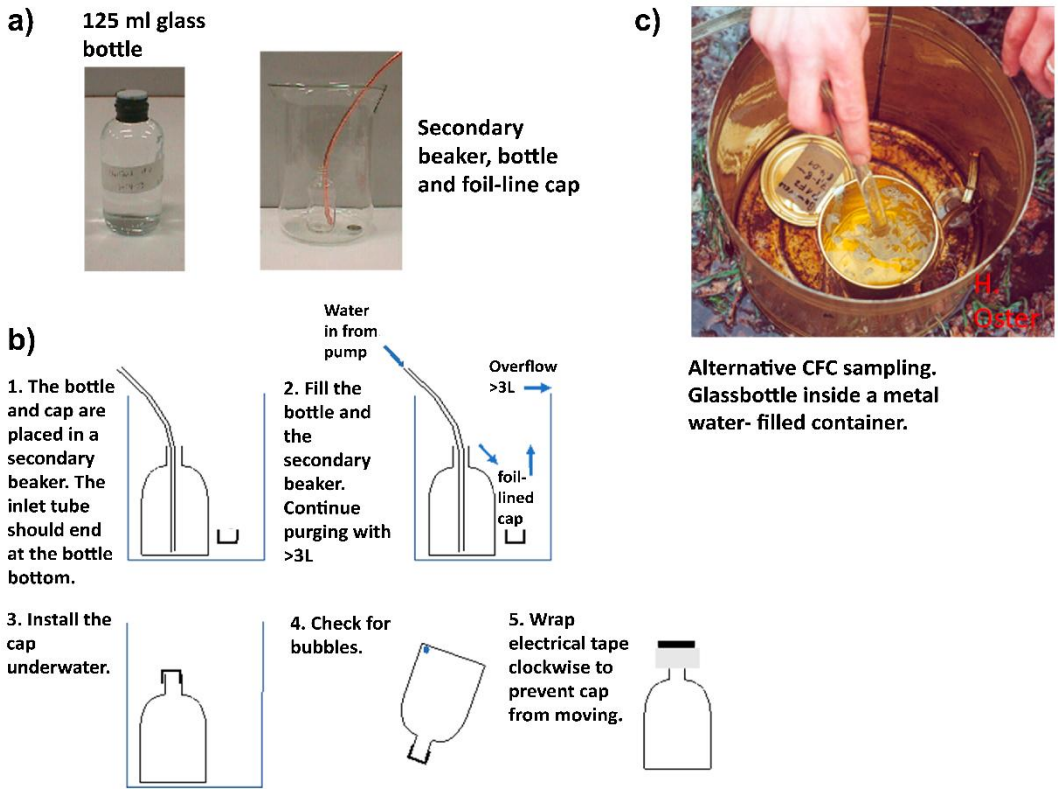

Figure 26 - Sampling water for CFCs. a) Narrow-mouth glass bottle with foil-lined cap. b) Bottles should be filled by inserting a tube to the bottom, flushing more than 3L, and then installing the cap with no headspace. c) Alternatively, a metal container can be used instead of the beaker of (b).

The purge-and-trap method is typically used to analyze CFCs because of their relatively high solubility in water. CFC-free carrier gas—typically N_2 or He—is bubbled through the water inside a sparging chamber and then through a trap that retains CFCs but not the carrier gas or oxygen. Traps are typically filled with a porous polymer and are held at about −30 °C. After sufficient stripping, the trap is warmed to release CFCs, which are then routed into a GC for analysis. Both packed and capillary columns have been used and typically CFC-11, CFC-12, and CFC-113 can be analyzed in a single run. Because of the possibility of sample contamination during sampling, CFCs are often analyzed in triplicate or more.

6.4 Calculation of Tracer Age

The calculation of CFC tracer ages is similar to that of SF_6. The procedure involves comparing a measured concentration in a water sample with historical concentrations in the atmosphere. Henry's Law is used to relate the measured aqueous concentration of a

sample to the equilibrium gas-phase concentration. Because the Henry Coefficient is temperature dependent, and because the partial pressure of CFCs in the atmosphere depends on total pressure, both the recharge temperature and pressure (i.e., elevation) are needed for age dating.

If groundwater contains excess air and, therefore, some excess CFCs above equilibrium solubility, the amount of excess air could be subtracted from the measured concentration. However, because CFCs are much more soluble than tracers such as SF_6, corrections for excess air are seldom made. For example, the calculated age of a sample that recharged in 1975 with 5 cc/kg—ΔNe of 45 percent, which is moderately large—would change by less than one year for CFC-11, CFC-12, and CFC-113.

The temperature and salinity dependence of the Henry Coefficient was investigated by Warner and Weiss (1985) and Bu and Warner (1995) who provided empirical equations for calculating the equilibrium constant (K_h) for the solubility form of Henry's Law expressed by Equation (23) in Section 5.4.

Values for K_h and e at various temperatures for fresh water are shown in Table 7. If the recharge temperature (T), salinity (S), and elevation—hence P—are known, Equation (26) [i.e., $C = K_h(T,S)x\big(P - e(T)\big)$] can be solved for the dry air mole fraction (x) and then x can be computed for a measured aqueous concentration (C) as shown in Equation (26). The dry air mole fraction can then be compared to the history of the CFCs in the atmosphere to obtain a recharge date as illustrated in Figure 25.

$$x = \frac{C}{K_h(T,S)\big(P - e(T)\big)} \tag{26}$$

Table 7 - Values of K_h for CFC-11, CFC-12, CFC-113, and water vapor (e) at various temperatures for fresh water (salinity = 0).

Temperature (°C)	K_h CFC-11 mol kg^{-1}atm^{-1}	K_h CFC-12 mol kg^{-1}atm^{-1}	K_h CFC-113 mol kg^{-1}atm^{-1}	e atm
0	0.03871	0.00942	0.01263	0.0060
10	0.02113	0.00548	0.00653	0.0121
20	0.01288	0.00353	0.00378	0.0230
30	0.00865	0.00247	0.00241	0.0418
40	0.00633	0.00187	0.00168	0.0726

K_h for CFC-11 and CFC-12 from Warner and Weiss (1985); K_h for CFC-113 from Bu and Warner (1995); e from Antoine (1888) and Equation (6) of this book.

A general procedure for calculating a tracer age for CFCs is as follows:

1. Measure the aqueous concentration (C) in a groundwater sample.
2. Estimate the recharge elevation (Z) of the sample.
3. Compute the recharge pressure (P) using Equation (5) in Section 2.3 of this book.
4. Estimate the recharge temperature for the sample. This could use noble gas thermometry, if available, or could be taken as the average annual temperature of the recharge zone for the sample.
5. Estimate the recharge salinity for the sample. In many cases, this is assumed to be zero for fresh water in the recharge area.
6. Compute the equilibrium constant (K_h) for the temperature and salinity of the recharge area. This could be computed using the equations of Warner and Weiss (1985) and Bu and Warner (1995), or could be approximated from the values given in Table 7.
7. Compute the vapor pressure of water (e) at the recharge temperature. This could be computed using empirical equations such as Antoine (1888) that is presented in Equation (6) of Section 2.3 of this book, or could be interpolated from the values given in Table 7.
8. Compute the mole fraction (x) of CFCs in the atmosphere that would have resulted in the measured aqueous concentration using Equation (26).
9. Compare the computed mole fraction—which is essentially equivalent to the mixing ratio—to the atmospheric history (Figure 24) to derive the estimated year the sample recharged.
10. Compute the age as sample date minus recharge year.

6.5 Sensitivity of Age to Input Parameters

The procedure outlined in the previous section for calculating a tracer age from a measured concentration of CFCs involves numerous parameters (recharge temperature, salinity, elevation) that are uncertain to some degree. In this section, we summarize the sensitivity of the computed age to uncertainty in recharge temperature and elevation.

Figure 27 shows the relationship between the CFC tracer age and various input parameters for a water sample having aqueous concentrations of 1.5, 0.7, and 0.1 pmole/kg for CFC-11, CFC-12, and CFC-113 respectively. The sample was assumed to have been collected in the year 2015, and the age was calculated as 2015 minus the computed recharge year. The recharge temperature and recharge elevation were varied to illustrate the sensitivity of the computed age to these parameters.

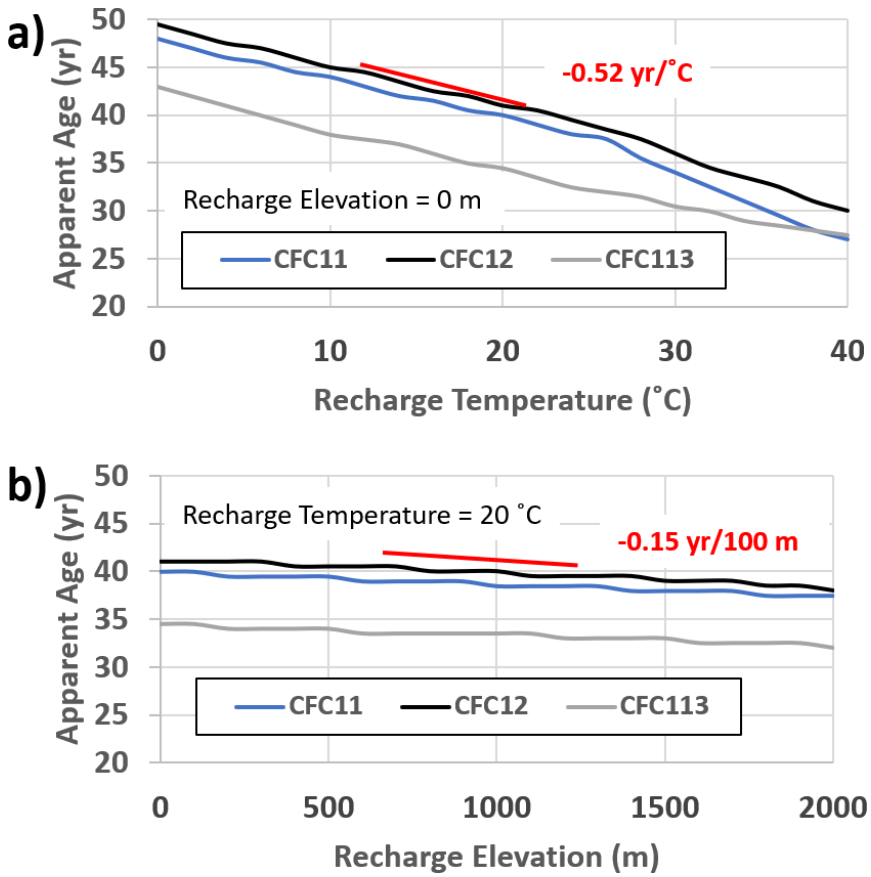

Figure 27 - Sensitivity of CFC tracer ages to input parameters. The tracer age of a hypothetical sample having CFC concentrations of 1.5, 0.7, and 0.1 pmole/kg for CFC-11, CFC-12, and CFC-113, respectively, were computed for various values of recharge temperature and recharge elevation as indicated. The sensitivities—change in age per change in parameter—are shown in red.

The sensitivity of the tracer age to recharge temperature is about −0.52 year/°C for recharge temperatures ranging from 0 to 40 °C. In other words, if the assumed recharge temperature was 1 °C warmer than the true value, the tracer age would be 0.5 years younger than the true age. The sensitivity to recharge elevation is about −0.15 year/100 m, so using a recharge elevation that is 100 m greater than the true elevation results in an age that is 0.15 years younger. The relationship is not smooth because of an artifact of the numerical simulation that uses annual average atmospheric concentrations instead of continuous values.

6.6 Discussion of Tracer-Specific Issues

The CFC dating method is conceptually straightforward but depends on assumptions such as conservative geochemical behavior in the subsurface and the atmosphere being the only source for CFCs in groundwater. In addition, the reduction of CFC atmospheric concentration since the late 1990s results in a non-uniqueness in the age-concentrations relationship. These issues are briefly discussed in this section.

To function as age-dating tracers, CFC concentrations in groundwater cannot be altered by biogeochemical processes in the subsurface. Minimal sorption of CFCs has been demonstrated in column experiments consisting of ground Ottawa sand (Ciccioli et al., 1980) and CFCs may be considered stable with respect to microbial degradation under aerobic conditions (Lovely & Woodward, 1992). However, for soils and sediments containing modest *fractions of organic carbon* (e.g., foc > 0.03 percent) and under reducing conditions, both sorption and microbial degradation can strongly affect CFC concentrations.

In general, CFC-12 is the least affected by these processes and comparisons of tracer ages derived from the different CFCs have been used to identify biogeochemical processes affecting CFC-11 and CFC-113 (Cook et al., 1995). In laboratory studies, for example, Archbold and others (2012) showed that both CFC-11 and CFC-113 degraded in the presence of zero-valent iron with half-lives of less than one day. In a field study, Cook and others (1995) showed stability of CFC-12 but almost complete degradation of CFC-11 and modest sorption of CFC-113 in a sandy aquifer near Sturgeon Falls, Ontario, Canada. As a general guide, CFC-11 tends to be most affected by microbial degradation under anerobic conditions whereas CFC-113 is most affected by sorption onto organic matter in soils and sediments.

Contamination of groundwater samples by sources other than the atmosphere can alter CFC concentrations in groundwater. Although the absolute concentration from other sources is often small, it can result in values that exceed atmospheric solubility and make dating impossible. Contamination sources include seepage from septic tanks, landfills, releases from polyurethane foam waste, leaky sewer lines, leakage from underground storage tanks, and recharge from rivers that are contaminated with CFCs, often from sewage effluents (Cook, Plummer, et al., 2006). Samples for CFC analyses can also become contaminated during collection, often when plastics are used in the collection process. While sampling equipment such as plastic discharge lines may not inherently contain CFCs, their exposure to the modern atmosphere along with slow desorption into groundwater samples can lead to contamination. When measured concentrations exceed atmospheric solubility, it is easy to recognize such contamination but identifying trace amounts of CFCs that simply elevate groundwater concentrations is difficult. Eliminating the possibility of contamination during sampling—using proper materials and abundant flushing—is extremely important.

As shown in Figure 24, atmospheric concentrations of CFCs started declining in the late 1990s to early 2000s, resulting in a non-uniqueness in the relationship between age and concentration. Although dating waters that recharged since 2000 is problematic with CFCs, it is still possible to date waters that recharged between about 1950 and 2000. In the future, it may be possible to date young waters using the declining limb of the atmospheric curve

along with some other tracer and/or hydrogeologic information that identifies the water as being recharged after about 2000.

6.7 Summary

CFCs are relatively stable gases and atmospheric concentrations increased monotonically from the 1940s to the late 1990s. During this period, it was possible to relate measured concentrations in groundwater samples to the atmospheric concentration each year and hence estimate a recharge year.

Although waters that recharged after the late 1990s—when CFC atmospheric concentrations started declining—cannot be uniquely dated, it is still possible to date older waters with this technique. Measurements of CFCs, while still somewhat specialized, are less complicated than tracers such as ^{3}H and noble gases. The process of calculating a tracer age involves measuring an aqueous concentration, calculating the atmospheric (gas-phase) concentration that would be in equilibrium (after corrections for excess air) with the aqueous concentration, and comparing the atmospheric-equivalent value with the history of CFCs in the atmosphere.

In addition to the non-uniqueness for young groundwaters, the primary limitations to CFC dating are the existence of non-atmospheric sources of CFCs and non-conservative transport behavior under certain biogeochemical conditions in the subsurface. CFC-11 can microbially degrade under reducing conditions, and CFC-113 can sorb onto aquifer solids. Despite these limitations, excellent agreement between CFC ages (especially CFC-12) and other tracers has been reported (Cook et al., 1995; Ekwurzel et al., 1994; Plummer et al., 1993). Into the future, it may be possible to date young waters using the declining limb of the atmospheric curve along with some other tracer and/or hydrogeologic information that identifies the water as being recharged after about 2000.

7 Wrap Up

Groundwater age refers to the elapsed time for a parcel of water to move along a flow path from recharge to the point of collection. Several environmental tracers can provide estimates of groundwater age, which in turn can highly constrain rates of groundwater movement and recharge. The use of ^3H, $^3H/^3He$, SF_6, and CFCs for age dating groundwater that is less than about 60 years old are described in this book.

Except for ^3H, these dating methods involve dissolved gases and so the book also reviews basic concepts of gas dissolution in groundwater. ^3H is one of the most widely used tracers of groundwater age and has been used to distinguish pre-bomb—before the 1950s—from post-bomb waters. Precise dating may be possible for waters recharged since about 1990 in the southern hemisphere and 2000 in the northern hemisphere. In the coming decades, ^3H is likely to be used more frequently as a precise dating tool, especially for surface waters where gas exchange with the atmosphere is problematic for other techniques.

The $^3H/^3He$ dating method substantially extends the dating range of ^3H alone and is one of the most robust of the young groundwater age-dating methods. Although the basic age equation for $^3H/^3He$ is straightforward, its application is sometimes complicated by the fact that ^3He is present in very small abundance and as a dissolved gas. The application of this method will improve as we better understand processes such as the formation of excess air and gas stripping. Analytical costs for $^3H/^3He$ are currently high but advances in portable mass spectrometry and gas separation techniques could substantially reduce costs.

The SF_6 dating method relies on its monotonic increase in the atmospheric concentration since about 1975. The nearly linear increase in atmospheric SF_6 since 1980 results in water mixtures having an SF_6 concentration that maps to approximately the average age of the mixture. Limitations in the SF_6 method result from subsurface sources and the sensitivity of apparent ages to excess air. As atmospheric concentrations continue to increase, the SF_6 method will become more robust, with diminished influence of subsurface (terrigenic) SF_6 on young waters.

The CFC dating method also relies on a unique atmospheric concentration through time. This existed from about 1940 to 1990, but declining atmospheric concentrations result in non-unique apparent ages for waters recharged since 1990. Nevertheless, it is still possible to date waters older than 1990 with CFCs and this method is still a powerful tool for distinguishing “old” from “modern” water.

While some researchers have argued against the quantitative use of groundwater age in favor of using raw tracer concentrations, calculated ages are useful for conceptualizing and understanding groundwater flow paths and turnover times. Because

the tracer concentration (age) is related to the entire upstream flow field, the tracers discussed in this book are powerful tools for understanding groundwater flow systems. By integrating these tracer methods into numerical models of groundwater flow, we expect significant improvement in the uniqueness of such models and their ability to forecast future conditions.

However, molecular diffusion, hydrodynamic dispersion, and convergence of groundwater flow paths result in groundwater samples that contain a spectrum of ages rather than a single age. While many practical groundwater issues involve waters that were recharged within the past 60 years, the spectrum of ages in many aquifers exceeds the dating range of the tracers presented in this book. Emerging tracers such as radioactive ^{39}Ar ($t_{1/2} = 269$ years) are likely to further our understanding of groundwater flow systems, their sustainability as sources of water supply, and strategies for protecting the quality of water in the flow systems.

8 Exercises

Exercise 1

Exercise 1 is in two parts: a) and b).

a) Use Equation (4) in Section 2.3 to calculate the concentrations of dissolved He, Ne, N_2, Ar, Kr, and Xe (in units of ccSTP/g) in equilibrium with the moist atmosphere at a temperature of 10 °C and an elevation of 450 m above mean sea level. The equation is shown here.

$$C_{i,eq} = \frac{\big(P - e(T)\big)x_i}{K_{w,i}(T,S)}$$

where:

$C_{i,eq}$ = concentration of air-saturated water (ASW, ccSTP/g)

P = atmospheric pressure (atm)

$e(T)$ = vapor pressure of water at temperature T (atm)

$K_{w,i}(T,S)$ = Henry Coefficient of gas i at temperature T and salinity S (g-atm/ccSTP)

x_i = fraction of gas i (mixing ratio) in the dry atmosphere

As with all equations, it is important to use consistent units throughout the calculation (i.e., for $C_{i,eq}$ in units of ccSTP/g, and P and e in atm, $K_{w,i}$ should be in g-atm/ccSTP).

Assume that the recharge salinity is zero. Use Table 1 (Section 2.1) for Henry Coefficient. A good approximation for atmospheric pressure is $P = P_0 \exp\left(-\frac{Z}{Z_s}\right)$ where P_0 is the pressure at elevation (Z) of zero (i.e., 1 atm) and Z_s is a scaling factor equal to 8,300 as shown in Equation (5). Use the Antoine equation $e = 10^{A-\frac{B}{C+T}}$ where $A = 8.07131$, $B = 1730.63$, $C = 233.426$ and T is temperature in °C and e is the vapor pressure of water in units of mmHg as shown in Equation (6). Both Equation (5) and Equation (6) follow Equation (4) in Section 2.3. e needs to be converted to units of atm for use in Equation (4).

b) Now add 0.003 ccSTP/g of UA to each of these values. On a percentage basis, calculate how much this changes the concentrations relative to the equilibrium values computed in Exercise 1a).

Solution to Exercise 1
Return to where text linked to Exercise 1

Exercise 2

The following results are obtained from fitting the CE model to four measured gas concentrations (C_m). Three parameters were varied to find the best fit simulated concentrations (C_S) shown. Estimated measurement errors are shown for each dissolved gas concentration. Calculate the p-value for these model results. How confident would you be in using this model to determine $^3H/^3He$ age for this groundwater sample? All concentrations are in units of ccSTP/g.

Gas	Measured Concentration	Error (σ)	Best-fit simulated concentration
Xe	1.238×10^{-8}	3.71×10^{-10}	1.202×10^{-8}
Kr	8.302×10^{-8}	2.49×10^{-9}	8.624×10^{-8}
Ar	3.876×10^{-4}	1.16×10^{-5}	3.854×10^{-4}
Ne	2.495×10^{-7}	7.49×10^{-9}	2.489×10^{-7}

Solution Exercise 2

Return to where text linked to Exercise 2

Exercise 3

Lab results for a groundwater sample reveal tritium activity of 3.5 TU. Based on a local, precipitation-weighted atmospheric ^3H function, you estimate background tritium as 8.5 TU. What is the minimum age for this groundwater?

Solution to Exercise 3

Return to where text linked to Exercise 3

Exercise 4

A times series of ^{3}H values in precipitation from Lincoln, Nebraska, USA, (Michel et al., 2018) is available and a groundwater sample collected in 2012 has a measured tritium concentration of 4.5 TU. In the spreadsheet provided on the web page for this book↗, annual ^{3}H has been determined as an unweighted mean value (annual mean) and a weighted mean based on monthly precipitation from Lincoln, Nebraska, USA↗.

Construct a decay curve and answer the following questions:

a) What is the minimum groundwater age for this sample, based on Equation (13)?
b) Compare the answer above to the minimum age determined using a graphical method.

Solution to Exercise 4↴

Return to where text linked to Exercise 4↑

Exercise 5

Lab analysis and noble gas modeling reveal tritium activity of 0.72 TU and $^3\mathrm{He}_{\mathrm{trit}}(t) = 6.8$ TU for a groundwater sample collected from a short-screened well in 2019.

What is the $^3\mathrm{H}/\,^3\mathrm{He}$ tracer age of this groundwater?

Exercise 5↴

Return to where text linked to Exercise 5↑

Exercise 6

A groundwater sample was analyzed for He, Ne, and ^{3}H with the following results:

$^4\mathrm{He} = 5.29 \times 10^{-8}$ ccSTP/g

$\mathrm{Ne} = 2.14 \times 10^{-7}$ ccSTP/g

$\delta\,^3\mathrm{He} = 32$ %

$^3\mathrm{He} = 5.6$ TU

The sample is thought to have recharged at an elevation of 500 m and the mean annual temperature at the site is 17.5 °C.

Calculate the $^3\mathrm{H}/\,^3\mathrm{He}$ tracer age assuming no fractionation of the excess air component. Assume that the He/Ne ratio of excess air is 0.2882.

A useful unit conversion: 1 ccSTP/g = 4.021×10^{14} TU.

Solution to Exercise 6↴

Return to where text linked to Exercise 6↑

Exercise 7

a) The SF_6 concentration of a groundwater sample collected in 2018 was 2.6 fmole/kg. An fmole is a femtomole which is an amount of substance equal to 10^{-15} moles. The mean annual temperature in the recharge zone of the aquifer is 15 °C and the elevation of the water table in the recharge zone is 800 m.

Calculate the tracer age of this sample.

b) An analysis of noble gases indicates that the sample in Exercise 7(a) contains 0.003 ccSTP/g of UA.

Recalculate the tracer age of the sample including excess air.

Solution to Exercise 7

Return to where text linked to Exercise 7

9 References

Aeschbach-Hertig, W., Beyerle, U., Holocher, J., Peeters, F., & Kipfer, R. (2002). Excess air in groundwater as a potential indicator of past environmental changes. Study of environmental change using isotope techniques. In International Atomic Energy Agency (Ed.),. *Study of environmental change using isotope techniques: Proceedings of an international conference held in Vienna, Austria, April 23–27, 2001* (pp. 174–183). Universität Konstanz. http://nbn-resolving.de/urn:nbn:de:bsz:352-243968↗.

Aeschbach-Hertig, W., El-Gamal, H., Wieser, M., & Palcsu, L. (2008). Modeling excess air and degassing in groundwater by equilibrium partitioning with a gas phase. *Water Resources Research, 44*(8), W08449. https://doi.org/10.1029/2007WR006454↗.

Aeschbach-Hertig, W., Peeters, F., Beyerle, U., & Kipfer, R. (1999). Interpretation of dissolved atmospheric noble gases in natural waters. *Water Resources Research*, *35*(9), 2779–2792. https://doi.org/10.1029/1999WR900130↗.

Aeschbach-Hertig, W., Peeters, F., Beyerle, U., & Kipfer, R. (2000). Palaeotemperature reconstruction from noble gases in ground water taking into account equilibration with entrapped air. *Nature*, *405*(6790), 1040–1044. https://doi.org/10.1038/35016542↗.

Aeschbach-Hertig, W., & Solomon, D. K. (2013). Noble gas thermometry in groundwater hydrology. In: P. Burnard (Ed.), *The noble gases as geochemical tracers. Advances in isotope geochemistry* (pp. 81–122). Springer. https://doi.org/10.1007/978-3-642-28836-4_5↗.

Allison, G.B., & Hughes, M.W. (1977). The history of tritium fallout in southern Australia as inferred from rainfall and wine samples. *Earth Planet. Sci. Lett. 36(2)*, 334–340.

Andrews, J. N., & Kay, R. L. F. (1982). Natural production of tritium in permeable rocks. *Nature*, *298*(5872), 361–363. https://doi.org/10.1038/298361a0↗.

Andrews, J. N., & Lee, D. J. (1979). Inert gases in groundwater from the Bunter Sandstone of England as indicators of age and paleoclimatic trends. *Journal of Hydrology*, *41*(3–4), 233–252. https://doi.org/10.1016/0022-1694(79)90064-7↗.

Antoine, C. (1888), Tensions des vapeurs; Nouvelle relation entre les tensions et les températures [Vapor pressure: A new relationship between pressure and temperature]. *Comptes Rendus des Séances de l'Académie des Sciences* (in French), *107*: 681–684, 778–780, 836–837.

Archbold, M. E., Elliot, T., & Kalin, R. M. (2012). Carbon isotopic fractionation of CFCs during abiotic and biotic degradation. *Environmental Science & Technology*, *46*(3), 1764–1773. https://doi.org/10.1021/es203386a↗.

Harnisch, J., & Eisenhauer, A. (1998). Natural CF_4 and SF_6 on Earth. *Geophysical Research Letters, 25(13),* 2401-2404.

Ballentine, C. J., & Hall, C. M. (1999). Determining paleotemperature and other variables by using an error-weighted, nonlinear inversion of noble gas concentrations in water.

Geochimica et Cosmochimica Acta, 63(16), 2315–2336. https://doi.org/10.1016/S0016-7037(99)00131-3↗.

Begemann, F., & Libby, W. F. (1957). Continental water balance, ground water inventory and storage times, surface ocean mixing rates and world-wide water circulation patterns from cosmic-ray and bomb tritium. *Geochimica et Cosmochimica Acta, 12(4)*, 277-296.

Beyerle, U., Rueedi, J., Leuenberger, M., Aeschbach-Hertig, W., Peeters, F., Kipfer, R., & Dodo, A. (2003). Evidence for periods of wetter and cooler climate in the Sahel between 6 and 40 kyr BP derived from groundwater. *Geophysical Research Letters*, *30*(4). https://doi.org/10.1029/2002GL016310↗.

Böhlke, J. K. (2002). Groundwater recharge and agricultural contamination. *Hydrogeology Journal, 10*, 153–179. https://doi.org/10.1007/s10040-001-0183-3↗.

Böhlke, J. K., & Denver, J. M. (1995). Combined use of groundwater dating, chemical, and isotopic analyses to resolve the history and fate of nitrate contamination in two agricultural watersheds, Atlantic coastal plain, Maryland. *Water Resources Research, 31*(9), 2319–2339. https://doi.org/10.1029/95WR01584↗.

Böhlke, J. K., Jurgens, B. C., Uselmann, D. J., & Eberts, S. M. (2014). Educational webtool illustrating groundwater age effects on contaminant trends in wells. *Groundwater*, *52*(S1), 8–9. https://doi.org/10.1111/gwat.12261↗.

Böhlke, J. K., Verstraeten, I. M., & Kraemer, T. F. (2007). Effects of surface-water irrigation on sources, fluxes, and residence times of water, nitrate, and uranium in an alluvial aquifer. *Applied Geochemistry*, *22*(1), 152–174. https://doi.org/10.1016/j.apgeochem.2006.08.019↗.

Brown, R. M., & Barry, P. J. (1979). A review of HTO evaporation studies at Chalk River Nuclear Laboratories. Isotopes in lake studies. In International Atomic Energy Agency (Ed)., *Advisory group meeting on the application of nuclear techniques to the study of lake dynamics: Panel proceedings series* (pp. 73–86). Vienna, Austria, 29 August–2 September 1977.

Bu, X., & Warner, M. J. (1995). Solubility of chlorofluorocarbon 113 in water and seawater. *Deep Sea Research Part I: Oceanographic Research Papers, 42(7),* 1151-1161.

Bullister, J. L., & Weiss, R. F. (1988). Determination of CCl3F and CCl2F2 in seawater and air. *Deep Sea Research Part A. Oceanographic Research Papers, 35(5)*, 839-853.

Bullister, J. L. (1989). Chlorofluorocarbons as time-dependent tracers in the ocean. *Oceanography*, *2*(2), 12–17. http://www.jstor.org/stable/43925263↗.

Bullister, J. L., & Wisegarver, D. P. (2008). The shipboard analysis of trace levels of sulfur hexafluoride, chlorofluorocarbon-11 and chlorofluorocarbon-12 in seawater. *Deep Sea Research Part I: Oceanographic Research Papers*, *55*(8), 1063–1074. https://doi.org/10.1016/j.dsr.2008.03.014↗.

Bullister, J. L., Wisegarver, D. P., & Menzia, F. A. (2002). The solubility of sulfur hexafluoride in water and seawater. *Deep Sea Research Part I: Oceanographic Research Papers, 49*(1), 175–187. https://doi.org/10.1016/S0967-0637(01)00051-6↗.

Busenberg, E., & Plummer, L. N. (1992). Use of chlorofluorocarbons (CCl3F and CCl2F2) as hydrologic tracers and age-dating tools: The alluvium and terrace system of central Oklahoma. *Water Resources Research, 28*(9), 2257-2283. https://doi.org/10.1029/92WR01263↗.

Busenberg, E., & Plummer, L. N. (1997). Use of sulfur hexafluoride as a dating tool and as a tracer of igneous and volcanic fluids in ground water, *Geological Society of America Abstracts of Programs, 296*, A-78, 1997.

Busenberg, E., & Plummer, L. N. (2000). Dating young groundwater with sulfur hexafluoride: Natural and anthropogenic sources of sulfur hexafluoride. *Water Resources Research, 36*(10), 3011–3030. https://doi.org/10.1029/2000WR900151↗.

Busenberg, E., & Plummer, L. N. (2010). A rapid method for the measurement of sulfur hexafluoride (SF_6), trifluoromethyl sulfur pentafluoride (SF_5CF_3), and Halon 1211 (CF_2ClBr) in hydrologic tracer studies. *Geochemistry, Geophysics, Geosystems, 11*(11), Q11001. https://doi.org/10.1029/2010GC003312↗.

Busenberg, E., Plummer, L. N., Cook, P. G., Solomon, D. K., Han, L. F., Gröning, M., & Oster, H. (2006). *Sampling and analytical methods.* International Atomic Energy Agency. http://www-pub.iaea.org/MTCD/publications/PDF/Pub1238_web.pdf↗.

Cauquoin, A., Jean-Baptiste, P., Risi, C., Fourré, É., Stenni, B., & Landais, A. (2015). The global distribution of natural tritium in precipitation simulated with an Atmospheric General Circulation Model and comparison with observations. *Earth and Planetary Science Letters, 427*, 160–170. https://doi.org/10.1016/j.epsl.2015.06.043↗.

Cey, B. D., Hudson, G. B., Moran, J. E., & Scanlon, B. R. (2008). Impact of artificial recharge on dissolved noble gases in groundwater in California. *Environmental Science & Technology, 42*(4), 1017–1023. https://doi.org/10.1021/es0706044↗.

Ciccioli, P., Cooper, W. T., Hammer, P. M., & Hayes, J. M. (1980). Organic solute-mineral surface interactions: A new method for the determination of groundwater velocities. *Water Resources Research, 16*(1), 217–223. https://doi.org/10.1029/WR016i001p00217↗.

Clark, J. F., Wanninkhof, R. I. K., Schlosser, P., & Simpson, H. J. (1994). Gas exchange rates in the tidal Hudson River using a dual tracer technique. *Tellus B: Chemical and Physical Meteorology, 46*(4), 274–285. https://doi.org/10.3402/tellusb.v46i4.15802↗.

Clever, H. L. (Ed.). (1979). *IUPAC solubility data series, Vol. 2: Krypton, xenon and radon—Gas solubilities*. Pergamon.

Cook, P. G. (2020). *Introduction to isotopes and environmental tracers as indicators of groundwater flow*. The Groundwater Project. https://doi.org/10.21083/978-1-7770541-8-2↗.

Cook, P. G., & Dogramaci, S. (2019). Estimating recharge from recirculated groundwater with dissolved gases: An end-member mixing analysis. *Water Resources Research, 55*(7), 5468–5486. https://doi.org/10.1029/2019WR025012↗.

Cook, P. G., Lamontagne, S., Berhane, D., & Clark, J. F. (2006). Quantifying groundwater discharge to Cockburn River, southeastern Australia, using dissolved gas tracers ^{222}Rn and SF_6. *Water Resources Research, 42*(10), W10411. https://doi.org/10.1029/2006WR004921↗.

Cook, P. G., Plummer, L. N., Busenberg, E., Solomon, D. K., & Han, L. F. (2006). Effects and processes that can modify apparent CFC age. In International Atomic Energy Agency (Ed.), *Use of chlorofluorocarbons in hydrology: A guidebook* (pp. 31–58). International Atomic Energy Agency. http://www-pub.iaea.org/MTCD/publications/PDF/Pub1238_web.pdf↗.

Cook, P. G., Solomon, D. K., Plummer, L. N., Busenberg, E., & Schiff, S. L. (1995). Chlorofluorocarbons as tracers of groundwater transport processes in a shallow, silty sand aquifer. *Water Resources Research, 31*(3), 425–434. https://doi.org/10.1029/94WR02528↗.

Copia, L., Wassenaar, L. I., Terzer-Wassmuth, S., Belachew, D. L., & Araguás-Araguás, L. J. (2021). Comparative evaluation of ^{2}H-versus ^{3}H-based enrichment factor determination on the uncertainty and accuracy of low-level tritium analyses of environmental waters. *Applied Radiation and Isotopes, 176*, 109850. https://doi.org/10.1016/j.apradiso.2021.109850↗.

Copia, L., Wassenaar, L. I., Terzer-Wassmuth, S., Hillegonds, D. J., Klaus, P. M., & Araguás-Araguás, L. J. (2020). Proficiency testing of 78 international laboratories measuring tritium in environmental waters by decay counting and mass spectrometry for age dating and water resources assessment. *Rapid Communications in Mass Spectrometry, 34*(17), e8832. https://doi.org/10.1002/rcm.8832↗.

Davis, S. N., & Murphy, E. (1987). *Dating ground water and the evaluation of repositories for radioactive waste*. United States.

Drever, J. I. (1988). *The geochemistry of natural waters* (Vol. 437). Prentice Hall.

Eastoe, C. J., Watts, C. J., Ploughe, M., & Wright, W. E. (2012). Future use of tritium in mapping pre-bomb groundwater volumes. *Groundwater, 50*(1), 87–93. https://doi.org/10.1111/j.1745-6584.2011.00806.x↗.

Ekwurzel, B., Schlosser, P., Smethie, W. M., Jr., Plummer, L. N., Busenberg, E., Michel, R. L.,... & Stute, M. (1994). Dating of shallow groundwater: Comparison of the transient tracers ^{3}H/ ^{3}He, chlorofluorocarbons, and 85Kr. *Water Resources Research, 30*(6), 1693–1708. https://doi.org/10.1029/94WR00156↗.

Gardner, P., & Solomon, D. K. (2009). An advanced passive diffusion sampler for the determination of dissolved gas concentrations. *Water Resources Research, 45*(6), W06423. https://doi.org/10.1029/2008WR007399↗.

Garrels, R. M., & Christ, C. L. (1965). *Solutions, minerals and equilibria*. Harper & Row.

Gilmore, T., Cherry, M., Gastmans, D., Humphrey, E., & Solomon, D. K. (2021). The $^{3}H/^{3}He$ groundwater age-dating method and applications. *Derbyana, 42*, 1–23. https://doi.org/10.14295/derb.v42.740↗.

Gilmore, T. E., Genereux, D. P., Solomon, D. K., Farrell, K. M., & Mitasova, H. (2016). Quantifying an aquifer nitrate budget and future nitrate discharge using field data from streambeds and well nests. *Water Resources Research, 52*(11), 9046–9065. https://doi.org/10.1002/2016WR018976↗.

Gilmore, T. E., Genereux, D. P., Solomon, D. K., & Solder, J. E. (2016). Groundwater transit time distribution and mean from streambed sampling in an agricultural coastal plain watershed, North Carolina, USA. *Water Resources Research, 52*(3), 2025–2044. https://doi.org/10.1002/2015WR017600↗.

Hall, C. M., Castro, M. C., Lohmann, K. C., & Ma, L. (2005). Noble gases and stable isotopes in a shallow aquifer in southern Michigan: Implications for noble gas paleotemperature reconstructions for cool climates. *Geophysical Research Letters, 32*(18), L18404. https://doi.org/10.1029/2005GL023582↗.

Han, L. F., Gröning, M., Plummer, L. N., & Solomon, D. K. (2006). Comparison of the CFC technique with other techniques (^{3}H, $^{3}H/^{3}He$, ^{85}Kr). In International Atomic Energy Agency (Ed.), *Use of chlorofluorocarbons in hydrology: A guidebook* (pp. 191–198). IAEA. http://www-pub.iaea.org/MTCD/publications/PDF/Pub1238_web.pdf↗.

Harms, P. A., Visser, A., Moran, J. E., & Esser, B. K. (2016). Distribution of tritium in precipitation and surface water in California. *Journal of Hydrology, 534*, 63-72.

Harnisch, J., & Eisenhauer, A. (1998). Natural CF_4 and SF_6 on Earth. *Geophysical Research Letters, 25*(13), 2401–2404. https://doi.org/10.1029/98GL01779↗.

Hartley, D. E., Kindler, T., Cunnold, D. M., & Prinn, R. G. (1996). Evaluating chemical transport models: Comparison of effects of different CFC-11 emission scenarios. *Journal of Geophysical Research: Atmospheres, 101*(D9), 14381–14385. https://doi.org/10.1029/96JD00865↗.

Heaton, T. H. E., & Vogel, J. C. (1981). "Excess air" in groundwater. *Journal of Hydrology, 50*, 201–216. https://doi.org/10.1016/0022-1694(81)90070-6↗.

Herzberg, O., & Mazor, E. (1979). Hydrological applications of noble gases and temperature measurements in underground water systems: Examples from Israel. *Journal of Hydrology, 41*(3-4), 217–231. https://doi.org/10.1016/0022-1694(79)90063-5↗.

Ho, D. T., Schlosser, P., Smethie, W. M., & Simpson, H. J. (1998). Variability in atmospheric chlorofluorocarbons (CCl3F and CCl2F2) near a large urban area: Implications for groundwater dating. *Environmental Science & Technology*, *32*(16), 2377–2382. https://doi.org/10.1021/es980021h↗.

Horvatinčić, N. (1980). Radiocarbon and tritium measurements in water samples and application of isotopic analysis in hydrology. *Fizika*, *12*(S2), 201–218. http://pascal-francis.inist.fr/vibad/index.php?action=getRecordDetail&idt=PASCALGEODEBRGM8220254863↗.

Intergovernmental Panel on Climate Change (IPCC). (1995). *Summary for policymakers and technical summary of the Working Group 1 Report*. IPCC.

International Atomic Energy Agency/World Meteorological Organization (IAEA/MO). (2020). *The Global Network of Isotopes in Precipitation (GNIP) database* [Data set]. International Atomic Energy Agency. http://www-naweb.iaea.org/napc/ih/IHS_resources_gnip.html↗.

Jenkins, W. J. (1981). Mass spectrometric measurement of tritium and ^{3}He. In *Proceedings of the consultation. group meeting on low-level tritium measurements*, *International Atomic Energy Agency*, (pp. 179–189).

Jenkins, W. J., & Clarke, W. B. (1976). The distribution of ^{3}H in the western Atlantic Ocean. *Deep Sea Research and Oceanographic Abstracts*, *23*(6), 481–494. https://doi.org/10.1016/0011-7471(76)90860-3↗.

Jurgens, B. C., Böhlke, J. K., & Eberts, S. M. (2012). *TracerLPM (Version 1): An Excel® workbook for interpreting groundwater age distributions from environmental tracer data* (Techniques and Methods Report 4-F3). US Geological Survey.

Katz, B. G., Lee, T. M., Plummer, L. N., & Busenberg, E. (1995). Chemical evolution of groundwater near a sinkhole lake, northern Florida: 1. Flow patterns, age of groundwater, and influence of lake water leakage. *Water Resources Research*, *31*(6), 1549–1564. https://doi.org/10.1029/95WR00221↗.

Kaufman, S., & Libby, W. F. (1954). The natural distribution of tritium. *Physical Review*, *93(6)*, 1337.

Keutsch, F. N., & Saykally, R. J. (2001). Water clusters: Untangling the mysteries of the liquid, one molecule at a time. *PNAS*, *98*(19), 10533–10540. https://doi.org/10.1073/pnas.191266498↗.

Kipfer, R., Aeschbach-Hertig, W., Peeters, F., & Stute, M. (2002). Noble gases in lakes and ground waters. *Reviews in mineralogy and geochemistry*, *47*(1), 615–700. https://doi.org/10.2138/rmg.2002.47.14↗.

Koh, D. C., Plummer, L. N., Busenberg, E., & Kim, Y. (2007). Evidence for terrigenic SF6 in groundwater from basaltic aquifers, Jeju Island, Korea: Implications for groundwater dating. *Journal of Hydrology, 339(1-2),* 93-104.

Kovács, T., Feng, W., Totterdill, A., Plane, J. M. C., Dhomse, S., Gómez-Martín, J. C., Stiller, G. P., Haenel, F. J., Smith, C., Forster, P. M., García, R. R., Marsh, D. R., & Chipperfield, M. P. (2017). Determination of the atmospheric lifetime and global warming potential of sulfur hexafluoride using a three-dimensional model, *Atmospheric Chemistry & Physics, 17*, 883–898. https://doi.org/10.5194/acp-17-883-2017↗.

Krey, P. W., Lagomarsino, R. J., & Toonkel, L. E. (1977). Gaseous halogens in the atmosphere in 1975. *Journal of Geophysical Research, 82(12),* 1753-1766.

LaBolle, E. M., Fogg, G. E., & Eweis, J. B. (2006). Diffusive fractionation of ^{3}H and ^{3}He in groundwater and its impact on groundwater age estimates. *Water Resources Research, 42*(7). https://doi.org/10.1029/2005WR004756↗.

Lehmann, B. E., Davis, S. N., & Fabryka-Martin, J. T. (1993). Atmospheric and subsurface sources of stable and radioactive nuclides used for groundwater dating. *Water Resources Research, 29*(7), 2027–2040. https://doi.org/10.1029/93WR00543↗.

Lippmann, J., Stute, M., Torgersen, T., Moser, D. P., Hall, J. A., Lin, L.,... & Onstott, T. C. (2003). Dating ultra-deep mine waters with noble gases and ^{36}Cl, Witwatersrand Basin, South Africa. *Geochimica et Cosmochimica Acta, 67*(23), 4597–4619. https://doi.org/10.1016/S0016-7037(03)00414-9↗.

Lovelock, J. E. (1971). Atmospheric fluorine compounds as indicators of air movements. *Nature, 230*(5293), 379–379. https://doi.org/10.1038/230379a0↗.

Lovelock, J. E., Maggs, R. J., & Wade, R. J. (1973). Halogenated hydrocarbons in and over the Atlantic. *Nature, 241*(5386), 194–196. https://doi.org/10.1038/241194a0↗.

Lovley, D. R., & Woodward, J. C. (1992). Consumption of freons CFC-11 and CFC-12 by anaerobic sediments and soils. *Environmental Science & Technology, 26*(5), 925–929. https://doi.org/10.1021/es00029a009↗.

Lucas L. L., & Unterweger M. P. (2000). Comprehensive review and critical evaluation of the half-life of tritium. *Journal of Research of the National Institute of Standards & Technology, 105*(4), 541–549. https://doi.org/10.6028/jres.105.043↗.

Maiss, M., & Brenninkmeijer, C. A. (1998). Atmospheric SF_6: Trends, sources, and prospects. *Environmental Science & Technology, 32*(20), 3077–3086. https://doi.org/10.1021/es9802807↗.

Maloszewski, P., & Zuber, A. (1982). Determining the turnover time of groundwater systems with the aid of environmental tracers: I. Models and their applicability. *Journal of Hydrology, 57*(3–4), 207–231. https://doi.org/10.1016/0022-1694(82)90147-0↗.

Maloszewski, P., & Zuber, A. (1996). Lumped parameter models for the interpretation of environmental tracer data. In International Atomic Energy Agency (Ed.), *Manual on mathematical models in isotope hydrogeology* (TECDOC-910). (pp. 9–58). International Atomic Energy Agency.

Mamyrin, B. A., & Tolstikhin, I. N. (2013). Helium isotopes in nature. *Elsevier*.

Manning, A. H., & Solomon, D. K. (2003). Using noble gases to investigate mountain-front recharge. *Journal of Hydrology, 275*(3–4), 194–207. https://doi.org/10.1016/S0022-1694(03)00043-X↗.

Manning, A. H., Solomon, D. K., & Sheldon, A. L. (2003). Applications of a total dissolved gas pressure probe in ground water studies. *Groundwater, 41*(4), 440–448. https://doi.org/10.1111/j.1745-6584.2003.tb02378.x↗.

Marston, T. M., Parry, W. T., Bowman, J. R., & Solomon, D. K. (2012). Tritium content of clay minerals. *Clays and Clay Minerals, 60*(2), 186–199. https://doi.org/10.1346/CCMN.2012.0600208↗.

McMahon, P. B., Carney, C. P., Poeter, E. P., & Peterson, S. M. (2010). Use of geochemical, isotopic, and age tracer data to develop models of groundwater flow for the purpose of water management, northern High Plains aquifer, USA. *Applied Geochemistry, 25*(6), 910–922. https://doi.org/10.1016/j.apgeochem.2010.04.001↗.

McMahon, P. B., Plummer, L. N., Böhlke, J. K., Shapiro, S. D., & Hinkle, S. R. (2011). A comparison of recharge rates in aquifers of the United States based on groundwater-age data. *Hydrogeology Journal*, *19*(4), 779–800. https://doi.org/10.1007/s10040-011-0722-5↗.

Michel, R. L., Jurgens, B. C., and Young, M. B. (2018). *Tritium deposition in precipitation in the United States, 1953–2012*. US Geological Survey. https://doi.org/10.3133/sir20185086↗.

Mercury, L., Pinti, D. L., & Zeyen, H. (2004). The effect of the negative pressure of capillary water on atmospheric noble gas solubility in ground water and palaeotemperature reconstruction. *Earth and Planetary Science Letters, 223*(1–2), 147–161. https://doi.org/10.1016/j.epsl.2004.04.019↗

Molina, M. J., & Rowland, F. S. (1974). Stratospheric sink for chlorofluoromethanes: Chlorine atom-catalysed destruction of ozone. *Nature, 249*(5460), 810–812. https://doi.org/10.1038/249810a0↗.

Montzka, S. A., Butler, J. H., Elkins, J. W., Thompson, T. M., Clarke, A. D., & Lock, L. T. (1999). Present and future trends in the atmospheric burden of ozone-depleting halogens. *Nature, 398*(6729), 690–694. https://doi.org/10.1038/19499↗.

Morgenstern, U., & Taylor, C. B. (2009). Ultra low-level tritium measurement using electrolytic enrichment and LSC. *Isotopes in Environmental and Health Studies, 45*(2), 96–117. https://doi.org/10.1080/10256010902931194↗.

National Oceanic and Atmospheric Administration (NOAA). (1976). *U.S. standard atmosphere*. NASA.

Noguchi, H., Fukutani, S., Yokoyama, S., & Kinouchi, N. (2001). Deposition of tritiated water vapour to a water surface in an outdoor field. *Radiation Protection Dosimetry, 93*(2), 167–172. https://doi.org/10.1093/oxfordjournals.rpd.a006425↗.

O'Brien, K. (1979). Secular variations in the production of cosmogenic isotopes in the Earth's atmosphere. *Journal of Geophysical Research: Space Physics, 84(A2)*, 423-431.

Oms, P. E., Du Bois, P. B., Dumas, F., Lazure, P., Morillon, M., Voiseux, C., Le Corre, C., Cossonnet, C., Solier, L., & Morin, P. (2019). Inventory and distribution of tritium in the oceans in 2016. *Science of the Total Environment, 656*, 1289–1303. https://doi.org/10.1016/j.scitotenv.2018.11.448↗.

Oster, H., Sonntag, C., & Münnich, K. O. (1996). Groundwater age dating with chlorofluorocarbons. *Water Resources Research, 32*(10), 2989–3001. https://doi.org/10.1029/96WR01775↗.

Peck, A. J. (1969). Entrapment, stability, and persistence of air bubbles in soil water. *Soil Research, 7*(2), 79–90. https://doi.org/10.1071/SR9690079↗.

Phillips, F. M., Mattick, J. L., Duval, T. A., Elmore, D., & Kubik, P. W. (1988). Chlorine 36 and tritium from nuclear weapons fallout as tracers for long-term liquid and vapor movement in desert soils. *Water Resources Research, 24*(11), 1877–1891. https://doi.org/10.1029/WR024i011p01877↗.

Plummer, L. N., & Busenberg, E. (2006). Chlorofluorocarbons in the atmosphere. In International Atomic Energy Agency (Ed.), *Use of chlorofluorocarbons in hydrology: A guidebook* (pp. 9–16). International Atomic Energy Agency. https://www-pub.iaea.org/MTCD/Publications/PDF/Pub1238_web.pdf↗.

Plummer, L. N., Busenberg, E., & Cook, P. G. (2006). Principles of chlorofluorocarbon dating. In International Atomic Energy Agency (Ed.), *Use of chlorofluorocarbons in hydrology: A guidebook* (pp. 17–30). International Atomic Energy Agency.

Plummer, L. N., Busenberg, E., Cook, P. G., Oster, H., Han, L. F., & Groening, M. (2006). *Selected case studies using CFC data*. International Atomic Energy Agency

Plummer, L. N., Busenberg, E., & Han, L. F. (2006). CFCs in binary mixtures of young and old groundwater. In International Atomic Energy Agency (Ed.), *Use of chlorofluorocarbons in hydrology: A guidebook* (pp. 59–72). International Atomic Energy Agency.

Plummer, N., Dunkle, S. A., & Busenberg, E. (1993). *Data on chlorofluorocarbons (CCl3F and CCl2F2) as dating tools and hydrologic tracers in shallow ground water of the Delmarva Peninsula* (No. 93-484). US Geological Survey. https://doi.org/10.3133/ofr93484↗.

Poreda, R. J., Cerling, T. E., & Salomon, D. K. (1988). Tritium and helium isotopes as hydrologic tracers in a shallow unconfined aquifer. *Journal of Hydrology, 103*(1–2), 1–9.

https://doi.org/10.1016/0022-1694(88)90002-9↗.

Poulsen, D. L., Cook, P. G., & Dogramaci, S. (2020). Excess air correction of SF_6 and other dissolved gases in groundwater impacted by compressed air from drilling or well development. *Water Resources Research, 56*(8), e2020WR028054. https://doi.org/10.1029/2020WR028054↗.

Puckett, L. J., Tesoriero, A. J., & Dubrovsky, N. M. (2011). Nitrogen contamination of surficial aquifers - A growing legacy. *Environmental Science & Technology, 45*(3), 839–844. https://doi.org/10.1021/es1038358↗.

Reilly, T. E., Plummer, L. N., Phillips, P. J., & Busenberg, E. (1994). The use of simulation and multiple environmental tracers to quantify groundwater flow in a shallow aquifer. *Water Resources Research, 30*(2), 421–433. https://doi.org/10.1029/93WR02655↗.

Ronen, D., Berkowitz, B., & Magaritz, M. (1989). The development and influence of gas bubbles in phreatic aquifers under natural flow conditions. *Transport in Porous Media, 4*(3), 295–306. https://doi.org/10.1007/BF00138041↗.

Rozanski, K., Gonfiantini, R., & Araguás-Araguás, L. (1991). Tritium in the global atmosphere: Distribution patterns and recent trends. *Journal of Physics G: Nuclear and Particle Physics, 17*(S), S523. https://doi.org/10.1088/0954-3899/17/S/053↗.

Sander, R. (1999). Compilation of Henry's law constants for inorganic and organic species of potential importance in environmental chemistry (Version 3). https://www.ready.noaa.gov/documents/TutorialX/files/Chem_henry.pdf.

Sanford, W. E., Shropshire, R. G., & Solomon, D. K. (1996). Dissolved gas tracers in groundwater: Simplified injection, sampling, and analysis. *Water Resources Research, 32*(6), 1635–1642. https://doi.org/10.1029/96WR00599↗.

Sano, Y., Marty, B., & Burnard, P. (2013). Noble gases in the atmosphere. In P. Burnard (Ed.), *The noble gases as geochemical tracers. Advances in isotope geochemistry* (pp. 17–31). Springer. https://doi.org/10.1007/978-3-642-28836-4_2↗.

Scanlon, B. R., Healy, R. W., & Cook, P. G. (2002). Choosing appropriate techniques for quantifying groundwater recharge. *Hydrogeology Journal, 10*(1), 18–39. https://doi.org/10.1007/s10040-001-0176-2↗.

Schlosser, P., Stute, M., Dörr, H., Sonntag, C., & Münnich, K. O. (1988). Tritium/ ^{3}He dating of shallow groundwater. *Earth and Planetary Science Letters, 89*(3–4), 353–362. https://doi.org/10.1016/0012-821X(88)90122-7↗.

Schlosser, P., Stute, M., Sonntag, C., & Otto Münnich, K. (1989). Tritiogenic ^{3}He in shallow groundwater. *Earth and Planetary Science Letters, 94*(3–4), 245–256. https://doi.org/10.1016/0012-821X(89)90144-1↗.

Schultz, T. R., Randall, J. H., Wilson, L. G., & Davis, S. N. (1976). Tracing sewage effluent recharge, Tucson, Arizona. *Groundwater, 14*(6), 463–471. https://doi.org/10.1111/j.1745-6584.1976.tb03140.x↗.

Sepall, O., & Mason, S. G. (1960). Vapor/liquid partition of tritium in tritiated water. *Canadian Journal of Chemistry, 38*(10), 2024–2025.

Shapiro, S. D., LeBlanc, D., Schlosser, P., & Ludin, A. (1999). Characterizing a sewage plume using the ^{3}H-^{3}He dating technique. *Groundwater, 37(6)*, 861-878.

Simmonds, P. G., Rigby, M., Manning, A. J., Park, S., Stanley, K. M., McCulloch, A., Henne, S., Graziosi, F., Maione, M., Arduini, J., Reimann, S., Vollmer, M. K., Mühle, J., O'Doherty, S., Young, D., Kummel, P. B., Fraser, P. J., Weiss, R., F., Salameh, P. K., …Prinn, R. G. (2020). The increasing atmospheric burden of the greenhouse gas sulfur hexafluoride (SF 6). *Atmospheric Chemistry and Physics, 20*(12), 7271–7290.

https://doi.org/10.5194/acp-20-7271-2020↗.

Solomon, D. K. (2000). ^{4}He in groundwater. In P. G. Cook & A. L. Herczeg (Eds.), *Environmental tracers in subsurface hydrology* (pp. 425–439). Springer.

Solomon, D. K., & Cerling, T. E. (1987). The annual carbon dioxide cycle in a montane soil: Observations, modeling, and implications for weathering. *Water Resources Research, 23*(12), 2257–2265. https://doi.org/10.1029/WR023i012p02257↗.

Solomon, D. K., & Cook, P. G. (2000). ^{3}H and ^{3}He. In P. G. Cook & A. L. Herczeg (Eds.), *Environmental tracers in subsurface hydrology* (pp. 397–424). Springer.

Solomon, D. K., & Sudicky, E. A. (1991). Tritium and Helium 3 isotope ratios for direct estimation of spatial variations in groundwater recharge. *Water Resources Research, 27*(9), 2309–2319. https://doi.org/10.1029/91WR01446↗.

Solomon, D. K., Cole, E., & Leising, J. F. (2011). Excess air during aquifer storage and recovery in an arid basin (Las Vegas Valley, USA). *Hydrogeology Journal, 19*(1), 187–194. https://doi.org/10.1007/s10040-010-0659-0↗.

Solomon, D. K., Cook, P. G., & Plummer, L. N. (2006). Models of groundwater ages and residence times. In International Atomic Energy Agency (Ed.), *Use of chlorofluorocarbons in hydrology: A guidebook* (pp. 73–88). International Atomic Energy Agency.

Solomon, D. K., Genereux, D. P., Plummer, L. N., & Busenberg, E. (2010). Testing mixing models of old and young groundwater in a tropical lowland rain forest with environmental tracers. *Water Resources Research, 46*(4), W04518.

https://doi.org/10.1029/2009WR008341↗.

Solomon, D. K., Plummer, L. N., Busenberg, E., & Cook, P. G. (2006). Practical applications of CFCs in hydrological investigations. In International Atomic Energy Agency (Ed.), *Use of chlorofluorocarbons in hydrology: A guidebook* (pp. 89–104). International Atomic Energy Agency.

Solomon, D. K., Poreda, R. J., Schiff, S. L., & Cherry, J. A. (1992). Tritium and helium: 3 as groundwater age tracers in the Borden Aquifer. *Water Resources Research, 28*(3), 741–755. https://doi.org/10.1029/91WR02689↗.

Solomon, D. K., Schiff, S. L., Poreda, R. J., & Clarke, W. B. (1993). A validation of the $^{3}H/^{3}He$ method for determining groundwater recharge. *Water Resources Research, 29*(9), 2951–2962. https://doi.org/10.1029/93WR00968↗.

Solomon, D. K., Gilmore, T. E., Solder, J. E., Kimball, B., & Genereux, D. P. (2015). Evaluating an unconfined aquifer by analysis of age-dating tracers in stream water. *Water Resources Research, 51(11)*, 8883-8899.

Stanley, R. H., Baschek, B., Lott, D. E., III, & Jenkins, W. J. (2009). A new automated method for measuring noble gases and their isotopic ratios in water samples. *Geochemistry, Geophysics, Geosystems, 10*(5), Q05008. https://doi.org/10.1029/2009GC002429↗.

Stonestrom, D. A., Andraski, B. J., Cooper, C. A., Mayers, C. J., & Michel, R. L. (2013). On the conversion of tritium units to mass fractions for hydrologic applications. *Isotopes in Environmental and Health Studies, 49*(2), 250–256.

https://doi.org/10.1080/10256016.2013.766610↗.

Stute, M., Forster, M., Frischkorn, H., Serejo, A., Clark, J. F., Schlosser, P., Broecker, W. S., & Bonani, G. (1995). Cooling of tropical Brazil (5 °C) during the last glacial maximum. *Science, 269*(5222), 379–383. https://doi.org/10.1126/science.269.5222.379↗.

Sun, T., Hall, C. M., Castro, M. C., Lohmann, K. C., & Goblet, P. (2008). Excess air in the noble gas groundwater paleothermometer: A new model based on diffusion in the gas phase. *Geophysical Research Letters, 35*(19), L19401. https://doi.org/10.1029/2008GL035018↗.

Taylor, C. B. (1968). A comparison of tritium and strontium-90 fallout in the Southern Hemisphere. *Tellus, 20(4)*, 559-576.

Terzer-Wassmuth, S., Araguás-Araguás, L. J., Copia, L., & Wassenaar, L. I. (2022). High spatial resolution prediction of tritium (^{3}H) in contemporary global precipitation. *Scientific Reports, 12*(1), 10271. https://doi.org/10.1038/s41598-022-14227-5↗.

Thompson, G. M., Hayes, J. M., & Davis, S. N. (1974). Fluorocarbon tracers in hydrology. *Geophysical Research Letters, 1*(4), 177–180. https://doi.org/10.1029/GL001i004p00177↗.

Tolstikhin, I. N., & Kamensky, I. L. (1969). Determination of groundwater age by the T- ^{3}H method. *Geochemistry International, 6*, 810–811.

Torgersen, T., Jenkins, W. J., & Clarke, W. B. (1979). The tritium/helium-3 method in hydrology. In *International symposium on isotope hydrology, proceedings series* (Vol. 2) (pp. 917–929) [Symposium]. United Nations Educational, Scientific and Cultural Organisation (UNESCO), June 19–23, 1978, Neuherberg, Germany. International Atomic Energy Agency.

http://inis.iaea.org/Search/search.aspx?orig_q=RN:10465819↗.

Turnadge, C., & Smerdon, B. D. (2014). A review of methods for modelling environmental tracers in groundwater: Advantages of tracer concentration simulation. *Journal of Hydrology, 519*, 3674–3689. https://doi.org/10.1016/j.jhydrol.2014.10.056↗.

United Nations (UN). (1998). *Kyoto protocol to the United Nations framework convention on climate change* (FCCC/CP/1997/L.7/Add.1). United Nations. https://unfccc.int/resource/docs/convkp/kpeng.pdf↗.

United Nations Environmental Programme (UNEP). (1987). *Montreal protocol on substances that deplete the ozone layer*. United Nations Environmental Programme. https://www.unep.org/ozonaction/who-we-are/about-montreal-protocol↗.

United States Geological Survey (USGS). (2016). GAMACTT: Groundwater age mixtures and contaminant trends tool (Version 1) [Computer software]. US Geological Survey. https://ca.water.usgs.gov/projects/gamactt/↗.

Visser, A., Broers, H. P., & Bierkens, M. F. P. (2007). Dating degassed groundwater with $^{3}H/^{3}He$. *Water Resources Research, 43*(10), W10434. https://doi.org/10.1029/2006WR005847↗.

Visser, A., Fourré, E., Barbecot, F., Aquilina, L., Labasque, T., Vergnaud, V., & Esser, B. K. (2014). Intercomparison of tritium and noble gases analyses, $^{3}H/^{3}He$ ages and derived parameters excess air and recharge temperature. *Applied Geochemistry, 50*, 130–141. https://doi.org/10.1016/j.apgeochem.2014.03.005↗.

Visser, A., Schaap, J. D., Broers, H. P., & Bierkens, M. F. P. (2009). Degassing of $^{3}H/^{3}He$, CFCs and SF_6 by denitrification: Measurements and two-phase transport simulations. *Journal of Contaminant Hydrology, 103*(3–4), 206–218. https://doi.org/10.1016/j.jconhyd.2008.10.013↗.

Volk, C. M., Elkins, J. W., Fahey, D. W., Dutton, G. S., Gilligan, J. M., Loewenstein, M., Podolske, J. R., Chan, K. R., & Gunson, M. R. (1997). Evaluation of source gas lifetimes from stratospheric observations. *Journal of Geophysical Research: Atmospheres, 102*(D21), 25543–25564. https://doi.org/10.1029/97JD02215↗.

Wanninkhof, R., Ledwell, J. R., Broecker, W. S., & Hamilton, M. (1987). Gas exchange on Mono Lake and Crowley Lake, California. *Journal of Geophysical Research: Oceans, 92*(C13), 14567–14580. https://doi.org/10.1029/JC092iC13p14567↗.

Wanninkhof, R., Ledwell, J. R., & Watson, A. J. (1991). Analysis of sulfur hexafluoride in seawater. *Journal of Geophysical Research: Oceans, 96*(C5), 8733–8740. https://doi.org/10.1029/91JC00104↗.

Wanninkhof, R., Mulholland, P. J., & Elwood, J. W. (1990). Gas exchange rates for a first-order stream determined with deliberate and natural tracers. *Water Resources Research, 26*(7), 1621–1630. https://doi.org/10.1029/WR026i007p01621↗.

Warner, M. J., & Weiss, R. F. (1985). Solubilities of chlorofluorocarbons 11 and 12 in water and seawater. *Deep Sea Research Part A. Oceanographic Research Papers, 32*(12), 1485–1497. https://doi.org/10.1016/0198-0149(85)90099-8↗.

Watson, A. J., & Liddicoat, M. I. (1985). Recent history of atmospheric trace gas concentrations deduced from measurements in the deep sea: Application to sulphur hexafluoride and carbon tetrachloride. *Atmospheric Environment (1967), 19*(9), 1477–1484. https://doi.org/10.1016/0004-6981(85)90285-9↗.

Weiss, R. F. (1970). The solubility of nitrogen, oxygen and argon in water and seawater. *Deep Sea Research and Oceanographic Abstracts, 17*(4), 721–735). https://doi.org/10.1016/0011-7471(70)90037-9↗.

Weiss, R. F. (1971). Solubility of helium and neon in water and seawater. *Journal of Chemical & Engineering Data, 16*(2), 235–241. https://doi.org/10.1021/je60049a019↗.

Weiss, R. F., & Kyser, T. K. (1978). Solubility of krypton in water and sea water. *Journal of Chemical and Engineering Data, 23*(1), 69–72. https://doi.org/10.1021/je60076a014↗.

Wells, M. J., Gilmore, T. E., Mittelstet, A. R., Snow, D., & Sibray, S. S. (2018). Assessing decadal trends of a nitrate-contaminated shallow aquifer in western Nebraska using groundwater isotopes, age-dating, and monitoring. *Water, 10*(8), 1047. https://doi.org/10.3390/w10081047↗.

Wells, M. J., Gilmore, T. E., Nelson, N., Mittelstet, A., & Böhlke, J. K. (2021). Determination of vadose zone and saturated zone nitrate lag times using long-term groundwater monitoring data and statistical machine learning. *Hydrology and Earth System Sciences, 25*(2), 811–829. https://doi.org/10.5194/hess-25-811-2021↗.

Wilson, R. D., & Mackay, D. M. (1996). SF_6 as a conservative tracer in saturated media with high intragranular porosity or high organic carbon content. *Groundwater, 34*(2), 241–249. https://doi.org/10.1111/j.1745-6584.1996.tb01884.x↗.

World Health Organisation (WHO). (2008). *Guidelines for drinking-water quality: Second addendum to third edition.Vol. 1: Recommendations*. World Health Organisation. https://apps.who.int/iris/bitstream/handle/10665/204412/9789241547604_eng.pdf↗.

10 Boxes

Box 1 The Total Dissolved Gas Pressure (*TDGP*) Probe

The *TDGP* of groundwater can be measured with a probe as illustrated in Figure Box 1-1. A *TDGP* probe consists of small-diameter tubing that is permeable to gases (including water vapor) but is not permeable to liquid water. One end of the tube is connected to a pressure sensor and the other end is plugged. When placed in water, gas inside the tube will either migrate into the water (if the *TDGP* is less than the initial gas pressure inside the tube) or dissolved gases from the water will migrate into the tube (if the *TDGP* is greater than the initial gas pressure). For example, if the probe is inserted into a bottle of carbonated water, the probe will read the pressure of CO_2 that was used to create the carbonated water but will not respond to the fluid pressure. If the probe is inserted into degassed water, it will read zero pressure independent of the fluid pressure.

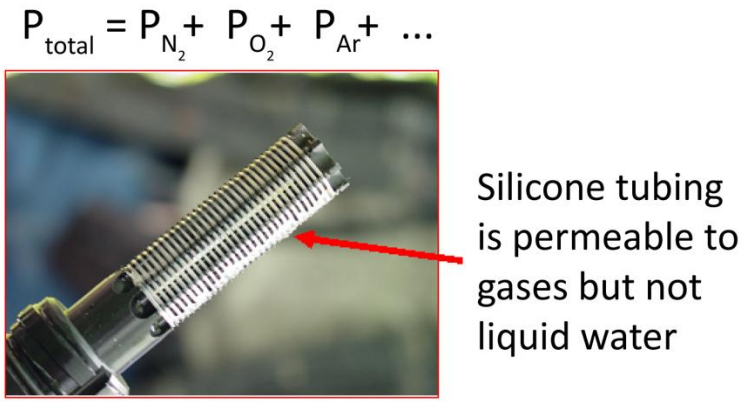

Figure Box 1-1 - Dissolved gas pressure probe.

Return to where text linked to Box 1

Box 2 Procedure for Sampling Wells

So-called *copper tube samples* are easy to transport or ship to the lab given that

1. the ends of the copper tube are not damaged or bent so far as to break, and
2. the samples do not freeze, which can expand and break the copper tube.

An example copper tube configuration consists of 0.95 cm diameter copper tubing of about 50 cm in length. A copper tube of this size will contain about 18 to 20 mL of water sample (Solomon et al., 1992, Solomon et al., 1993). Figure Box 2-1 shows key aspects of copper-tube sampling, including

1. inspection of groundwater flowing through the outlet tubing to be sure bubbles—from degassing and/or air leakage in pump tubing—are not present prior to sampling, and
2. tilting the copper tube upward to allow bubbles to escape the copper tube prior to sealing.

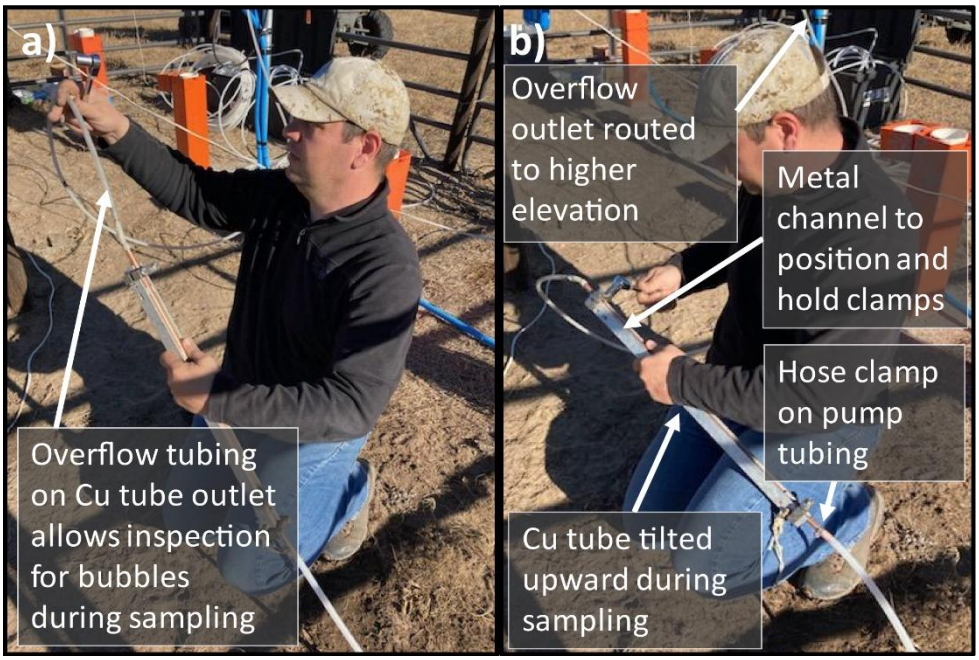

Figure Box 2-1 - Key procedures for sampling groundwater from wells, using the copper tube (Cu tube) method (modified from Gilmore et al., 2021 and used with permission).

Before collecting water samples, wells should be purged according to standard procedures, withdrawing, and disposing of, a volume of well water at least three times the bore volume, and/or when field parameters—e.g., conductivity, pH, temperature—stabilize. When sampling a well using a submersible pump, it is ideal to purge the well by placing the pump near the top of the water column in the well. Purging with the pump near the top of the water column helps to remove well water that may be partially equilibrated with the air in the well casing. The pump inlet can then be lowered toward the well screen before collecting the sample.

When the tubing is filled with a groundwater sample, each end of the tube is sealed with a refrigeration clamp (Figure Box 2-1a) that is machined to very precise specifications to provide a completely airtight seal but not pinch off the copper tubing to the point that it breaks. Figure Box 2-1b shows an example metal channel used to position and hold clamps while they are tightened.

Return to where text linked to Box 2

Box 3 Procedure for Sampling from Streambeds

In some cases, groundwater samples are collected from small diameter wells or from piezometers in sandy, permeable streambeds (Figure Box 3-1). The same general considerations apply as when sampling wells, but streambed piezometer diameters are typically too small to allow use of a submersible pump. In this case, a small inertial pump (i.e., a *check valve*) can be attached to the end of the copper tube using flexible rubber tubing (Figure Box 3-1b). An overflow line is attached to the copper tube (Figure Box 3-1c), which is lowered into the piezometer and used to purge the piezometer and collect the sample water. It is helpful to attach a 3-way valve to the outlet of the overflow tube. One side of the three-way valve can be used to discharge groundwater as it is pumped. The other side of the three-way valve is connected to a syringe, which can be used to apply backpressure on the water sample in the copper tube. Backpressure serves two purposes,

1. forcing the check valve to stay closed while refrigeration clamps are tightened, and
2. increasing pressure on the water sample in the copper tube, which helps to minimize formation of bubbles in samples with high total dissolved gas pressure.

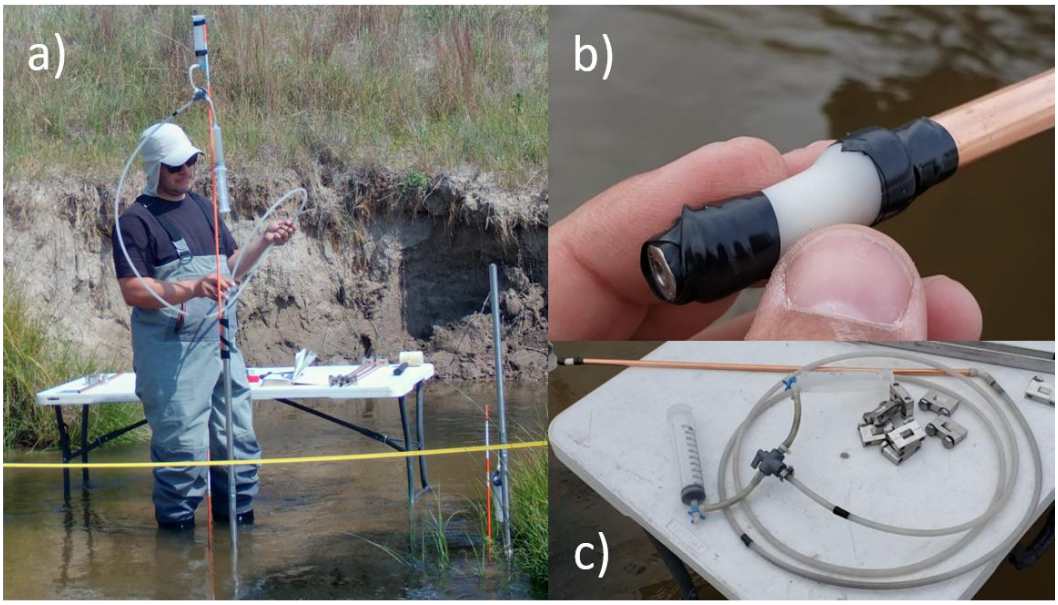

Figure Box 3-1 - Noble gas sampling in the streambed of a gaining stream, showing a) piezometer being sampled for noble gases, b) inertial pump (Waterra® check valve) attached to a copper tube, and c) sampling rig, with inertial pump, copper tube, and overflow tubing with 3-way valve and syringe to apply backpressure on the noble gas sample.

Return to where text linked to Box 3

11 Exercise Solutions

Solution Exercise 1

The solution to Exercise 1 has two parts: a) and b).

a) Equation (4) is duplicated here.

$$C_{i,eq} = \frac{\big(P - e(T)\big)x_i}{K_{w,i}(T,S)}$$

Common values needed for all gases are P and $e(T)$. We calculate P as:

$$P = P_0 \exp\left(-\frac{Z}{Z_s}\right) = 1 \text{ atm } \exp\left(-\frac{450 \text{ m}}{8300 \text{ m}}\right) = 0.947 \text{ atm}$$

We calculate e at 10 °C and convert to atmospheres as shown in the next equation.

$$\text{e} = 10^{A-\frac{B}{C+T}} = 10^{\left(8.07131-\frac{1730.63}{233.426+10}\right)} = 9.16 \text{ mmHg } \frac{1\text{atm}}{760 \text{ mmHg}} = 0.0121 \text{ atm}$$

Using $K_{h,i}$ at 10 °C from Table 1 and x_i from Table 2, we have the values shown in this table.

i	$K_{h,i}$ (atm g/ccSTP)	x_i	$C_{i,eq}$ (ccSTP/g)
He	111	5.24×10^{-6}	$\frac{(0.947-0.0121)5.24\times10^{-6}}{111} = 4.41\times10^{-8}$
Ne	89.0	1.82×10^{-5}	$\frac{(0.947-0.0121)1.82\times10^{-5}}{89.0} = 1.91\times10^{-7}$
N_2	53.2	0.781	$\frac{(0.947-0.0121)0.781}{53.2} = 1.37\times10^{-2}$
Ar	23.9	9.34×10^{-3}	$\frac{(0.947-0.0121)9.34\times10^{-3}}{23.9} = 3.65\times10^{-4}$
Kr	12.4	1.14×10^{-6}	$\frac{(0.947-0.0121)1.14\times10^{-6}}{12.4} = 8.60\times10^{-8}$
Xe	6.52	8.7×10^{-8}	$\frac{(0.947-0.0121)8.7\times10^{-8}}{6.52} = 1.25\times10^{-8}$

b) Equation (9) is shown here.

$$C_i = \frac{\big(P - e(T)\big)\text{x}_i}{K_{w,i}(T,S)} + A'x_i$$

Values for x_i are given in Table 2, and are shown in the table in Solution Exercise 1a. The first term in Equation (9) was computed in Solution Exercise 1a. The second term (with $A' = 0.003$ ccSTP/g), concentration (C_i), and percent change are shown in the next table.

i	$A'x_i$ (ccSTP/g)	C_i (ccSTP/g)	Percent Change $\frac{C_i - C_{i,eq}}{C_{i,eq}} X\ 100\%$
He	1.57×10^{-8}	5.99×10^{-8}	36.0%
Ne	5.45×10^{-8}	2.46×10^{-7}	29.0%
N_2	2.34×10^{-3}	1.61×10^{-2}	17.0%
Ar	2.80×10^{-5}	3.93×10^{-4}	7.7%
Kr	3.42×10^{-9}	8.94×10^{-8}	4.0%
Xe	2.61×10^{-10}	1.27×10^{-8}	2.1%

As seen in this table, the addition of excess air has a much larger effect on the low solubility gases such as He and Ne than the higher solubility gases such as Kr and Xe.

Return to Exercise 1

Return to where text linked to Exercise 1

Solution Exercise 2

The model scenario involves four noble gases and three unknown parameters, which means there is one degree of freedom ($4 - 3 = 1$). Chi-squared calculations are provided in a spreadsheet that can be download from the web page for this book↗, yielding a chi-squared value of 2.67. Based on the provided chi-squared table, a value of 2.67 corresponds to $p = 0.10$, or a 10 percent chance that the chi-squared value results from random measurement error. Given this result, we would have confidence that the noble gas model yielded reasonable and useful results.

Return to Exercise 2↑

Return to where text linked to Exercise 2↑

Solution Exercise 3

Equation (13) is used to determine minimum groundwater age. A spreadsheet showing this solution is available on the web page for this book↗.

The average precipitation-weighted ^{3}H for the last five years is 8.5 TU.

$$Age_{min} = \frac{-\ln\left(\frac{3.5}{8.5}\right)}{\left(\frac{\ln(2)}{12.32}\right)} = \frac{-\ln(0.4118)}{0.05626\ \mathrm{yr}^{-1}} = 16 \text{ years}$$

Return to Exercise 3↑

Return to where text linked to Exercise 3↑

Solution Exercise 4

The solution to Exercise 4 has two parts: a) and b).

a) Using Equation (13) the minimum groundwater age is determined as:

The average precipitation-weighted ^{3}H for the last five years is 7.7 TU.

$Age_{min} = -\ln(4.5/7.7)/(\ln(2)/12.32)) = 9$ years (rounded down to capture a minimum)

b) Based on the plotted decay curve and ^{3}H function, we can estimate a minimum groundwater age of nine years and a range of potential minimum age between four and 20 years.

The graphical solution steps, based on information in Section 3.4, are:

1. Use the provided atmospheric ^{3}H function.
   - The data provided are annual averages and the problem statement indicates we can assume these are weighted by precipitation.
2. Calculate the first point of the decay curve:
   Year = 2012
   $C_m = 4.5$ TU
3. Calculate the second point of the decay curve:
   $C_0 = C_m(\exp(\lambda\Delta t)$
   $C_0 = 4.5 \text{ TU } (\exp\left(\frac{\ln(2)}{12.32 \text{ yrs}}(2012 \text{ yrs} - 1950 \text{ yrs})\right)$
   Year = 1950
   $C_0 = 147$ TU
4. Therefore, the two points for plotting the decay curve are:
   Year : ^{3}H (TU)
   2012 : 4.5 TU
   1950 : 147 TU

More detail is provided in the following graphs and the spreadsheet provided on the web page for this book↗. Based on the plotted decay curve and the precipitation-weighted ^{3}H curve, the estimated minimum groundwater age is $2012 - 2003 = 9$ years. Using the mean annual ^{3}H curve, plus or minus one standard deviation, we can estimate uncertainty in minimum groundwater age. The decay curve crosses the annual mean minus one standard deviation line at about 2008. The decay curve crosses the annual mean plus one standard deviation line at about 1992. Thus, the full range of potential minimum ages is about 4 to 20 years.

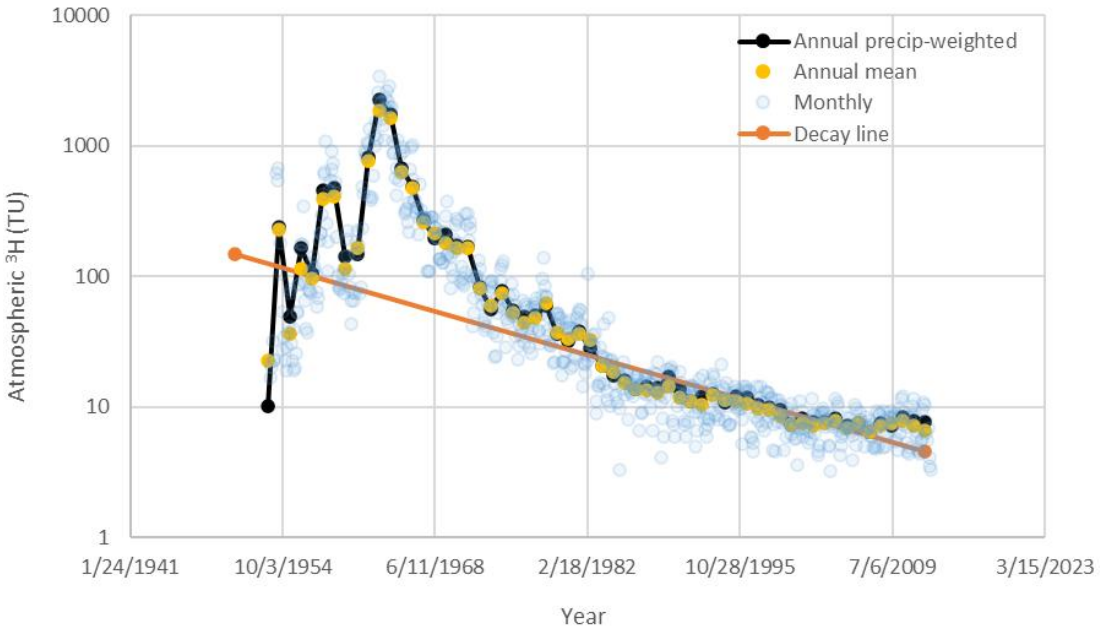

A shorter period of the same graph, zoomed in on the period of time when there are intersections of the decay line and the recharge concentration curve.

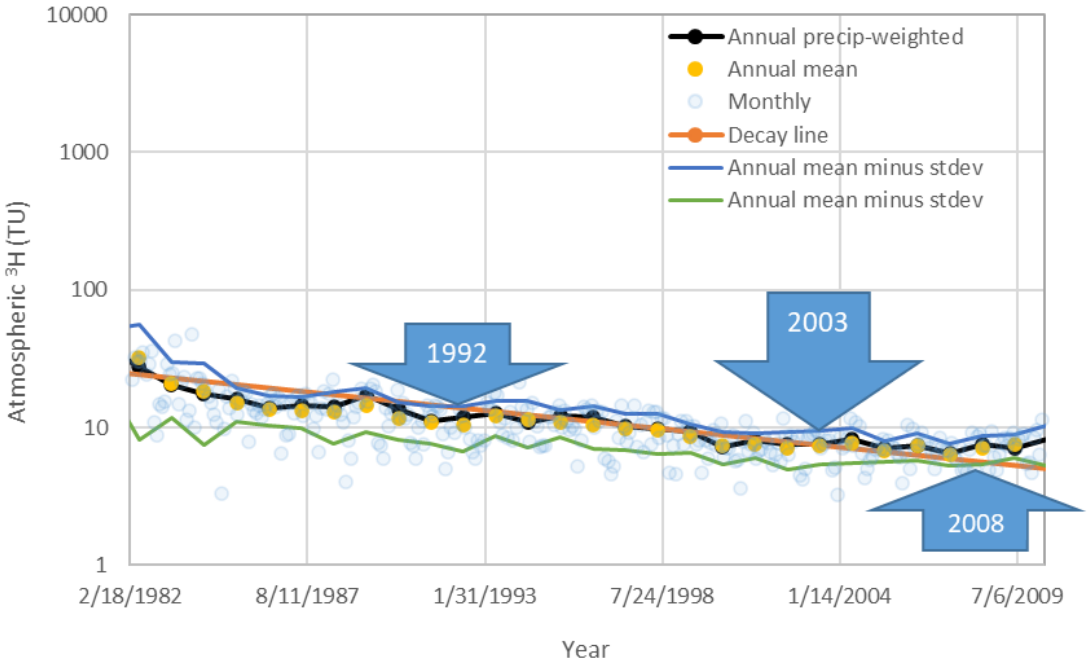

Return to Exercise 4

Return to where text linked to Exercise 4

Solution Exercise 5

Calculate the $^3H/^3He$ age using Equation (14) as shown here.

$$Age = \frac{\ln\left(1 + \frac{6.8}{0.72}\right)}{\frac{\ln(2)}{12.32}} = 41.7 \text{ years}$$

Return to Exercise 5

Return to where text linked to Exercise 5

Solution Exercise 6

Equation (21) is shown here.

$$^3\mathrm{He}_{\mathrm{trit}} =$$

$$^4\mathrm{He}_{\mathrm{m}}(R_m - R_{terr}) - {}^4\mathrm{He}_{\mathrm{sol}}(R_{sol} - R_{terr}) - \left(\frac{^4\mathrm{He}}{\mathrm{Ne}}\right)_{\mathrm{EA}} (\mathrm{Ne}_{\mathrm{m}} - \mathrm{Ne}_{\mathrm{sol}})(R_a - R_{terr})$$

Working from left to right through the right-hand side of Equation (21), values that must be calculated are R_m, $^3\mathrm{He}_{\mathrm{sol}}$, R_{sol}, and $\mathrm{Ne}_{\mathrm{sol}}$.

R_a is known (1.382×10^{-6}) and, in the absence of other evidence, R_{terr} is assumed to be 2×10^{-8}.

Measured concentrations of ^{4}He and Ne, and the assumed ^{4}He/Ne ratio, are given in the problem statement. R_m can be determined from $\delta\ ^3$He = 32 percent,

where:

$$\begin{aligned}
\delta\ ^3\mathrm{He} &= \left(\frac{R_m}{R_a} - 1\right) 100\% \\
32\% &= \frac{R_m}{R_a} 100\% - 1(100\%) \\
0.32 &= \frac{R_m}{R_a} 1.0 - 1(1.0) \\
0.32{+}1 &= \frac{R_m}{R_a} \\
1.32 &= \frac{R_m}{R_a} \\
R_m &= 1.32 \quad R_a = 1.32\ (1.382\text{x}10^{-6}) = 1.824\text{x}10^{-6}
\end{aligned}$$

$^3\mathrm{He}_{\mathrm{sol}}$ and $\mathrm{Ne}_{\mathrm{sol}}$ are determined from Equation (4).

$$c_{i,eq} = \frac{\big(P - e(T)\big)x_i}{K_{w,i}(T,S)}$$

We need to compute P at 500 m, e at 17.5 °C, and $K_{w,i}$ at 17.5 °C. P is calculated as:

$$P = P_0 \exp\left(-\frac{Z}{Z_s}\right) = 1\ \mathrm{atm} \exp\left(-\frac{500\ \mathrm{m}}{8300\ \mathrm{m}}\right) = 0.942\ \mathrm{atm}$$

e at 17.5 °C is calculated and converted to atmospheres as shown here.

$$e = 10^{A - \frac{B}{C+T}} = 10^{\left(8.07131 - \frac{1730.63}{233.426+17.5}\right)} = 14.94\ \mathrm{mmHg}\ \frac{1\mathrm{atm}}{760\ \mathrm{mmHg}} = 0.0197\ \mathrm{atm}$$

Table 1 gave K_w values for He and Ne at 10 °C and 20 °C but not at 17.5 °C. The empirical equations of Weiss (1971) could be used, or the values could be linearly interpolated between 10 °C and 20 °C.

For He, with $K_{w,He}$ in $\frac{\text{atm g}}{\text{ccSTP}}$:

$$K_{w,He} \text{ at } 17.5\ ^\circ\text{C} = K_{w,He} \text{ at } 10\ ^\circ\text{C} + \frac{(17.5^\circ\text{C} - 10^\circ\text{C})}{(20^\circ\text{C} - 10^\circ\text{C})}\left(K_{w,He} \text{ at } 20\ ^\circ\text{C} - K_{w,He} \text{ at } 10\ ^\circ\text{C}\right)$$

$$= 111 + \frac{(17.5\ ^\circ\text{C} - 10\ ^\circ\text{C})}{(20\ ^\circ\text{C} - 10\ ^\circ\text{C})}(114 - 111) = 113.25\ \frac{\text{atm g}}{\text{ccSTP}}$$

For Ne:

$$K_{w,Ne} \text{ at } 17.5\ ^\circ\text{C} = K_{w,Ne} \text{ at } 10\ ^\circ\text{C} + \frac{(17.5\ ^\circ\text{C} - 10\ ^\circ\text{C})}{(20\ ^\circ\text{C} - 10\ ^\circ\text{C})}\left(K_{w,Ne} \text{ at } 20\ ^\circ\text{C} - K_{w,Ne} \text{ at } 10\ ^\circ\text{C}\right)$$

$$= 89.0 + \frac{(17.5\ ^\circ\text{C} - 10\ ^\circ\text{C})}{(20\ ^\circ\text{C} - 10\ ^\circ\text{C})}(96.0 - 89.0) = 94.25\ \frac{\text{atm g}}{\text{ccSTP}}$$

We also need the mixing ratios (x_i) of ^{4}He and Ne, which are given Table 4.

^{4}He makes up 99.9 percent of atmospheric He, and He makes up 0.000524 percent of dry atmospheric air, so $x_{He} = (5.24\text{x}10^{-6})(0.999) = 5.235\text{x}10^{-6}$

Ne makes up 0.001818 percent of dry atmospheric air, so $x_{Ne} = 1.818\text{x}10^{-5}$.

Returning to Equation (4) for He, the concentration is calculated as shown here.

$$C_{^4He,eq} = \frac{(0.942 - 0.0197)(5.235\text{x}10^{-6})}{113.25} = 4.261\text{x}10^{-8}\ \frac{\text{ccSTP}}{\text{g}}$$

And then we do the same for Ne.

$$C_{Ne,eq} = \frac{(0.942 - 0.0197)(1.818\text{x}10^{-5})}{94.25} = 1.778\text{x}10^{-7}\ \frac{\text{ccSTP}}{\text{g}}$$

The last variable needed to solve Equation (21) is R_{sol}

$$R_{sol} = \alpha R_a = 0.98\ (1.382\text{x}10^{-6}) = 1.354\text{x}10^{-6}$$

Substituting the above values into Equation (21), we calculate $^3\text{He}_{\text{trit}}$ as follows.

$$^3\text{He}_{\text{trit}} = {}^4\text{He}_{\text{m}}(1.824\text{x}10^{-6} - 2\text{x}10^{-8}) - {}^4\text{He}_{\text{sol}}(1.354\text{x}10^{-6} - 2\text{x}10^{-8}) - (0.2882)(\text{Ne}_{\text{m}} - \text{Ne}_{\text{sol}})(1.382\text{x}10^{-6} - 2\text{x}10^{-8})$$

$$^3\text{He}_{\text{trit}} = 5.29\text{x}10^{-8}(1.824\text{x}10^{-6} - 2\text{x}10^{-8}) - (4.261\text{x}10^{-8})(1.354\text{x}10^{-6} - 2\text{x}10^{-8}) - (0.2882)(2.14\text{x}10^{-7} - 1.778\text{x}10^{-7})(1.382\text{x}10^{-6} - 2\text{x}10^{-8})$$

$$^3He_{trit} = 2.43x10^{-14}\ \frac{ccSTP}{g}$$

Converting $^3He_{trit}$ in $\frac{ccSTP}{g}$ to TU

$$^3He_{trit} = (2.43x10^{-14})(4.021x10^{14}) = 9.8\ TU$$

Finally, the $^3H/\ ^3He$ age based on Equation (14) as shown here.

$$Age = \frac{\ln\left(1 + \frac{9.8}{5.6}\right)}{\frac{\ln(2)}{12.32\ years}} = 18\ years$$

Return to Exercise 6

Return to where text linked to Exercise 6

Solution Exercise 7

The solution to Exercise 7 is in two parts: a) and b).

a) We first solve for the mole fraction of SF_6 that would be in equilibrium with the measured concentrations at a temperature of 15 °C and elevation of 800 m. This was shown in Equation (25) for UA as shown here.

$$x = \frac{C}{K_h(P - e) + A'}$$

We need to first compute P at 800 m, e at 15 °C, and K_h at 15 °C. P is calculated as shown here.

$$P = P_0 \exp\left(-\frac{Z}{Z_s}\right) = 1 \text{ atm } \exp\left(-\frac{800 \text{ m}}{8300 \text{ m}}\right) = 0.908 \text{ atm}$$

e at 15 °C is calculated and converted to atmospheres as shown here.

$$e = 10^{A - \frac{B}{C+T}} = 10^{\left(8.07131 - \frac{1730.63}{233.426+15}\right)} = 12.73 \text{ mmHg } \frac{1\text{atm}}{760 \text{ mmHg}} = 0.0167 \text{ atm}$$

Table **6** gave K_h values at 10 °C and 20 °C but not at 15 °C. We could use the empirical equations of Bullister and others (2002), or we can linearly interpolate between 10 °C and 20 °C as shown in the following equations.

$$\begin{aligned} K_h \text{ at } 15\,^\circ\text{C} &= K_h \text{ at } 10\,^\circ\text{C} + \frac{(15\,^\circ\text{C} - 10\,^\circ\text{C})}{(20\,^\circ\text{C} - 10\,^\circ\text{C})} (K_h \text{ at } 20\,^\circ\text{C} - K_h \text{ at } 10\,^\circ\text{C}) \\ &= 0.0003969 + \frac{(15\,^\circ\text{C} - 10\,^\circ\text{C})}{(20\,^\circ\text{C} - 10\,^\circ\text{C})}(0.0002739 - 0.0003969) \\ &= 0.0003354 \frac{\text{mole}}{\text{kg atm}} \end{aligned}$$

So, the mole fraction becomes (with $A' = 0$) as shown in the following equation.

$$\begin{aligned} x &= \frac{2.6\text{x}10^{-15} \frac{\text{moles}}{\text{kg}}}{0.0003354 \frac{\text{mole}}{\text{kg atm}}(0.908 \text{ atm} - 0.0167 \text{ atm}) + 0} \\ &= 8.70\text{x}10^{-12} \\ &= 8.7 \text{ pptv} \end{aligned}$$

Next the atmospheric curve shown in Figure 20 is utilized to find the year that the atmosphere had a mole fraction (essentially equal to the mixing ratio) of 8.7 pptv as shown below. This is approximately 2015. Since the sample was collected in 2018, it has an apparent tracer age of 2018 – 2015 = 3 years.

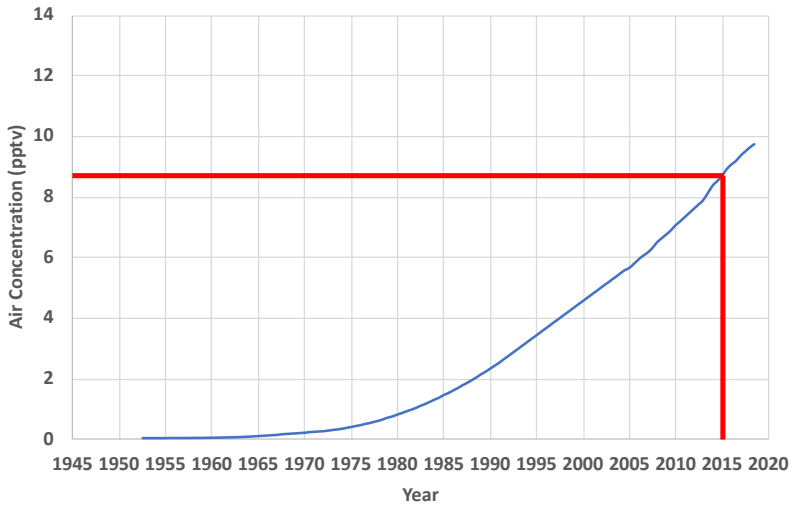

b) To add 0.003 ccSTP/g = 3.0 ccSTP/kg of excess air, we must convert ccSTP/kg to moles/kg. Equation (3) showed this conversion as duplicated here.

$$n = \frac{PV}{RT} = \frac{(1\text{ atm})(\text{ccSTP})}{82.05746\ \frac{\text{ccSTP atm}}{\text{K mole}}(273.15\text{ K})} = \frac{1\text{ atm}\left(3.0\ \frac{\text{ccSTP}}{\text{kg}}\right)}{82.05746\ \frac{\text{ccSTP atm}}{\text{K mole}}(273.15\text{ K})}$$

$$= 0.000134\ \frac{\text{moles}}{\text{kg}}$$

With excess air, Equation (25) can be used to calculate the mole fraction of SF_6 in the atmosphere that would have resulted in the measured concentration. This is duplicated here.

$$x = \frac{2.6\text{x}10^{-15}\ \frac{\text{moles}}{\text{kg}}}{0.0003354\ \frac{\text{mole}}{\text{kg atm}}(0.908\text{ atm} - 0.0167\text{ atm}) + 0.000134\ \frac{\text{moles}}{\text{kg}}}$$

$$= 6.01\text{x}10^{-12} = 6.01\text{ pptv}$$

Then the atmospheric curve in Figure 20 is utilized to find the year that the atmosphere had a mole fraction (essentially equal to the mixing ratio) of 6.01 pptv as shown below. This is approximately 2006.5. Since the sample was collected in 2018, it has an apparent tracer age of 2018 − 2006.5 = 11.5 years. This is 8.5 years older than the tracer age when excess air was not included and illustrates the importance of including excess air for calculating SF_6 tracer ages.

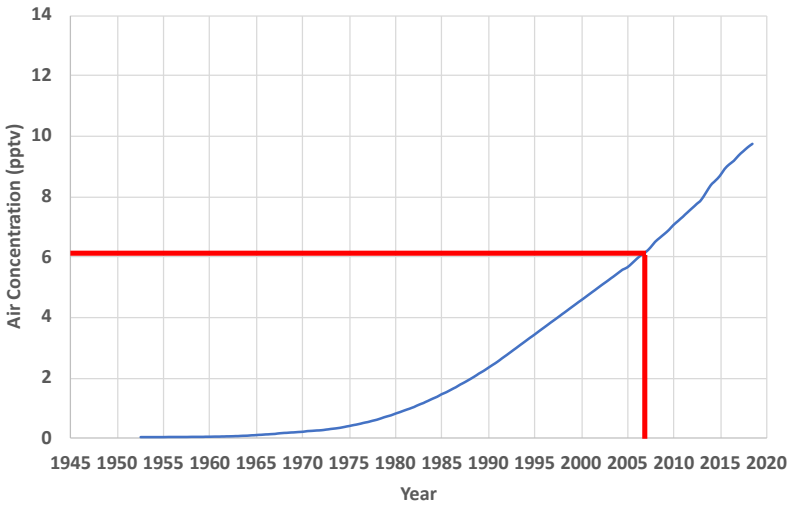

Return to Exercise 7

Return to where text linked to Exercise 7

12 Notations

A = amount of gas trapped in the porous media per unit mass of water (molM^{-1}, typically in ccSTP/g, ccSTP/kg, or mole/kg)

A' = amount of excess air in units consistent with c_i (e.g. molM^{-1}, typically in ccSTP/g, ccSTP/kg, or mole/kg)

Age = elapsed time since groundwater recharge, i.e., exposure to atmosphere (T)

Age_{min} = minimum age of the sample (T)

C = aqueous concentration (molM^{-1}, typically in mole/kg or TU for ^{3}H)

C_o = concentration at an arbitrary time; a convenient choice is 1950 when the precipitation ^{3}H record begins after 1950. (molM^{-1}, typically in mole/kg or TU for ^{3}H)

$\mathrm{C_{Ar}}$ = concentration of Ar in water (L^{3}M^{-1}, typically in ccSTP/g)

$C_{background}$ = ^{3}H concentration in precipitation at the time the sample was collected (TU)

c_i^{water} = concentration of gas *i* in the water phase (L^{3}M^{-1}, typically in ccSTP/g)

c_i = concentration of gas *i* in the water phase (L^{3}M^{-1}, typically in ccSTP/g)

$C_{i,eq}$ = concentration of air saturated water, ASW, (L^{3}M^{-1}, typically in ccSTP/g or ccSTP/kg)

C_i^{gas} = concentration of gas *i* in the gas phase (moles/L)

$C_{m,i}$ = measured concentration of the *i*th gas (moles/L)

$C_{m,\mathrm{Ne}}$ = measured concentration of dissolved Ne (ccSTP/g)

C_{meas} = sample concentration (L^{3}M^{-1}, typically in ccSTP/g)

$C_{\mathrm{N_2}}$ = concentration of $\mathrm{N_2}$ in water (L^{3}M^{-1}, typically in ccSTP/g)

$C_{\mathrm{O_2}}$ = concentration of $\mathrm{O_2}$ in water (L^{3}M^{-1}, typically in ccSTP/g)

$c_{s,i}$ = simulated concentration of the *i*th gas (L^{3}M^{-1}, typically in ccSTP/g or ccSTP/kg)

$C_{sol,\mathrm{Ne}}$ = theoretical concentration of Ne in equilibrium with the atmosphere (L^{3}M^{-1}, typically in ccSTP/g or ccSTP/kg)

Δt = sample time $-C_0$ time (T)

e = temperature dependent vapor pressure of water ($ML^{-1}T^{-2}$, typically in atm or mmHg)

$e(T)$ = vapor pressure of water at temperature T ($ML^{-1}T^{-2}$, typically in atm or mmHg)

F = fractionation factor (dimensionless)

$^3He_{atm}$ = ^3He derived from atmospheric sources (L^3M^{-1})

$^3He_{EA}$ = ^3He derived from excess air (L^3M^{-1})

^3He_m = ^3He measured in the groundwater sample (L^3M^{-1})

$^3He_{sol}$ = ^3He concentration at solubility equilibrium with the atmosphere at recharge temperature and elevation (L^3M^{-1})

$^3He_{terr}$ = ^3He from terrigenic sources, including crustal ^3He ($^3He_{crust}$) and mantle ^3He ($^3He_{man}$) (L^3M^{-1})

^4He_m = Measured concentration of ^4He (L^3M^{-1})

K_h = temperature- and salinity-dependent equilibrium constant ($molM^{-2}LT^2$ typically in moles $kg^{-1}atm^{-1}$)

$K_{w,Ar}$ = dimensioned Henry Coefficient for Ar ($molM^{-2}LT^2$, typically in moles $kg^{-1}atm^{-1}$)

$K^{cc}_{w,i}$ = dimensionless Henry Coefficient for gas i (dimensionless)

$K_{w,i}$ = Henry Coefficient for gas i ($molM^{-2}LT^2$, typically in moles $kg^{-1}atm^{-1}$)

$K_{w,i}(T,S)$ = Henry Coefficient of gas i at temperature T and salinity S ($molM^{-2}LT^2$, typically in moles $kg^{-1}atm^{-1}$)

K_{w,N_2} = dimensioned Henry Coefficient for N_2 ($molM^{-2}LT^2$, typically in moles $kg^{-1}atm^{-1}$)

K_{w,O_2} = dimensioned Henry Coefficient for O_2($molM^{-2}LT^2$, typically in moles $kg^{-1}atm^{-1}$)

L_{vz} = vertical distance from land surface to the water table (L)

λ = tritium decay constant (T^{-1}, 0.05626 yr^{-1})

P = atmospheric pressure ($ML^{-1}T^{-2}$, typically in atm)

P_0 = pressure at elevation zero ($ML^{-1}T^{-2}$, 1 atm)

p_i = partial pressure of gas *i* in the gas phase ($ML^{-1}T^{-2}$, typically in atm)

q = recharge rate (LT^{-1}, typically in mm/yr)

R_m = measured $^3He/^4He$ ratio; commonly referred to simply as R, as in the notation R/R_a (dimensionless)

R_{terr} = $^3He/^4He$ ratio for terrigenic He, given in Table 4, (dimensionless)

S = salinity of the sample (MM^{-1}), often in part per thousand (1000 MM^{-1})

σ_i = measurement error of the *i*th gas (L^3M^{-1}, typically in ccSTP/kg)

T = temperature (typically in °C)

t = time of sampling (T)

$TDGP$ = total dissolved gas pressure ($ML^{-1}T^{-2}$)

t_{vz} = vadose zone transport time (T)

θ_{vz} = mobile water content (dimensionless)

x = dry air mole fraction (dimensionless)

x_i = fraction of gas *i* (mixing ratio) in the dry atmosphere (dimensionless)

Z = elevation (L)

Z_s = scaling factor (dimensionless)

13 About the Authors

D. Kip Solomon, PhD is a professor at the University of Utah and was formerly the chair of the Department of Geology and Geophysics. He was also appointed as the Darcy Lecturer by the National Groundwater Association and has served on numerous national committees including: National Research Council Committee on Improving Practices for Regulating and Managing Low-Activity Radioactive Waste, National Research Council Committee on Conceptual Models in Fractured Unsaturated Zones, United States Representative for various Advisory Groups at the International Atomic Energy Agency, and the editorial board for the journal *Groundwater*. Dr. Solomon's research interests include the use of environmental tracers to evaluate groundwater flow and solute transport processes in local- to regional-scale aquifers. He has developed the use of dissolved gases including helium-3, CFCs, and SF_6 to evaluate groundwater travel times, location and rates of recharge, and the sustainability of groundwater resources. He constructed and operates one of only a few labs in the world that measures noble gases in groundwater. His research results have been documented in more than 100 journal articles, book chapters, and technical reports.

Troy Gilmore, PhD is an Associate Professor at the University of Nebraska-Lincoln. His appointments include the Conservation and Survey Division (Nebraska's Geological Survey) in the School of Natural Resources and the Biological Systems Engineering Department. He is a Faculty Fellow with the Daugherty Global Water for Food Institute and Associated Faculty with North Carolina State University. Dr. Gilmore's research interests include the use of environmental tracers, mostly in agricultural landscapes where aquifer and surface water contamination from agrichemicals is a concern. Emerging projects include image-based hydrology leveraging existing archives of ground-based time-lapse imagery (gaugecam.org↗). He also focuses on extension and outreach projects, for communication of scientific information to key water resources decision-makers. His research has been documented in 39 journal articles. His extension activities include 11 extension workshops and online training modules, videos, and story maps hosted at NebraskaWAVES.org↗.

Please consider signing up to the GW-Project mailing list to stay informed about new book releases, events, and ways to participate in the GW-Project. When you sign up to our email list, it helps us build a global groundwater community. Sign up↗.

Modifications to Original Release

Changes from the Original Version to Version 2

Original Version: February 8, 2024, Version 2: March 5, 2026

General: updated the Table of Contents to include this modification section

Page numbers refer to the original PDF.

page ii, added Version 2

page 43, Equation 20, the minus sign was changed to a plus sign